2-7-2023

Probing Amyloid-beta protein structure and dynamics with a selective antibody

Shikha Grover
University of Missouri-St. Louis, shikhagroveraug14@gmail.com

Probing Amyloid-β protein structure and dynamics with a selective antibody

Shikha Grover
M.S., Chemistry, University of Missouri-St. Louis, 2020
M. Sc., Chemistry, Delhi University, Delhi, India, 2016
B. Sc., Chemistry, Delhi University, Delhi, India, 2014

A Dissertation

Submitted to the Graduate School at the

THE UNIVERSITY OF MISSOURI-ST. LOUIS

In partial fulfillment of the requirements for the degree

Doctor of Philosophy

in

CHEMISTRY

with an emphasis in Biochemistry

May 2023

Advisory Committee

Prof. Michael R. Nichols, Ph.D. (Chairperson)

Prof. James K. Bashkin, D. Phil

Prof. Keith J. Stine, Ph.D.

Prof. Chung F. Wong, Ph.D.

ACKNOWLEDGEMENT

I would whole-heartedly like to express my gratitude to UMSL Department of Chemistry & Biochemistry for offering me a doctoral position in Chemistry (Biochemistry). I have thoroughly enjoyed my PhD journey being part of Dr. Nichols Laboratory. Dr. Nichols has been such a kind and supportive mentor to me. Words would fall short of the ceaseless encouragement and expertise I have received from him over the past years. I had a little hands-on experience in the biochemistry laboratory before joining Nichols lab. I have gained immense knowledge and research expertise as a biochemist and have continued to strengthen problem-solving and troubleshooting while navigating toward the goals of my research project. All thanks to you.

I am thrilled to have Dr. Stine, Dr. Bashkin, and Dr. Wong on my dissertation committee. I had a great opportunity to take classes with them and be a teaching assistant for their courses. I have learned a lot from them. They have continued to extend their valuable feedback and suggestions during all the times I needed help. Dr. Stine has been welcoming whenever I have reached out regarding CGSA related matters. Dr. Bashkin and Dr. Wong have helped me strengthen my research skills through the Biochemistry Problem seminar course and I have had a great time each semester with the discussions we have had in our Journal club. I would like to thank Dr. Bashkin for his continuous encouragement and compliments on my work. To all the teachers and mentors, I have had in my life, I am indebted.

Dr. Nyasha Makoni trained me in many research techniques when I first started working in Nichols Lab. I had a great time with her. Thank you for loving my cooked

food and our happy times together. Dr. Kapur Dhami was a great guide for me while navigating through problems encountered during my work. The first 2-3 years in the laboratory were one of the greatest times of my life because of thoughtful conversations with Dr. Makoni and Dr. Dhami. I will never be able to thank Cristina Sinobas for being the best lab mate and a true friend. Thank you for considering me one of the rarest personalities and for listening patiently to all my problems. Thank you for your texts even when I reach home to ensure my healthy being. I am grateful for the friendship shared with new lab members Ryan Domalewski and Nathan Zeller. It has been easy to talk to Ryan about the research work and to know about his experience until now. Nathan Zeller has contributed immensely to the lab and my research project. He provided all the help possible when the purifications columns had taken a setback. I have always wondered how Nichols lab can attract such wonderful and passionate undergraduate students and MS student researchers. I have enjoyed my time working with Thao, Anna, Gabe, Antanisha, Evan, Nicholas, Marina, Hannah, Bree, and Emma. I appreciate all the ELISA studies and western blot analysis work done.

During my time at UMSL, I have had a huge advantage of collaborative work with two of the labs at Washington University. I would like to thank postdoctoral student Dr. Saketh Chemuru from Dr. Gross's laboratory at the Danforth campus for helping us with the epitope-mapping studies conducted on Aβ42 protofibrils. I am thankful to Yingyue Zhou from Marco Colonna's lab at Med School Washington University for a collaborative study on the effect of complement protein on Aβ42 monomer aggregation of which we have a paper published. I had a great time working with you. I would like to extend my gratitude towards Danish Gul from Dr. Chubiz lab and Ariel from Dr. Olivas

lab in Biology department for all the research expertise offered for site-directed mutagenesis study. Thank you for letting me use the thermocycler and gel reagents. The work helped me enhance my knowledge of molecular biology tools. Danish Gul has been a great friend to me throughout. Thanks to Ariel Bulmash who is more excited about my graduation and can't wait to attend. I appreciate our conversations in the cell-culture lab.

All the PhD graduate students from other groups have been a great source of encouragement. I would like to thank Dr. Deva Talasila for her friendship over the years, especially with driving me to the lab when I did not have a car and for selfless support and care. I would also like to thank all the graduate students I have met from the beginning of my program to the end. They were a big part of my journey. I have had a great time as President of the Chemistry Graduate Student Association and connecting with Melanie Shadrick and the rest of the CGSA members. My leadership skills have been enhanced to a great extent. Thanks to all.

My friends from India Mansi, Harshi, Nitika, Vibhav, Adesh, Savita, Shaifali, Vaishali, and Anshul have been my world for me. Mansi, you have helped me immensely in unbelievable ways and I can't thank you enough for being such a great part of my life. You all have continued to be there for me and cheered me up when the valleys of PhD overwhelmed me. Without their support, I wouldn't be here.

Special thanks to my siblings Shivani Grover and Rakshit Grover who have been with me through all the ups and downs. Thank you, Shivani, for visiting me several times and traveling with me. Thank you for your help in cooking for me during my study work and for helping me format my PhD document. Special thanks to Rishab Sakhuja for being my greatest hope to complete PhD. Thank you for all the emotional support needed to

achieve this. Thanks to my extended family from India and the ones in United States who continue to pray for my well-being. I would never be able to thank my parents Vivek Kumar Grover and Ranjana Grover enough for encouraging me towards pursuing PhD in the first place and for the sacrifices they have made for us kids. I know you have missed having me around while I continue to live my dream. I'm blessed. I love you so much. Forever grateful to Nirankar.

TABLE OF CONTENTS

ACKNOWLEDGEMENT ..... **ii**

TABLE OF CONTENTS ..... **v**

LIST OF TABLES ..... **x**

LIST OF FIGURES ..... **xi**

LIST OF ABBREVIATIONS ..... **xv**

ABSTRACT ..... **xvii**

CHAPTER 1. INTRODUCTION **1**

1.1.Alzheimer's disease (AD) 1

1.1.1. Etiology and neuropathology 1

1.1.2. Early onset and late onset AD 2

1.1.3. Clinical stages of AD 3

1.1.4. Overview of senile plaques 4

1.2.Role of amyloid-β 4

1.2.1. Aβ protein generation from APP 4

1.2.2. Amyloid hypothesis 7

1.2.3. Relevant and abundant Aβ isoforms formed 8

1.2.4. Aβ detection in AD brain 9
1.2.5. Molecular basis of Aβ protein aggregation 9
1.3. Role of conformationally varied oligomeric Aβ species 10
1.3.1. Resolving Aβ structural conformations 11
1.3.2. Premise behind oligomeric Aβ species 11
1.3.3. Protofibrils: Morphology and physical properties 12
1.3.4. Significance of soluble Aβ protofibril species studies 13
1.4. Anti-amyloid-β immunotherapy 16
1.4.1. Adaptive immune system overview 16
1.4.2. Relevance of antibodies in AD research 17
1.4.3. Conformational-selective antibodies as therapeutics 18
CHAPTER 2. METHODS 21
2.1. Size-exclusion chromatography (SEC) of Aβ42 21
2.1.1. Aβ42 protofibril purification prep by SEC 21
2.1.2. Aβ42 monomer purification by SEC 23
2.2. Aβ42 fibril preparation 24
2.3. Immunization of rabbits and cloning of monoclonal antibodies 25
2.3.1. Immunization of rabbits 25
2.3.2. Biotinylation of Aβ protofibrils 25
2.3.3. Circular dichroism 26
2.3.4. Isolation of splenetic B-cells 26
2.3.5. Agar plate preparation 27
2.3.6. Formulation of LB broth 27
2.3.7. Preparation of competent DH5α E. coli cells 27

2.3.8. Cloning of assembled DNA fragments into pRab293 plasmid 28
2.3.9. Transformation of plasmid into DH5-α competent cells 29
2.3.10. Preparation of gridded patch plate for correct plasmid determination 30
2.3.11. Colony PCR of E. coli cell colonies 30
2.3.12. Gel electrophoresis of cell colonies 31
2.3.13. Mini-prep and sequencing of positive colonies 31
2.3.14. Maxi-prep of sequenced E. coli colonies 32
2.3.15. Plasmid DNA purity and concentration determination 33
2.3.16. Re-amplification of mAb HC and LC plasmid into E. coli cells 35
2.4. Expression and purification of monoclonal antibodies 35
2.4.1. FreeStyle 293 cell-culture 35
2.4.2. Transfection of HC and LC plasmid into FreeStyle 293 cells 36
2.4.3. High-throughput transfection 40
2.4.4. Collection of supernatants from FreeStyle cells 42
2.4.5. Dot blot to detect monoclonal antibody 42
2.4.6. Protein A/G affinity column 43
2.5. Site-directed mutagenesis experiments 44
2.5.1. Polymerase chain reaction (PCR) 44
2.5.2. Ligation reaction 45
2.5.3. Transformation of plasmid into E. coli cells and sequencing the product 46
2.6. Aβ enzyme linked immunosorbent assay (ELISA) 46
2.6.1. Aβ indirect ELISA 46
2.6.2. Aβ titer ELISA 47
2.6.3. Aβ antigen competition ELISA 47

2.6.4. Aβ antibody competition sandwich ELISA 48
2.7. Thioflavin T (ThT) fluorescence measurement 48
2.7.1. Aβ monomer aggregation assay (cuvette-based) 49
2.7.2. Aβ protofibril dynamic experiment 49
2.8. Atomic force microscopy (AFM) 50
2.9. Epitope determination of mAbSL on Aβ protofibril 50
2.9.1. Hydrogen-deuterium exchange/mass spectrometry (HDX-MS) 50
2.9.2. Fast photochemical oxidation of proteins/mass spectrometry (FPOP-MS).... 53
CHAPTER 3. DEVELOPMENT OF A CLASS OF MONOCLONAL ANTIBODIES SPECIFIC FOR Aβ42 PROTOFIBRILS 55
3.1. Isolation and characterization of soluble Aβ42 protofibrils and Aβ42 fibrils..... 58
3.2. SEC purification of Aβ42 monomer and oligomers 61
3.3. Production of serum polyclonal antibodies from immunization of rabbit with Aβ42 protofibrils..... 63
3.4. Cloning, expression, purification, and characterization of monoclonal antibodies selective for Aβ42 protofibrils..... 69
3.4.1. Cloning of HC and LC 74
3.4.2. Cell-culture and transfection of 293 F cells with heavy-chain and light-chain plasmid..... 79
3.4.3. Expression and affinity purification of secreted monoclonal antibodies..... 81
3.4.4. Monoclonal antibodies offer great selectivity towards protofibrils..... 83
3.4.5. High-throughput transfection using deep-well plate..... 85
3.5. Conclusion 86
CHAPTER 4. PROPERTIES OF MONOCLONAL PROTOFIBRIL-SELECTIVE ANTIBODY 91

4.1. Monoclonal antibody inhibits Aβ42 monomer aggregation 93

4.1.1. Concentration-dependent effect of selective monoclonal antibody 93

4.1.2. Effect of a non-selective monoclonal antibody 96

4.2. Monoclonal antibody interacts with Aβ42 protofibrils 99

4.3. Aβ42 protofibrils and monoclonal antibody complex imaged using atomic force microscopy 102

4.4. Conclusion 105

CHAPTER 5. EPITOPE MAPPING OF Aβ42 PROTOFIBRILS..... 109

5.1. Antibody competition study of monoclonal antibody with antibodies Ab5 and Ab 2.1.3..... 111

5.2. Hydrogen-deuterium exchange-mass spectrometry..... 113

5.2.1. Differential uptake of deuterium by conformationally distinct Aβ42 species 114

5.2.2. Conformational epitope of selective monoclonal antibody on Aβ protofibrils involves N-and C-terminal region 117

5.3. Fast photochemical oxidation of proteins-mass spectrometry..... 120

5.3.1. FPOP also shows intermediate structure of protofibril..... 120

5.3.2. FPOP shows an involvement of N-and C-terminus in the epitope mapping of Aβ protofibrils..... 122

5.4. Conclusion 124

CHAPTER 6. CONVERSION OF A SELECTIVE ANTIBODY TO A NON-SELECTIVE ANTIBODY 126

CONCLUSION 133

BIBLIOGRAPHY 134

VITA……...160

LIST OF TABLES

CHAPTER 1. INTRODUCTION

Table 1.1 Conformational-selective antibodies know in AD research 20

CHAPTER 2. METHODS

Table 2.1. Illustrates the concentration obtained and % yield of various preps where Aβ42 protofibril (PF) and monomer (M) have been isolated by SEC using Superdex 75 column..... 22

Table 2.2. Illustrates the concentration obtained and % yield of various preps where Aβ42 monomer has been isolated by SEC using Superdex 200 column..... 23

Table 2.3. List of all the plasmids transfected in 293 F cell with the amount of each reagent used to generate monoclonal AbSL 37

Table 2.4. List of expressed mAbSL, volume of cell expression, volume of expression medium used, of cells used and volume of 293 Fectin-plasmid complex used..... 39

Table 2.5. List of all the plasmids transfected in 293 F cell with the amount of each reagent used to generate monoclonal AbSL in a high-throughput fashion..... 40

Table 2.6. High-throughput transfection. List of expressed mAbSL, volume of cell expression, volume of expression medium used, of cells used and volume of 293 Fectin-plasmid complex used 41

Table 2.7. Cycling instructions followed for mutagenesis reaction in the thermal cycler program. 45

CHAPTER 3. DEVELOPMENT OF A CLASS OF MONOCLONAL ANTIBODIES SPECIFIC FOR Aβ42 PROTOFIBRILS

Table 3.1. Sequence identities between mAbSL and Aβ mAb antibodies 79

Table 3.2. Notable amino acid differences between mAbSL and Aβ mAb antibodies 80

CHAPTER 4. PROPERTIES OF MONOCLONAL PROTOFIBRIL-SELECTIVE ANTIBODY

Table 4.1. Height, length and width analysis of Aβ42 fibrils and samples from Aβ42 protofibril dynamics……105

LIST OF FIGURES

CHAPTER 1. INTRODUCTION

Figure 1.1. Pathological hallmarks of Alzheimer's disease..... 2

Figure 1.2. Preclinical and Clinical stages of AD..... 3

Figure 1.3. Proteolytic cleavage of amyloid precursor protein..... 5

Figure 1.4. Aβ primary structure and aggregation pathway 8

Figure 1.5. Nucleation-dependent polymerization of aggregation process 10

Figure 1.6. Imaging Aβ protofibril and fibril structure by electron microscopy 13

Figure 1.7. Aβ42 protofibrils stimulate the release of TNFα..... 15

Figure 1.8. High-molecular weight Aβ42, represented as Aβ42 protofibrils pose cytotoxic effects..... 16

CHAPTER 2. METHODS

Figure 2.1. Design of cloning and expression of antibodies..... 34

Figure 2.2. Schematic illustration outlining the details of each step followed during 293 F cell-culture, transfection, expression and purification of monoclonal antibodies. ... 42

Figure 2.3 HDX-MS experimental workflow 53

CHAPTER 3. DEVELOPMENT OF A CLASS OF MONOCLONAL ANTIBODIES SPECIFIC FOR Aβ42 PROTOFIBRILS

Figure 3.1. Isolation and characterization of Aβ42 by SEC and CD spectra..... 61

Figure 3.2. SEC purification of Aβ42 using Superdex 200 column 63

Figure 3.3. AbSL antiserum displays selectivity for Aβ42 protofibrils..... 65

Figure 3.4. AbSL ELISA optimization and recognition of Aβ42 protofibrils with high affinity..... 66

Figure 3.5. AbSL PAC 56-1 selectively recognizes protofibrils over monomers and fibrils 67

Figure 3.6. Competition ELISA data with a fixed concentration of Aβ42 protofibrils (18 ng/well) coated in the plate 68

Figure 3.7. Affinity-purified ELISA data 69

Figure 3.8. Distinct areas of Aβ pathology recognized by AbSL 70

Figure 3.9. Biotinylation of Aβ42 protofibrils does not alter their characteristics 72

Figure 3.10. Aβ42 protofibril-selective monoclonal antibodies obtained using SPIN® coupled with biotinylated protofibrils..... 74

Figure 3.11. Second round screen of 36 antibody-expressing HEK 293 supernatants..... 75

Figure 3.12. Details of assembled fragment and linearized vector sent by Exon Bio to be used for cloning of positive monoclonal antibody hits..... 76

Figure 3.13. Cloning of the variable region for mAbSL 512 HC and LC antibodies was carried out as described..... 77
Figure 3.14. Agarose gel electrophoresis after colony PCR of patch plate colonies..... 78
Figure 3.15. Expression of mAbSL antibodies confirmed by dot blot of 293 F cell expression supernatant..... 81
Figure 3.16. Purification of mAbSL antibodies. FreeStyle 293 cells were co-transfected with mAbSL HC and LC plasmidsbsorbance at 280 nm..... 83
Figure 3.17. mAbSL and Aβ mAb antibodies expressed in-house display different Aβ42 protofibril selectivity..... 83
Figure 3.18. ELISA reveal affinities of mAbSL 113 for Aβ42 species..... 85
Figure 3.19. High-throughput expression permitted rapid assessment of multiple mAbSL antibodies..... 87

CHAPTER 4. PROPERTIES OF MONOCLONAL PROTOFIBRIL-SELECTIVE ANTIBODY

Figure 4.1. Indirect ELISA with a protofibril-selective antibody and a non-selective antibody..... 92
Figure 4.2. AbSL monoclonal antibody inhibits Aβ aggregation at sub-stoichiometric ratios..... 94
Figure 4.3. mAbSL monoclonal antibody inhibits Aβ aggregation at sub-stoichiometric ratios..... 96
Figure 4.4. mAb Aβ monoclonal antibody inhibits Aβ aggregation at sub-stoichiometric ratios..... 98

Figure 4.5. Protofibril dynamics in the presence of mAbSL monoclonal antibody at 10-fold difference 100
Figure 4.6. Protofibril dynamics in the presence of mAbSL monoclonal antibody 102
Figure 4.7. Images of Aβ42 fibrils (5 μM) 103
Figure 4.8. Morphological differences between Aβ42 fibrils and Aβ42 protofibril samples from protofibril dynamics 104
Figure 5.1. Cryo-EM density maps and atomic models of Aβ fibrils. 110
Figure 5.2. Atomic resolution structure of monomorphic Aβ42 amyloid fibrils 111
Figure 5.3. Probing the mAbSL epitope on Aβ42 protofibrils with an antibody competition ELISA 113
Figure 5.4. Amino acid sequence and pepsin digestion of Aβ42 protofibrils 115
Figure 5.5. HDX-MS plots for peptides obtained from Aβ42 species 117
Figure 5.6. HDX-MS epitope mapping 119
Figure 5.7. FPOP-MS of Aβ42 species 121
Figure 5.8. FPOP epitope mapping 123
Figure 5.9. HDX epitope mapping for a non-selective antibody 124

CHAPTER 5. EPITOPE MAPPING OF Aβ42 PROTOFIBRILS

Figure 6.1. Key amino acid differences between conformational-selective Aβ antibody and Aβ non-selective antibody. 127
Figure 6.2. Proposed single or double amino acid substitutions in mAbSL 113 127
Figure 6.3. Introduction of a single nucleotide mutation in mAbSL 113 HC 128
Figure 6.4. Steps involved in site-directed mutagenesis 128
Figure 6.5. Design of Primer 1 shown 129

Figure 6.6. DNA gel analysis with using Primer 1 design..... 129

Figure 6.7. Successful PCR product formation with the use of primer 130

Figure 6.8. Transformation step was evaluated using Topshot cells 132

LIST OF ABBREVIATIONS

APTES, 3'-aminopropyl-triethoxysilane

AbSL, antibody St. Louis

aCSF, artificial cerebero spinal fluid

AD, Alzheimer's disease

ADDLs, Aβ derived diffusible ligands

AFM, atomic force microscopy

AICD, amyloid precursor protein intracellular domain

APOE, apolipoprotein

APP, amyloid precursor protein

APTES, 3-aminopropyl triethoxysilane

Aβ, amyloid-beta

BACE, β-site amyloid precursor protein-cleaving enzyme 1

BCA, bicinchoninic acid

CD, circular dichroism

CSF, artificial cerebero spinal fluid

CTF, carboxy-terminal fragment

DLB, dementia with Lewy bodies

DNA, deoxyribonucleic acids

ELISA, enzyme linked immunosorbent assay

FPOP-MS, Fast photochemical oxidation of proteins/mass spectrometry

FTD, frontotemporal dementia

HC, heavy chain

HDX-MS, Hydrogen-deuterium exchange/mass spectrometry

HFIP, hexafluoro isopropanol

HPCL, high performance liquid chromatography

HRP, horseradish peroxidase

IMAC, immobilized metal affinity chromatography

IPTG, Isopropyl-β-D-thiogalactopyranoside

LC, light-chain

mAbSL, monoclonal antibody St. Louis

MCI, mild cognitive impairment

MCI, mild cognitive impairment stage

MyD88, myeloid differentiation primary-response protein 88)

NFTs, Neurofibrillary tangles

PAGE, polyacrylamide gel electrophoresis

PCR, Polymerase chain reaction

PD, Parkinson's disease

PFs, protofibrils

PG, PicoGreen

PS1, presenilin 1

PS2, presenilin 2

sAPP, soluble amyloid precursor protein

SEC, size-exclusion chromatography

SEM, scanning electron microscopy

TEM, transmission electron microscopy

ThT, Thioflavin-T

TNF-α, tumor necrosis factor α

X-Gal, 5-bromo-4-chloro-3-indolyl-β-D-galactopyranoside

ABSTRACT

Alzheimer's disease (AD) is a progressive neurodegenerative disorder. The AD brain is characterized by significant neuronal loss and accumulation of insoluble fibrillar amyloid-β protein (Aβ) plaques and tau protein neurofibrillary tangles in the brain. However, over the last decade, many studies have shown that the neurodegenerative effect of Aβ may in fact be caused by various soluble oligomeric forms as opposed to the insoluble fibrils. Furthermore, the data suggest that a pre-fibrillar aggregated form, termed protofibrils, mediates direct neurotoxicity, and triggers a robust neuroinflammatory response.

Antibodies targeting the various conformation of Aβ are important therapeutic agents to prevent the progression of AD. We have generated conformationally-selective monoclonal antibody St. Louis (mAbSL) that selectively targets Aβ42 protofibrils compared to Aβ42 monomers and fibrils. The development aspects of these antibodies include the cloning of HC and LC variable fragments into the plasmid vector, transfection

of the plasmids into 293 F cells, collection of the supernatant and purification using Protein A or protein G affinity chromatography. Sequencing of the heavy and light chain variable regions for multiple antibodies identified sequence characteristics that may impart conformational selectivity to the antibodies. Thus, I have successfully developed, expressed, and characterized these conformationally selective antibodies using various ELISA formats.

Exploration of Aβ42 aggregation in the presence a selective (mAbSL 113) and a non-selective antibody (mAb Aβ 513) using spectroscopic and microscopic techniques is quintessential to looking at the effect of these antibodies on Aβ42 monomer aggregation and protofibril dynamics. It yielded a unique inhibitory mechanism on Aβ42 monomer aggregation offered by mAbSL antibodies. Aβ42 protofibril dynamics were prominently altered in the presence of mAbSL 113 with an insoluble complex formation by the antibody at low sub-stoichiometric molar ratios.

We focused on accurately determining the conformational epitope of our developed antibodies on Aβ42 protofibrils. The conformational epitope on Aβ42 protofibril was detected using a monoclonal antibody in various experimental formats like antibody competition ELISA, HDX-MS, and FPOP analysis. Our findings demonstrated new insights into monoclonal antibodies that target AD progression.

CHAPTER 1: INTRODUCTION

1.1. Alzheimer's disease (AD)

Neurodegenerative disorders such as Alzheimer's disease (AD), Parkinson's disease and Huntington's disease, dementia with Lewy bodies (DLB), and familial frontotemporal dementia (FTD) share a similar fundamental protein polymerization phenomenon termed amyloid formation (Landles and Bates 2004, Selkoe 2004). A typical pattern observed in such progressive disorders is the accrual of β-pleated sheet-rich protein aggregates that pose toxicity (Perrin et al. 2009).

1.1.1. Etiology and Neuropathology

Alzheimer's disease is usually an age-related neurodegenerative disorder we believe is initiated by the accumulation of amyloid-β (Aβ) in the brain and surrounded by neuritic and glial processes, compromising memory and cognitive abilities (Selkoe and Hardy 2016, Long and Holtzman 2019). The deposition of Aβ results in the formation of intercellular senile plaques that poses profound toxic effects on the neurons and synaptic function (Bloom 2014, Li and Selkoe 2020). The presence of senile plaques is followed by the formation of neurofibrillary tangles (NFTs), which consist of intraneuronal hyperphosphorylated tau filaments (Hardy and Higgins 1992, Ittner, Chua et al. 2016) (Figure 1.1). Tau is a cytoplasmic protein that involves microtubule-binding domains and gets assembled into tubulin, thereby stabilizing, and contributing to microtubule function (Lee, Goedert, et al. 2001). The severe Alzheimer's disease brain is characterized by densely packed, highly complex, and insoluble filaments of both neuronal proteins. These two neuronal proteins have synergistic effects on each other and go together in the

advancement of AD (Jeremic, Jiménez-Díaz, et al. 2021). The event invites responses from reactive astrocytes and activated microglia to surround the plaques and causes a cascade of neuroinflammatory storms (Selkoe 2004).

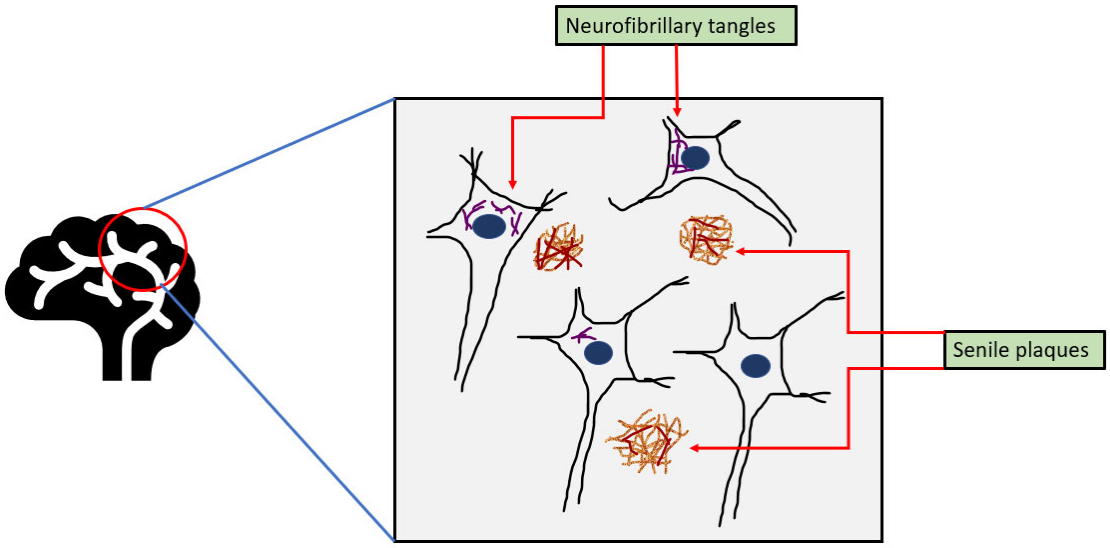

Figure 1.1. Pathological hallmarks of Alzheimer's disease. AD brain is marked by the deposition of two neuropathological hallmarks. Extracellular senile plaques composed of spherical deposits of Aβ enveloped by dystrophic neurites. Neurofibrillary tangles of abnormal tau filaments are represented as formed intracellularly. The presence and accretion of the two proteins deplete neuronal integrity (Selkoe 1998, Masters and Selkoe 2012).

1.1.2. Early-onset and late-onset AD

AD pathology initiated 20-30 years before the manifestation of clinical symptoms and the appearance of memory loss. Age is the main risk factor for AD development (Masters and Selkoe 2012, Zvěřová 2019). Genetic factors and environmental factors contribute tremendously towards developing familial or sporadic AD (Hardy 1997, Andreasen and Blennow 2002) Early-onset AD is associated with less than 1% of cases and is marked by the evolution of mutations in three genes encoding amyloid precursor protein (APP) (Selkoe 1998, Hashimoto, Ogino, et al. 2010), presenilin genes PS1 and

PS2 (Selkoe 1998, Selkoe 2011). Late-onset AD is due to several genetic and environmental factors as well as due to the gradual deposition of Aβ in the brain (Bekris, Yu et al. 2010, Selkoe and Hardy 2016). The dyshomeostasis of Aβ generation and clearance is a crucial process that determines the progression of AD. APOE allele e4 (late-onset) (Li, Kanekiyo, et al. 2012) is a genetic risk factor for AD that leads to impaired Aβ clearance and accretion of Aβ in neurons (Vandenberghe, Rinne, et al. 2016).

1.1.3. Clinical stages of AD

The brain components undergo major transformation contributing to the degeneration of neurons and synapses. There are various phases involved in this process ranging from preclinical Alzheimer's disease to the severe form of the disease (Figure 1.2). The dementia phase can be distinguished into mild, moderate, and severe AD. The biological changes in the brain initiate from the preclinical stage with no appearance of symptoms. Mild symptoms develop at the mild cognitive impairment stage (MCI) along with biomarker evidence. Mild dementia and moderate dementia stages affect patient's routine tasks, and the severe dementia stage affects almost all the mundane tasks of a patient (2022 AD facts and figures).

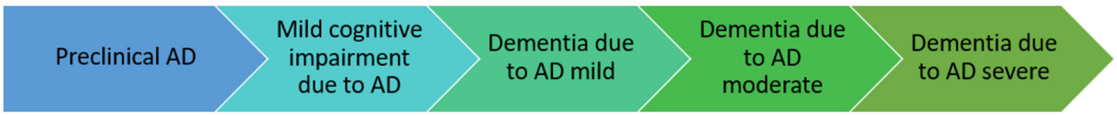

Figure 1.2. Preclinical and Clinical stages of AD. The preclinical AD stage marks the initiation of pathological hallmarks of AD with no symptoms. Mild cognitive impairment stage leads to the development of symptoms that interfere with the everyday activities of

a patient followed by later stages of dementia where the patients start to experience major symptoms of memory loss, inability to articulate thoughts, and cognitive decline (2022 AD facts and figures).

1.1.4. Overview of senile plaques

Neuritic plaques are found in the hippocampus, amygdala, and the cortices of frontal, temporal, and parietal lobes (Attems et al. 2005). In most AD cases, Aβ deposits are observed in the walls of blood vessels (cerebral amyloid angiopathy). Aβ immunocytochemistry led to the differentiation of mature plaques and diffuse plaques in the parenchyma and as vascular deposits (Iwatsubo et al. 1994). The mature plaques in the form of dense focal deposits were surrounded by dystrophic neurites and altered astrocytes. Dense plaques and blood vessel deposits contain a tightly packed spherical core of both Aβ40 and Aβ42 filaments (Jarrett et al. 1993). The diffuse plaques contain mostly loosely packed Aβ42 filaments and are granular at the microscopic level, devoid of immune cells around them (Thal et al. 2015). These are found in brain regions such as in cortex, cerebellum, striatum, and brainstem (Güntert et al. 2006).

1.2. Role of amyloid-β

1.2.1. Aβ protein generation from APP

Amyloid precursor protein (APP) is a transmembrane protein found in neurons and glial cells and is generated ubiquitously throughout our life span (Selkoe 2004, Haass et al. 2012). It gets catabolized into the Aβ peptide of 37-44 amino acids (Chen, Xu et al. 2017). The gene coding for APP lies on chromosome 21, which can be expressed as different isoforms (Folch, Ettcheto, et al. 2018). APP 695 is the one that undergoes proteolytic cleavage, facilitated by proteases α-, β- and γ-secretase by either an

amyloidogenic or non-amyloidogenic pathway (Figure 1.3). The amyloidogenic way utilizes the involvement of β- and γ-secretase enzyme that produces Aβ as the product, which self-assembles non-covalently to form amyloid fibrils (Andreasen and Blennow 2002, Ono, Condron, et al. 2009).

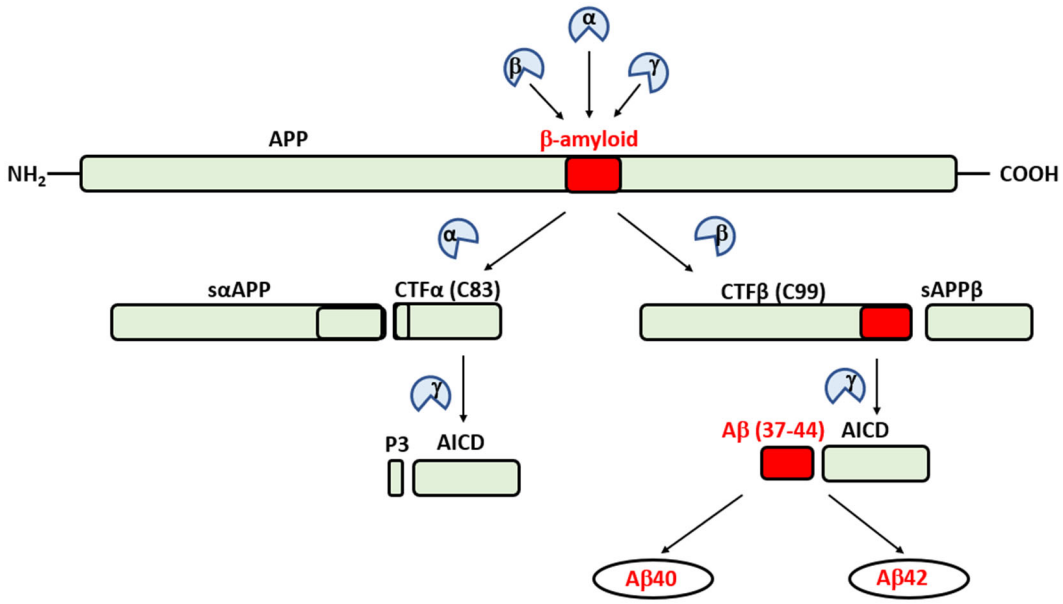

Figure 1.3. Proteolytic cleavage of the amyloid precursor protein. APP is an integral membrane protein, the cleavage of which takes place by either protease α- and β-secretase through a non-amyloidogenic pathway or by two aspartyl protease β- and γ-secretase by amyloidogenic pathway to yield Aβ 37-44 (Jeremic, Jiménez-Díaz, et al. 2021)

The non-amyloidogenic pathway is a regulatory or protective pathway that employs metalloprotease α-secretase which cleaves between residues 16 and 17 of Aβ domain. This cleavage produces the soluble sAPPα fragment in the extracellular region and a carboxy-terminal fragment called CTFα with 83 amino acid that stays attached to the membrane (Parkin, Trew, et al. 2002). The cleavage ensures that Aβ peptides cannot be formed (Figure 1.3). The CTFα fragment later gets cleaved by γ-secretase to generate a non-pathogenic hydrophobic P3 piece and APP intracellular domain (AICD). These two

pose a negative impact on memory (Nhan, Chiang, et al. 2015). However, sAPPα has been identified as being a regulatory factor for neuronal integrity, synaptic potentiation, and improved cognition (Palop, Chin, et al. 2007, Livingstone, Elder, et al. 2019). The protective pathway occurs in no raft areas of the plasma membrane (Ribarič 2018).

APP can be cleaved either directly by β- and γ-secretase or it can be re-internalized in the endosomes where these enzymes act upon it (Selkoe 2004). In both scenarios, β-secretase (BACE-1), an aspartyl protease, starts off the toxic pathway and generates soluble sAPPβ and a 99 amino acid CTFβ which is tethered to the membrane. CTFβ fragment is acted upon by γ-secretase which finally produces Aβ peptides of variable sizes (38-43 residues) and AICD fragment (Ribarič 2018, Southam, Stennard et al. 2019). γ-secretase consists of four complex transmembrane structures, the enzymatic activity being on presenilin 1 and presenilin 2 (Lemere, Lopera, et al. 1996, Bateman, Xiong et al. 2012). AICD fragment affects the mitochondria and disorganizes actin filaments (Ward, Concannon, et al. 2010, Folch, Ettcheto, et al. 2018). C99 fragment results in neuronal damage due to the expression of some genes (Bressler, Gray, et al. 1996, Kinoshita, Whelan, et al. 2002). APP can be cleaved in a cytosolic pathway by recruiting caspase which releases a C31 peptide that is detrimental to neuronal survival and synaptic functioning. Aβ is formed by further processing of γ-secretase (Nhan, Chiang et al. 2015). The toxic pathway occurs in lipid raft areas of the plasma membrane and is driven by mitochondrial disruption, polymorphism of APOE, neuroinflammation, calcium dyshomeostasis, hypoxia, and decrease in α-secretase activity (Lall, Mohammed et al. 2019). The key factors that can reduce Aβ production through the amyloidogenic pathway are the use of metal chelators, steroid hormones, and lowering of cholesterol in

the cells. Cholesterol disrupts the functioning of lipid rafts, ultimately affecting the site at which APP gets cleaved to undergo Aβ generation (Ribarič 2018).

1.2.2. Amyloid hypothesis

The amyloid cascade hypothesis states that the accretion of Aβ peptides and failure of Aβ clearance is the primary event in the AD brain which ultimately results in synaptic dysfunction, neurodegeneration, and a variety of symptoms (Hardy and Selkoe 2002, Hampel, Hardy, et al. 2021). The primary step is the conversion of Aβ monomer to the detrimental aggregates contributing to AD pathology (Karran and De Strooper 2022). The extensive research in this field using genetic evaluation, biochemical experimental evidence, and the use of various animal models that have been going on for decades, implicates the involvement of different forms of Aβ species responsible for the progression of AD (Selkoe et al. 2016; Powers et al. 2008). Aggregation of Aβ abnormally to form low molecular weight oligomers, and high molecular weight oligomers such as protofibrils and fibrils is held as a crucial process for the advancement of the disease (Figure 1.4) (Roychaudhuri, Yang, et al. 2009). The severity of the toxicity of amyloid is based strongly on the structure and aggregation state of Aβ (Ono and Tsuji 2020).

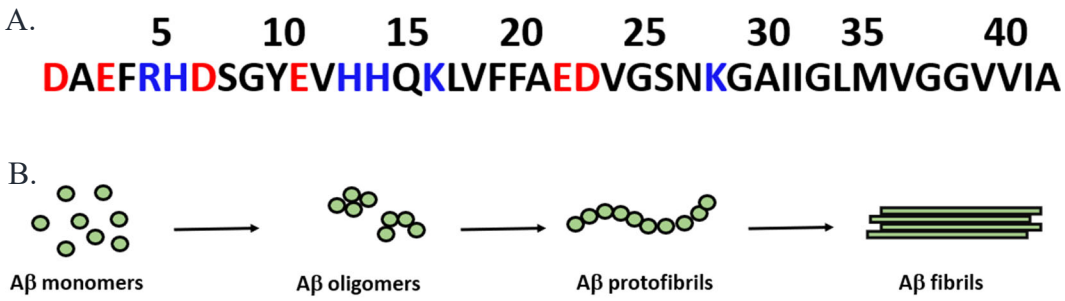

Figure 1.4. Aβ primary structure and aggregation pathway. A. The amino acid sequence of Aβ42 is shown. B. Aβ self-assembly consists of natively unstructured monomer self-associating to form a nucleus which transitions from soluble intermediate assembly termed as protofibrils and finally to generate Aβ fibrillar assembly.

1.2.3. Relevant and abundant Aβ isoforms formed

Mutations on presenilin lead to early-onset familial AD, favoring the production of Aβ40 or Aβ42 peptide, with 40 and 42 amino acids respectively. These two forms predominate in the formation when APP glycoprotein is cleaved by the enzymes (Ono and Tsuji 2020). Thus, the ratio of Aβ42/Aβ40 determines the possibility of AD onset with Aβ42 being the primary trigger (Suzuki et al. 1994, Scheuner et al. 1996, Gu and Guo 2013). Aβ40 is the predominant one whereas Aβ42 nucleates more readily (Fernandez, Klutkowski et al. 2014, Zhang, Guo et al. 2018, Wolfe 2020) and is recognized to be the most pathogenic form of Aβ (Citron et al. 1994, Attems et al. 2005, Roychaudhuri et al. 2017, Pagnon de la Vega et al. 2021). Aβ42 possesses two additional C-terminal hydrophobic residues, namely, isoleucine and alanine, inherently making Aβ42 more prone to form higher-order assemblies (Jarrett, Berger et al. 1993, Hardy and Selkoe 2002, Wälti, Ravotti, et al. 2016). The Aβ peptide oligomerizes into distinct soluble conformations before polymerization into mature amyloid fibrils aggregating into spherical plaques (Selkoe 2004).

1.2.4. Aβ detection in AD brain

The increased amount of Aβ42 deposition vs Aβ40 has been observed in AD patients (Hardy 1997). A critical AD biomarker is reduced occurrence of Aβ42 in cerebral spinal fluid (Motter, Vigo-Pelfrey et al. 1995, Mehta, Pirttilä et al. 2000, Andreasen and Blennow 2002, Hölttä, Hansson et al. 2013), while Aβ40 levels remain constant, resulting in higher Aβ40/ Aβ42 ratio. Aβ42 clearance is regulated by microglia under normal conditions (Chung, Brazil et al. 1999, Mandrekar, Jiang et al. 2009, Ries and Sastre 2016). In AD, dysregulation, and elevation of Aβ levels result in deposition of insoluble aggregates in the brain components. (Heneka, Carson et al. 2015, Heneka, Golenbock et al. 2015). Positive positron emission tomography (PET) scans, cerebrospinal fluid testing for Aβ, and brain atrophy are imperative biomarkers to diagnose the presence of AD (Selkoe and Hardy 2016, van Dyck et al. 2022)

1.2.5. Molecular basis of Aβ protein aggregation

The unstructured Aβ monomer is well known to self-assemble by non-covalent interactions (Jarrett, 1993) by nucleation-dependent polymerization pathway into a polydisperse mixture with variety of aggregated structures mostly composed of β-sheet rich conformations. (Walsh, Hartley et al. 1999, Kirkitadze, Condron et al. 2001). Polymerization advancement takes place through stages of lag phase, growth phase and saturation phase (Figure 1.5) (Huang and Liu 2020). The lag phase refers to the time required to form a ‘nucleus’ which is a state that overcomes energy barrier and drives the kinetics of the amyloid pathway. This step is usually slow and reversible (Kodali and Wetzel 2007). The aggregation of monomers into low-molecular-weight oligomers takes place in this step. Growth phase marks the formation of more organized soluble structures

which have multiple conformations and consist of cross beta structure such as protofibrils (Jarrett and Lansbury 1993). Concentration of the protein, pH, temperature, ionic strength are the factors responsible for formation of conformationally-distinct aberrant structures. The saturation phase is where the beta-structured oligomers amass into disease-causing insoluble extracellular Aβ fiber. (Iannuzzi, Irace et al. 2015).

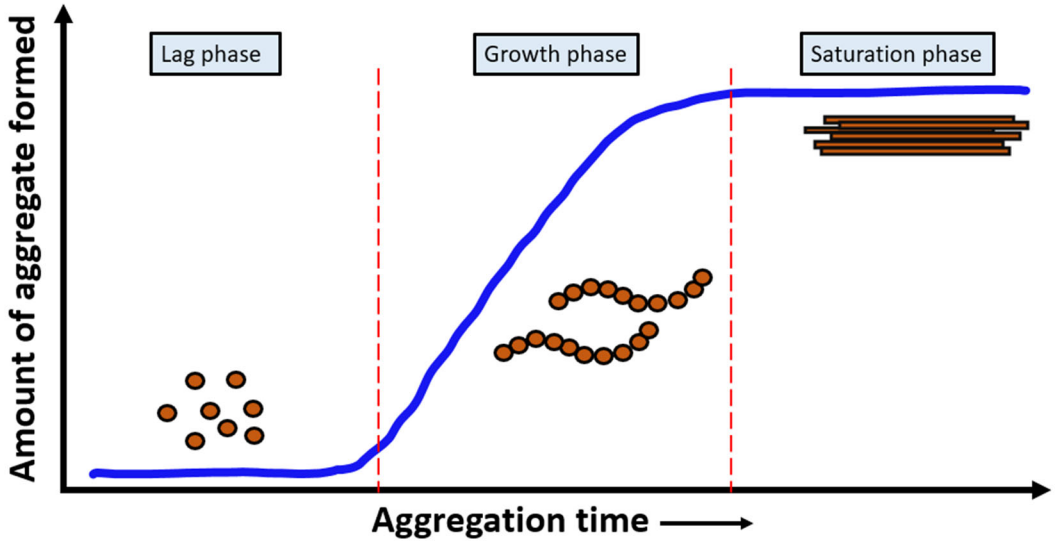

Figure 1.5. Nucleation-dependent polymerization of aggregation process. The sequence of events along the aggregation pathway are lag phase (misfolded monomer aggregation initiation), growth phase (formation of organized conformation-based oligomeric structures), and the saturation phase (association of protofibrils into structured fibrils).

1.3. Role of conformationally varied oligomeric Aβ species

McLean et al. performed western blot analysis on Alzheimer's patient's frontal cortex to measure soluble and insoluble Aβ fractions. Aggregated assemblies of were detected in AD patients as compared to control patients (McLean et al. 1999). Several such evidence led to extensive research to find right Aβ targets (Ono, Hasegawa et al. 2002, He, Luo et al. 2010, Youmans, Tai et al. 2012).

1.3.1. Resolving Aβ structural conformations

Aβ fibril structure is highly ordered with the diameter ranging from 7-10 nm and contains a high β-sheet content. Aromatic amino acid residues in the core region of β-sheet help stabilize the β-segments which are oriented perpendicular to the fibril axis. Mutations in Aβ residues to aromatic residue substitution favor amyloid fibril formation. (Bitan, Kirkitadze et al. 2003, Kayed, Head et al. 2003).

Several attempts to characterize Aβ42 fibril structure formed in vitro and one that formed in Alzheimer's patient brain have been made. It is critical to study the filaments from Aβ42 because it plays a central role in AD pathology. The structure resolved of Aβ42 fibrils by cryo-EM indicates the presence the S-shaped protofilament folds that is observed in two different the kinds of filaments examined (Yang, Arseni et al. 2022).

1.3.2. Premise behind oligomeric Aβ species

The link between Aβ plaques and cognitive decline has not been well established. The intermediate soluble Aβ oligomers being reported as neurotoxic and neuroinflammatory appears to be a plausible theory of explaining the non-correlation (Haass and Selkoe 2007, Ribarič 2018). Aβ oligomers are somewhat globular in shape (3-10 nm) called as Aβ-derived diffusible ligands (ADDLs) and they are composed mostly of Aβ40 and Aβ42 (Klein 2002, Baldassarre, Baronio et al. 2017). These have been biggest contributors of loss of alertness and memory (Kelly, He et al. 2017). The appearance of soluble oligomeric Aβ species results in oxidative stress, cell membrane disruption, ion channel formation and apoptosis of cells (Carrillo-Mora, Luna et al. 2014). Protofilaments (Serpell, Sunde et al. 2000). The conformational elements of small

oligomeric and prefibrillar species determine the pathogenicity of these misfolded, aggregated structures.

1.3.3. Protofibrils: Morphology and physical properties

Aβ protofibrils were discovered using size exclusion chromatography system represented by a large (>100 kDa, 200 nm length, 5 nm diameter) peak before Aβ42 monomers (Walsh, Lomakin et al. 1997). They are high-molecular weight, soluble intermediate aggregates with quite stable and developed structure found in the brain senile plaques (Coalier et al. 2013, Chen et al. 2017). Aβ42 protofibrils represent a polydisperse population of non-spherical, small curvilinear structures and remain soluble while centrifugation at 16,000-18,000 g (Kodali and Wetzel 2007). The hydrodynamic (R_H) radii range between 10 to 30 nm (Walsh, Lomakin et al. 1997, Harper, Wong et al. 1999, Nichols, Colvin et al. 2015). It can be viewed using electron microscopy (EM), consisting mostly of β-sheet secondary structure and partially random coils and α-helix (Walsh, Hartley et al. 1999).

SEC-purified Aβ42 protofibrils lie in the molecular weight range of 200-2000 kDa (Nichols, Colvin et al. 2015). Aβ42 protofibrils are much more stable than Aβ40 protofibrils (Coalier, Paranjape et al. 2013). These aberrant assemblies predominate when started with equal mixtures of Aβ40 and Aβ42 (Terrill-Usery, Colvin et al. 2016). Aβ42 protofibrils imaged by TEM displayed size of 50-100 nm in length whereas Aβ42 fibril in aCSF were determined to be >1 μM in length (Figure 1.6) (Paranjape, Terrill et al. 2013).

A. B.

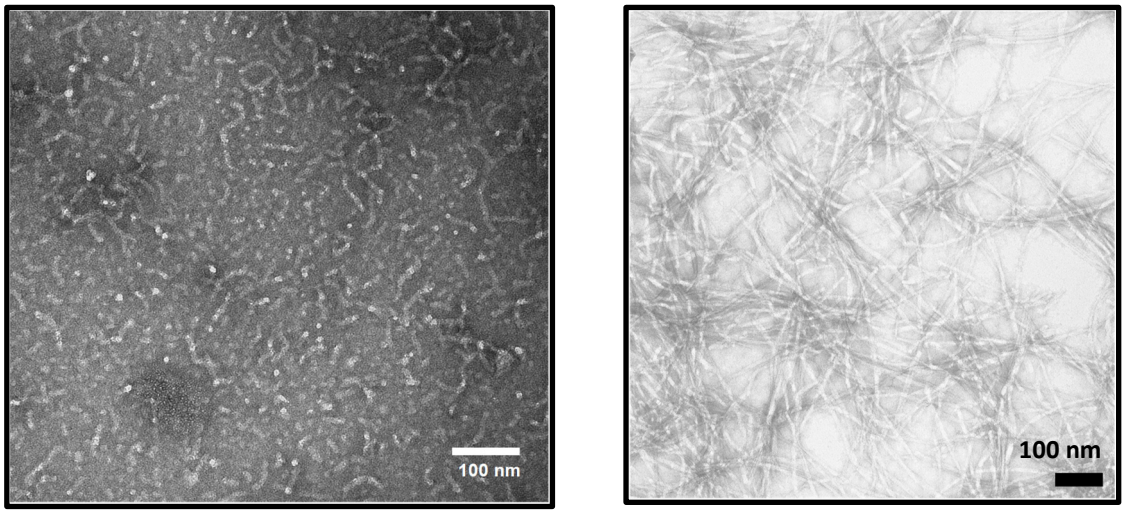

Figure 1.6. Imaging Aβ protofibril and fibril structure by electron microscopy. A. Protofibrils (52 μL) was applied to a copper formwar grid and imaged by transmission electron microscopy (TEM). The scale bar represents 100 nm. B. SEC-purified aged Aβ42 monomer (58 μM) solution was prepared in aCSF buffer. The fibrils formed when the monomer solution was agitated for 72 h at 25°C. The solution was centrifuged, supernatant removed, and pellet was reconstituted in a fresh aCSF buffer. TEM image obtained of the fibril pellet. The scale bar represents 100 nm (Paranjape, Terrill et al. 2013)

The diameter of protofibril is smaller as compared to the fibrils. Most groups have shown that the transition from protofibril to fibril is very slow and can take place without any observed changes in the diameter because of end-to-end attachments of monomers on protofibril ends (Harper et al. 1997, Harper et al. 1999). The conversion of protofibrils to fibril can also occur by lateral association (Nichols, Moss et al. 2002).

It has been observed that the Arctic mutation in APP results in high chances of the production of a species that forms protofibrils easily (Nilsberth, Westlind-Danielsson et al. 2001).

1.3.4. Significance of soluble Aβ protofibril species studies

Aβ protofibrils are treated as a precursor to fibrils and they have been known to behave as a seed for the aggregation process (Harper, Lieber et al. 1997). Iwatsubo's

group observed the deposition of Aβ in the brain when Aβ42 protofibrils were introduced into the brains of A7 mice overexpressing human APP and with the corresponding mutations (Hori, Hashimoto et al. 2015). Some research groups have clearly demonstrated Aβ protofibrils to be the causative agent for neuronal injury (Pike, Walencewicz et al. 1991, Busciglio, Lorenzo et al. 1992).

Protofibrils portray toxicity to neurons (Walsh, Hartley et al. 1999), disrupting the calcium ion-channels (Ye, Selkoe et al. 2003), inhibit hippocampus functioning (O'Nuallain, Freir et al. 2010). Over the years, it has been established that Aβ protofibrils have unique structural aspects that encourage stimulation of immune cells. Aβ protofibrils incite the release of proinflammatory cytokine such as tumor necrosis factor α because of microglial cells interaction and stimulation (Paranjape, Terrill et al. 2013, Gouwens, Makoni et al. 2016) much more robustly through Toll-like receptors and NLRP3 inflammasome (Udan, Ajit et al. 2008, Ajit, Udan et al. 2009, Paranjape, Gouwens et al. 2012) (Figure 1.7). It has been shown that micro vesicles trafficked from primary microglia binds to Aβ42 protofibrils at a greater affinity to Aβ42 monomers (Gouwens, Ismail et al. 2018). Aβ42 protofibrils have been indicated to generate pro and mature forms of intracellular interleukin-1β (IL-1β) protein through multiple pathways such as activation of Nod-like receptor (NLRP3) inflammasome or TLR/myeloid differentiation protein (MyD88) mediated priming (Terrill-Usery, Mohan et al. 2014).

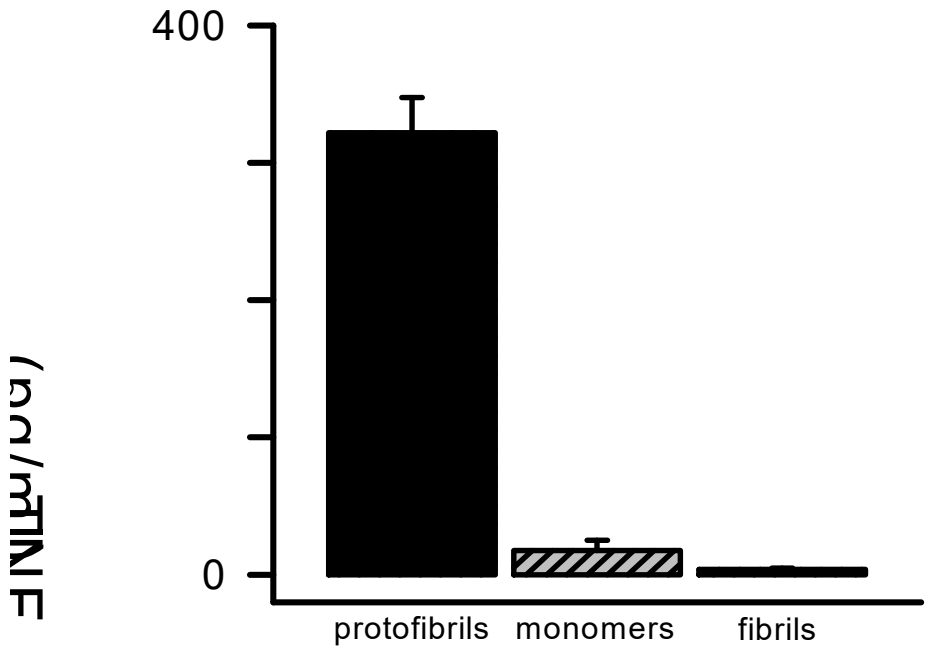

Figure 1.7. Aβ42 protofibrils stimulate the release of TNFα. Solutions of Aβ42 protofibrils, monomers and fibrils with final concentration of 15 μM were incubated with primary murine microglia cells for 6 h. Condition medium was tested for TNFα secretion by ELISA. Error bars represent the average ± std error of n=6 (Paranjape, Gouwens et al. 2012)

The protofibrils cause disruption of cellular homeostasis, loss of membrane integrity and fluidity, oxidative stress, calcium dysregulation, lipid peroxidation, inflammation, and synaptic toxicity (Ono and Tsuji 2020). High-molecular weight Aβ42, corresponding to Aβ42 protofibrils, displayed higher cytotoxicity and neurotoxicity in SH-SY5Y neuroblastoma than low-molecular weight Aβ42, representing small oligomers (Yasumoto, Takamura et al. 2019) (Figure 1.8). Aβ protofibrils affect neuronal membrane fluidity and directly causes mitochondrial respiratory chain impairment (Pohanka 2014).

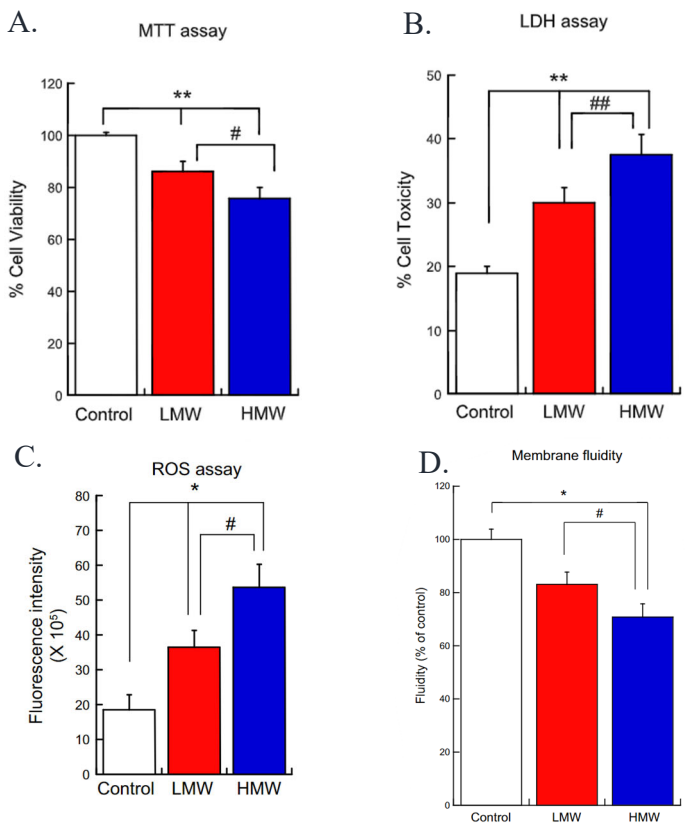

Figure 1.8. High-molecular weight Aβ42, represented as Aβ42 protofibrils pose cytotoxic effects. A. High-molecular weight Aβ42 are more toxic to the cells when examined by MTT assay. B. High-molecular weight Aβ42 are more cytotoxic than low-molecular weight Aβ42 when evaluated through LDH assay. B. High-molecular weight Aβ42. C. High-molecular weight Aβ42 induces more severe oxidative stress than low-molecular weight Aβ42 in SH-SY5Y cells. D. High-molecular weight Aβ42 affects fluidity of cell membrane to a greater extent than low-molecular weight Aβ42. (Yasumoto, Takamura et al. 2019)

1.4. Anti-amyloid-β immunotherapy

1.4.1. Adaptive immune system overview

Antibodies or immunoglobulins are proteins that are synthesized by B-cell lymphocytes. They are a part of the adaptive immune system. Immunoglobulins possess a variable region that confers the specificity of the antibodies (Neuberger et al. 2008). Constant domains help in purification using protein A/G. The region of the antigen that interacts with the antibody is called the epitope. Antibodies can be raised against any

protein, proteins with post-translational modifications, for other antibodies such as secondary antibodies. Immunization elicits an antigen-specific immune response. B-cells are activated in response to an antigen to produce and secrete their antibodies. Antigens are multivalent and can have many epitopes. Epitopes are regions on the antigen which can elicit an immune response. The serum contains antibodies produced from many clones of B-cells and these antibodies are polyclonal. Polyclonal antibodies can have desirable, broad specificities and have multiple epitopes. Monoclonal antibodies, on the other hand, arise from a single clone of cells (Saper et al. 2009). Monoclonal antibody generation is preferred because it ensures efficient, directed creation of desired specificity, large-scale production, reproducible behavior, scalable manufacturing, minimal animal usage, can be engineered for suitable needs (Bradbury, Trinklein et al. 2018).

B-cells, antibody producing cells, are difficult to culture and are short-lived in vitro. When they are fused in myeloma cell line forms an immortal hybridoma with both the chromosomes in one cell. This is called hybridoma technology. Recombinant antibody technology results in isolation of DNA sequences responsible for encoding HC and LC, which is then transfected in a heterologous host cell line. This is referred to as recombinant antibody technology. Antigen-specific B-cells are sorted into 96 well plate, cloned and express, culture, purification (Bradbury, Trinklein et al. 2018).

1.4.2. Relevance of antibodies in AD research

Antibodies are critical tools to infer details about all the different aspects of AD including research, diagnostic and therapy. Many antibodies were significantly involved in the detection of pathological hallmarks in AD brain (Wong, Quaranta et al. 1985).

Moreover, antibodies have allowed quantitative measurements of Aβ level in human fluids (Seubert, Vigo-Pelfrey et al. 1992). Interestingly, development of C-terminal selective antibody helped resolve the difference in the primary structure of Aβ40 and Aβ42 (Gravina, 1995).

1.4.3. Conformational-selective antibodies as therapeutics

Antibodies usually provide the clue for the existence of conformationally-diverse species in AD tissue samples from humans and mouse models (Georganopoulou et al. 2005). The development of conformational-selective antibodies has been instrumental in probing Aβ protofibrils and fibrils species in cell, animal models, and human fluids and tissues (Kayed et al. 2007, Deshpande et al. 2009, Koffie et al. 2009). There have been several pitfalls for the success of these antibodies. Nevertheless, these antibodies are successful in effective therapeutic targeting and have potential in AD therapeutics.

There has been an administration of anti-Aβ monoclinic antibodies (mAbs) as passive immunization agents for AD (Van Dyck et al. 2018). The murine form, 3D6, of Bapineuzumab (humanized IgG1 anti-Aβ mAb) was observed to be bound to the residues at N-terminal to phagocytose the fibrillar and soluble forms of Aβ in PDAPP transgenic mice brain (Bard et al. 2000). The murine precursor m266 of Solanezumab, an IgG1 mAb, has an affinity towards the middle residues 16-26 and cleared Aβ monomer in transgenic mice (DeMattos et al. 2001). Gantenerumab is the first fully human IgG anti-Aβ mAb. The epitope of this antibody includes a few residues from N-terminal and some from the central region. It made a significant contribution in reducing the Aβ plaque formation in PS2APP transgenic mice by employing microglia (Bohrmann et al. 2012).

Crenezumab binds to the mid-domain of Aβ peptide and has an affinity towards multiple conformations. It was engineered on an IgG4 backbone (Adolfsson et al. 2012).

Lecanemab (BAN2401), a humanized IgG1 conformational-selective monoclonal antibody and its murine version mAb158, binds with high selectivity to soluble Aβ protofibrils compared to monomeric Aβ and with moderate selectivity for fibrils (Lannfelt, Möller et al. 2014, Logovinsky, Satlin et al. 2016). Several research studies showed that BAN2401 diminished Aβ protofibril levels in brain tissues and CSF of AD transgenic mouse model and enhanced neuronal functioning (Englund, Sehlin et al. 2007, Söllvander, Nikitidou et al. 2018). The antibody was in its 4-year Phase 3 clinical trial earlier this year (Kwon, Iba et al. 2020) and the results displayed a reduction in cognitive decline but were associated with adverse events. Longer trials are needed to ensure safety and efficacy of the antibody candidate (van Dyck et al. 2022). Lecanemab has been making the way towards neuroimaging as in vivo positron emission tomography (PET) agents in the central nervous system. Radiolabeled single-chain variable fragment (scFv) region of Aβ selective antibody, mAb 158, was engineered with Fab fragment of TfR antibody recombinantly in the form a Tribody^{TM} structure to assist in interaction with transferrin receptor to cross the blood-brain barrier (BBB) (Syvänen, Fang et al. 2017).

Aducanumab is the first potential anti-amyloid treatment approved by US regulators for mild AD patients to tackle the underlying cause of AD. Biogen's aducanumab portrays selectivity towards soluble Aβ and insoluble Aβ and has been granted accelerated approval to pace down cognitive decline in AD patients when given at higher doses (Sevigny, Chiao et al. 2016).

Table 1.1 Conformational-selective antibodies known in AD research.

Drug	Company	Mechanism or specificity	Comment	Reference
Bapineuzumab, humanized monoclonal antibody, binds to N-terminal region of Aβ	Janssen/Pfizer	Binding towards oligomeric Aβ, slightly lower affinity towards monomer	No cognitive benefits, high ARIA, Phase III, discontinued	(Salloway, Sperling et al. 2009, Black, Sperling et al. 2010, Rinne, Brooks et al. 2010, Blennow, Zetterberg et al. 2012, Salloway, Sperling et al. 2014, Hu, Adedokun et al. 2015, Lacey, Bobula et al. 2015, Liu, Schmidt et al. 2015, Arrighi, Barakos et al. 2016, Ivanoiu, Pariente et al. 2016, Vandenberghe, Rinne et al. 2016, Ketter, Brashear et al. 2017, Suzuki, Iwata et al. 2017, Brashear, Ketter et al. 2018, Cehlar, Skrabana et al. 2018, Kwan, Konno et al. 2020)
Solanezumab, humanized monoclonal antibody IgG1, binds to central region of Aβ	Eli Lilly	Stabilize monomer Aβ and prevents formation of soluble Aβ, Does not target fibril	No cognitive benefits, low ARIA, Phase III	(Doody, Thomas et al. 2014, Suzuki, Iwata et al. 2017, Folch, Ettcheto et al. 2018, Honig, Vellas et al. 2018, Schwarz, Sundell et al. 2019, Se Thoe, Fauzi et al. 2021)
Crenezumab, MABT5102A or MABT, IgG4, mid-region of Aβ	Hoffmann-La Roche	Similar affinity with monomers, oligomers, fibrils, plaques	No cognitive decline, Phase III	(Goure, Krafft et al. 2014, Ramirez Aguilar, Acosta-Uribe et al. 2019, Kwan, Konno et al. 2020, Yoshida, Moein et al. 2020)
Gantenerumab, humanized IgG1, recognizes C-terminal and central region	Hoffmann-La Roche	Towards Aβ oligomers and fibrils, prevents fibril elongation	II and III	(Ostrowitzki, Deptula et al. 2012, Panza, Solfrizzi et al. 2014, Ostrowitzki, Lasser et al. 2017, Suzuki, Iwata et al. 2017, Panza, Seripa et al. 2018, Klein, Delmar et al. 2019, Kwan, Konno et al. 2020, Portron, Jordan et al. 2020)
Ponezumab, humanized IgG2 antibody, C-terminal region of Aβ40	Pfizer	Aβ1-40 oligomers and fibrils, not to monomers	II, discontinued	(Burstein, Zhao et al. 2013, Landen, Zhao et al. 2013, Miyoshi, Fujimoto et al. 2013, Goure, Krafft et al. 2014, Landen, Andreasen et al. 2017, Landen, Cohen et al. 2017, Kwan, Konno et al. 2020)
Lecanemab, BAN 2401, mAb158	Biogen/Eisai	Binds selectively to soluble Aβ protofibril, binds to fibrils as well	III, positive results, less ARIA observed, slows progression, improves cognition	(Logovinsky, Satlin et al. 2016, Satlin, Wang et al. 2016, Panza, Lozupone et al. 2019, Swanson, Zhang et al. 2021)
Aducanumab,	Biogen Neurimmune	Specificity towards aggregated Aβ	IV, Accelerated approval	(Ferrero, Williams et al. 2016, Sevigny, Chiao et al. 2016, Chiao, Bedell et al. 2019)

CHAPTER 2: METHODS

2.1. Size-exclusion chromatography (SEC) of Aβ42

Synthetic Aβ42 peptide was purchased from ERI Amyloid Laboratories, formerly called W. M. Keck Biotechnology Resource Laboratory (CT). Aβ was dissolved in 100% hexafluoro isopropanol (HFIP, Sigma-Aldrich, Saint Louis, MO) to obtain a 1 mM Aβ solution. Aliquots of the solution were prepared in sterile microcentrifuge tubes and were left uncovered at room temperature overnight in a fume hood for HFIP to entirely evaporate. Aliquots were vacuum-centrifuged the following day to obtain a thin-filmed tube with Aβ and stored in a desiccant at -20°C (Paranjape et al. 2012).

2.1.1. Aβ42 protofibril purification prep by SEC

An aliquot of lyophilized Aβ (0.9 mg) is pulled out from -20°C and was reconstituted in 100 µl of 50 mM NaOH solution and pipette mixed well. The solution was then treated with 900 µl of prefiltered (0.22 µm) artificial cerebrospinal fluid buffer (1mM Na_2PO_4, 130mM NaCl, 15mM $NaHCO_3$, 3mM KCl pH 7.8) or TRIS buffer pH 8. The mixture was incubated at room temperature for 20 minutes and was centrifuged at 17,000 g for 10 min to prevent insoluble fibrils from loading onto the column. The prepared Aβ42 was fractionated on a 25 ml Superdex 75 HR 10/30 column (GE Healthcare) with a fractionation range of 3-70 kDa using an AKTA fast protein liquid chromatography system (GE Healthcare) as previously described (Terrill-Usery, Colvin, et al. 2016). The column was washed with milliQ water and later with the appropriate buffer being used for 1 column volume. 1 ml of bovine serum albumin (2.5 mg/ml) was injected through the column to avoid any non-specific binding of Aβ prior to Aβ fraction isolation. Aβ sample was loaded onto the column using a 1 ml sample loop and Aβ42

protofibrils and monomers were eluted at 0.5 mL min^{-1} flowrate and 0.5 mL fractions were collected using a fraction collector into sterile, labeled, low-retention microcentrifuge tubes and immediately placed on ice. The delay volume between the UV detector and the fractions collected was monitored with BSA elution. Aβ42 concentrations were determined by in-line UV absorbance trace (Unicorn software 5.01) using an extinction coefficient of 1450 cm^{-1} M^{-1} at 280 nm. The purification typically yielded Aβ42 protofibrils and Aβ42 monomers is shown. The various preps of Aβ42 were purified using Superdex 75 which displayed essentially two peaks each time. Table 2.1 provides intricate details about the prep number, date, time of incubation after the reconstitution process with NaOH, fraction number, concentration, percentage yield of total Aβ42, and monomer specifically. (Table 2.1)

Table 2.1. Illustrates the concentration obtained and % yield of various preps where Aβ42 protofibril (PF) and monomer (M) have been isolated by SEC using Superdex 75 column. Reconstitution was carried out in NaOH with aCSF (pH 7.8)/tris (pH 8)/PBS (pH 7.4)/buffer.

Prep #	Date	Time of reconstitution (min)	Buffer	Aβ42	Fract. of highest conc.	Highest concentration (µM)	Total recovery (%)	Monomer recovery (%)
561	9/26/19	30	aCSF	PF	14,15	18	53	35
561	9/26/19	30	aCSF	M	29,30	33	53	35
585	09/22/20	30	aCSF	PF	13,14, 15	26	52	25
585	9/22/20	30	aCSF	M	29,30	24	52	25
586	10/1/20	30	aCSF	PF	13,14	36	50	19
586	10/1/20	30	aCSF	M	13,14	19	50	19
590	12/9/20	25	aCSF	PF	13,15	32	52	13
595	2/2/21	0	aCSF	PF	13,15	17	48	27
595	2/2/21	0	aCSF	M	29,31	17	48	27
597	3/15/21	0	PBS	PF	13,15	19	54	25
597	3/15/21	0	PBS	M	29,31	17	54	25
605	6/22/21	0	PBS	PF	14,15	33	54	25
605	6/22/21	0	PBS	M	30,31	20	a54	25
610	11/19/21	20	aCSF	PF	14,15	28	50	26
610	11/19/21	20	aCSF	M	30,31	23	50	26
617	2/20/22	10	TRIS	PF	14,15	27	54	32

617	2/20/22	10	TRIS	M	28,29	30	54	32
621	5/13/22	10	TRIS	PF	14,15	32	64	37
621	5/13/22	10	TRIS	M	28,29	37	64	37
622	6/21/22	20	aCSF	PF	14,15	30	46	21
622	6/21/22	20	aCSF	M	30,31	19	46	21
624	7/11/22	20	aCSF	PF	14,15	28	46	20
624	7/11/22	20	aCSF	M	30,31	20	46	20

2.1.2. Aβ42 monomer purification by SEC

Superdex 200 column has a better separation resolution (GE Healthcare) with a fractionation range of 10-600 kDa and was used on the AKTA FPLC system for chromatographic isolation of Aβ monomer. The separation range of the column is determined by the size of the beads used to pack the column. The dry Aβ aliquot (0.9 mg) was reconstituted in a solution containing 10 mM NH_4OH and 6 M guanidinium hydrochloride (GuHCl) and then incubated for 20 minutes at room temperature. The tube was spun at room temperature at 17,000 g for 10 min and was injected into the column. Aβ monomer and oligomeric fractions are obtained in the same way as described in the previous section.

The concentration obtained from the in-line UV absorbance curve was 94 μM (fraction 33) as mentioned in the first entry of Table 3.2. For most of the Aβ42 purification preps, aCSF pH 7.8 buffer was used for the reconstitution of dried Aβ42. Maximum recovery of total Aβ42 and the highest concentration of monomer was observed on 20 min incubation (Table 2.2).

Table 2.2. Illustrates the concentration obtained and % yield of various preps where Aβ42 monomer has been isolated by SEC using Superdex 200 column. Reconstitution was carried out in GuHCl, NH_4OH aCSF (pH 7.8)/tris (pH 8)/PBS (pH 7.4)/buffer.

Prep #	Date	Time of reconstitution (min)	Buffer	Fract. of highest conc.	Highest concentration (μM)	Total recovery (%)	Monomer recovery (%)
560	8/26/19	-	aCSF	33	94	48	20
563	10/9/19		aCSF	33,34	42	36	30
564	10/13/19		aCSF	32,33	37	27	24
565	10/15/19		aCSF	33	86	68	46
567	10/30/19		aCSF	32,33	55	43	33
583	9/1/20	5	aCSF	32,33	63	53	39
584	9/21/20	20	aCSF	33,34	63	55	37
586	11/8/20	20	aCSF	31,32	59	55	37
589	11/21/20	20	aCSF	33,34	53	59	38
591	12/10/20	20	aCSF	33,34	46	82	41
592	12/18/20	25	aCSF	33,34	56	89	49
594	1/20/21	20	aCSF	33,34	56	94	52
596	2/23/21	20	aCSF	33,34	57	72	43
599	3/27/21	20	aCSF	33,34	49	70	40
606	7/12/21	30	aCSF	33,34	57	55	32
607	8/30/21	20	aCSF	33,34	51	63	34
611	12/6/21	20	aCSF	33,34	47	60	28
613	12/21/21	60	TRIS	31,32	39	60	9

2.2. Aβ42 fibril preparation

Aβ42 fibrils were prepared from aged SEC-purified Aβ42 monomers (usually older than 3-4 months) stored in low-retention (siliconized) tubes at 4°C. Fibril formation in the Aβ42 monomer sample was confirmed by thioflavin T fluorescence using the Cary Eclipse fluorescence spectrophotometer. The sample proceeded to further steps if it displayed a high fluorescent signal as compared to the ThT control sample. The solution was spun by centrifugation at 17,000*g* for 10 min, the supernatant was removed, and the insoluble pellet was reconstituted in the same volume of freshly prepared aCSF or TRIS buffer. Thioflavin T fluorescence was measured again for the reconstituted pellets and the supernatant was removed to ensure that the fibrils did not get transferred into the supernatant.

2.3. Immunization of rabbits and cloning of monoclonal antibodies

2.3.1. Immunization of rabbits

SEC-purified Aβ42 protofibrils were shipped overnight on ice to Pacific Immunology (Ramona, CA). Two New Zealand White rabbits (PAC-12155 and PAC-12156) were immunized with 0.1 mg Aβ42 protofibrils in Complete Freund's Adjuvant. Two additional immunizations were administered at 25 and 46 days with 0.1 mg Aβ42 protofibrils in Incomplete Freund's Adjuvant. At 53 days, serum from an initial bleed of each rabbit was shipped overnight for testing at the University of Missouri-St. Louis. At 58 days, following confirmation that the serum was selective for Aβ42 protofibrils, a lethal intravenous injection of Euthasol solution was administered to each rabbit at a manufacturer- and veterinary-recommended dosage of 1 mL per 10 lbs of body weight. Euthanasia by intravenous injection of an overdose of pentobarbital sodium in combination with phenytoin sodium is consistent with the recommendations of the Panel on Euthanasia of the American Veterinary Medical Association. The spleens and bone marrow were harvested and sent to ExonBio for monoclonal antibody development.

2.3.2. Biotinylation of Aβ protofibrils

Aβ42 protofibrils were biotinylated using amine-based conjugation per vendor protocols (ThermoFisher Scientific). Aβ42 protofibrils (1 ml, 0.27 mg/ml) in aCSF pH 7.8 were mixed with N-hydroxysuccinimide (NHS)-polyethylene glycol (PEG)4-biotin ester at a 20-fold molar excess of biotin relative to Aβ and incubated for 30 min with orbital mixing at 25 °C. The labeling mixture was separated chromatographically on Superdex 75. Aβ42 protofibril fractions eluting in the void volume were collected, and concentrations were determined by in-line UV absorbance, pooled, and tested for biotin

incorporation using a modified indirect ELISA. The indirect ELISA was conducted in a similar manner to that described above with purified protofibril labeling product pool and unlabeled protofibrils coated on plates followed directly by the addition of streptavidin-HRP and completion of the ELISA. Following characterization of the biotinylated Aβ42 protofibrils, 1 ml of the product (22 μM, 0.1 mg/ml) was shipped overnight on ice to ExonBio.

2.3.3. Circular dichroism

Aβ42 protofibril samples were analyzed as previously described (Dhami, et al. 2022) without modification using a Jasco J-1500 circular dichroism spectrometer measurements. Wavelength scan spectra represent the average of 20 accumulations for each Aβ sample. Buffer control spectra were averaged and subtracted from Aβ sample spectra. Each data point ($[\theta]_{obs}$, deg) was converted to mean residue ellipticity ([θ], deg cm2 dmol-1) using a molecular weight of 4514 g/mol for Aβ42 divided by 42 residues.

2.3.4. Isolation of splenetic B-cells

Spleens from PAC-12155 and PAC-12156 rabbits were harvested 7 days after the final boost and transported from Pacific Immunology to ExonBio. Spleen lymphocytes were prepared on a Ficoll-Paque PLUS gradient by centrifugation at 1200g for 30 min and collected at the interface. Individual antigen-specific plasma cells were selected from the isolated splenocytes by Single Plasma Cell Interrogation (SPIN®) microfluidic technology utilizing biotinylated Aβ42 protofibrils as a probe. Heavy chain (HC) and light chain (LC) variable region mRNA was obtained from lysates of SPIN®-isolated individual B-cells, reverse-transcribed to DNA, PCR-amplified, and cloned into pRab293 HC and LC vectors. Cloning of plasmids monoclonal antibodies mAbSL 113 and 108

was performed at ExonBio, while others were cloned at University of Missouri-St. Louis uses similar methods.

2.3.5. Agar plate preparation

In the cell-culture hood, 7.5 g of solid agar was added to 500 ml of LB broth in a 500 ml conical flask under sterile conditions. The flask for covered with aluminum foil and autoclaved for 30 minutes. The flask was cooled to ~60°C and ampicillin (100 ug/ml) was added to the media and swirled well. The protocol calls for 20 agar plates. The media was poured ~20 ml or up to half the height of the 100 mm petri dish. The petri dish was capped and sealed. It was allowed to solidify at room temperature, and it took approximately 30 min. The plate was stored at 4°C in a sealed plastic bag for future use.

2.3.6. Formulation of LB broth

10 g of Tryptone, 5 g of Yeast extract, and 10 g of NaCl were mixed in a 1L sterile Erlenmeyer flask with 950 ml of milliQ water. The homogenized mixture was adjusted to the pH of 7.5 and the volume was brought to 1L. The homogenized solution was autoclaved. Usually, LB broth (Fisher Sci) was bought commercially for experiments. It was prepared in the lab while troubleshooting site-directed mutagenesis experiments.

2.3.7. Preparation of competent DH5α E. coli cells

A tube of 50 µl DH5α stock cells was thawed from a -80°C freezer and the cells were inoculated on the pre-warmed LB agar plate (without ampicillin) using the four-quadrant streak method on the first day. The agar plate was sealed and incubated in a 37°C incubator for 24 hours. A single colony of DH5α *E. coli* cells was transferred with an inoculation loop into a separate tube containing 10 ml LB media. The tube was kept

shaking at 225 rpm for 24 hours in a 37°C incubator on the second day. On the third day, 1 ml of the 10 ml overnight culture was put into a 100 ml fresh LB broth and kept for shaking in an incubator at 37°C for 3 hrs. It was transferred to two 50 ml conical tubes. In a separate beaker, 30 ml of 0.1 M $CaCl_2$ was prepared. 2 ml of 0.1 M $CaCl_2$ was mixed with 0.5 ml of 100% glycerol (final concentration 15-20%). The solution was filtered through a 0.2 μm syringe filter and was chilled on ice. 50 ml tubes were spun at 4,000 g for 10 mins and supernatants were discarded. The pellet was resuspended in 20 ml of 0.1 M $CaCl_2$ and transferred to the next conical tube to resuspend the second pellet. The cells were incubated on ice for 30 min and spun again at 4,000g at 4°C for 10 minutes with the supernatant discarded. The pellet was then resuspended in 2.5 ml of a prechilled solution of $CaCl_2$ and glycerol. 50 μl of the cell solution was aliquoted to sterile Eppendorf tubes and the aliquots were flash-frozen in liquid nitrogen. The bacterial cells were stored in an -80°C freezer and were later used for transformation whenever needed.

2.3.8. Cloning of assembled DNA fragments into pRab293 plasmid

Indirect ELISA was used to screen for numerous HEK supernatants that were shipped from ExonBio. Fourteen positive hits were selected for cloning and further characterization. DNA of these selected antibodies was obtained either in full plasmid form (ready for transformation) or assembled fragment form. The purpose of the protocol was to fully anneal the DNA-assembled fragments (Exon Bio) of the antibodies (a heavy chain and a light chain per antibody) into pRab293 vectors which has an ampicillin-resistant gene built in them. A specific thermocycler program was used to facilitate the annealing of DNA assembled fragments (contained V-region of either HC or LC) to corresponding linearized vectors that contained the IgG constant regions and amp^R gene

for selection (pRab293H2 or pRab293L3, respectively). Annealing reactions were conducted using a Phusion high-fidelity DNA polymerase kit (Thermo Scientific) and were comprised of 1 µL 5xPhusion HF buffer (Fischer Sci), 2 µL 10 ng/µL linearized vectors (ExonBio), 1 µL of diluted (1:10) DNA assembled fragments, and 1 µL of nuclease-free water. To facilitate DNA annealing, the thermocycler heat block was stimulated at 98°C for a 30s, decreased rapidly to 94°C for 1 min, started 90°C and 89°C cycle (20s/ step), and then the temperature gradually reduced to 30°C with a Δ_{Temp}/cycler = -2°C and ramp rate of 0.1°C/s and a step time of 20 sec.

2.3.9. Transformation of plasmid into DH5-α competent cells

The annealed plasmids were then immediately used to transform into $CaCl_2$-treated competent *DH5α* cells. Per transformation, 2 µL of the annealing plasmid of interest was pipetted into a 1.5 mL Eppendorf tube that contained 50 µL of pre-chilled competent *DH5α* cells, mixed by tapping the tube and incubated in an ice bucket for 30 min. The heavy chain and light chain plasmids were transformed into their own 1.5 ml tubes. The transformation was induced by heat-shock the tube at 42°C in a water bath for 1 min, followed by ice incubation for 1 min, reconstituted the mixture was in 1 mL S.O.C medium (cat. no. 15-544-034, ThermoFisher Scientific) and incubated the tube at 37°C with shaking at 225 rpm for 1 hour. Transformed cells were concentrated by microcentrifugation at 5000g for 10 min, followed by the removal of 900 uL of the supernatant, and reconstituted the cell pellet into the left-over 150 uL medium. All transformed cells were then aseptically spread with a sterile L-shaped spreader onto a pre-warmed LB-agar-ampicillin plate and incubated overnight at 37°C in a quiescent condition.

2.3.10. Preparation of gridded patch plate for correct plasmid determination

The next day, isolated bacterial colonies resulting from transformed cells on a transformation plate were transferred to a new LB-agar-ampicillin patch plate (with a toothpick) that was numerically labeled for further colony testing. The plates were called patch plates and were grown overnight at 37°C in quiescent condition and stored at -20°C until further colony assessment. Separate patch plates were prepared for heavy and light chain plasmids. The patch plates were used for colony PCR to screen for bacterial colonies that contained the correct insert of the plasmid of interest.

2.3.11. Colony PCR of E. coli cell colonies

The colony-wise screening was carried out from a patch plate using colony PCR followed by gel analysis to ensure the presence of the correct genetic construct of the plasmid. PCR reaction tube consists of a total 25 µL solution: 12.5 µL of 2X PCR Master mix (cat. no. FERK0171, ThermoFisher Scientific), 2.5 µL of 10 µM forward primer (pRab293-F, ATC CAC TTT GCC TTT CTC TC), 2.5 µL of 10 µM reverse primer (RabIgH-R3 for HC, ACC GTG GAG CTG GGT GTG T or RabIgK-R9 for LC, TGG TGG GAA GAT GAG GAC AG, ThermoFisher Scientific) and 7.5 µL of nuclease-free water. The cells from corresponding colonies were picked up from the patch plate and added to the numerically labeled PCR reaction tubes using a sterile pipette tip. The cells were thoroughly mixed with PCR solution. The thermocycler PCR program entailed initial denaturation performed at 98°C for 1 min, followed by 25 cycles of denaturation at 98°C for 5s, an annealing step at 60°C for 15 s, and an extension step at 72°C for 2 min 30 s. The final extension step was set up at 72°C for 10 min and the reaction tube was cooled to 10°C.

2.3.12. Gel electrophoresis of cell colonies

2% agarose gel was cast to screen colonies for PCR reactions and was run at 100V for 45 mins. The gel was prepared by adding 10 g of agarose powder, and 10 ml of 50X TAE buffer into 490 mL of deionized water (1:50) in a 1L glass bottle. Agarose was completely dissolved in the solution by heating it in a microwave oven. 20uL of 10mg/mL EtBr (DNA intercalating agent, carcinogen) was added to the gel solution after cooling it down. The agarose solution was slowly poured into the gel cassette with the combs being set to the correct position to create the sample wells. The gel was left for 30 minutes to solidify. 1X TAE buffer was used to cover the gel in the cassette. The first well has a 10 μL quick-load 2-log DNA ladder (0.1-10.0 kb) (cat. no. 50-152-6414, ThermoFisher Scientific). The rest of the lanes were loaded with 20 μL pre-mixed solution of PCR reaction with 1 μL of 6X loading dye (cat. no. FERK0171, ThermoFisher Scientific). The gel was run, and the positive inserts were identified as those which displayed the band around 500 kb with the gel imager. This confirms that the plasmid of interest has been incorporated into the competent bacterial cells.

2.3.13. Mini-prep and sequencing of positive colonies

Miniprep was performed using Purelink Quick Plasmid Miniprep Kit (cat. nos. K210006, K210010, ThermoFisher Scientific) to extract purified plasmid DNA on a small scale from the positive colonies. Overnight culture of bacterial colonies transformed with HC and LC plasmids with confirmed variable-chain inserts ($n \geq 3$ colonies) were grown overnight in a conical tube containing 5 mL LB broth and 5 μL 1000X Ampicillin (100 μg/mL) under sterile conditions at 37°C with continuous shaking. Liquid bacterial culture centrifuged at 5000 g for 10 min. Plasmid DNA was purified

using both Invitrogen™ PureLink™ Quick Plasmid Miniprep and Invitrogen™ PureLink™ HiPure Plasmid Maxiprep kits per recommended protocols. The supernatant discarded and harvested cell pellet was resuspended in 250 µL Resuspension buffer with RNase A (buffer stored at 4°C) by meticulously pipet-mixing the solution until it is homogenous. Lysis buffer (250 µL) was added to the tube and the tube was inverted gently 5 times to mix it well. The cell membrane was disrupted during this step and the contents came out in the solution. The mixture was incubated for 5 min at room temperature. It is followed by the addition of 350 µL precipitation buffer and vigorous shaking to homogenize the mixture. The lysate was centrifuged at 17,000 g for 10 min. The supernatant from this step contains our plasmid and was loaded onto a 2 mL wash tube spin column where the plasmid got bound to the column. It was centrifuged at 13,800 g for 1 min and the flow-through was discarded. Wash buffer containing ethanol (700 µL) was added to the column and centrifuged again two times to discard the flow-through. The spin column was placed in a 1.5 ml recovery tube and 30 µL of pre-heated TE buffer was poured into the center of the column. Incubation was done for 1 min at room temperature followed by centrifugation at 13,800 g for 2 min. The eluted purified plasmid DNA was procured, and purity and concentration were obtained using Nanodrop analysis. Samples were sent for sequencing at Eurofins Genomics.

2.3.14. Maxi-prep of sequenced E. coli colonies

Maxi-prep yields purified plasmid DNA at a large scale. Similar steps were followed for the mini-prep protocol except all the reagents were used with higher volume. Bacterial culture was initiated overnight by inserting the colony of interest in a 200 mL LB broth in a conical flask with 200 µL of 1000X Ampicillin. The flask was kept shaking

for 24 h at 37°C. Maxi-prep proceeded on the following day with the first application of 30 mL Equilibration buffer to the column (part of the kit). The cell lysate was prepared by centrifugation of 200 mL of overnight LB-Ampicillin culture at 5000 g for 10 min at room temperature. The medium was removed and 10 mL of resuspension buffer with RNase added to a conical tube. The pellet was mixed well until completely resuspended. Lysis buffer (10mL) added, and the tube inverted 5 times to mix the solution well. The mixture was incubated for 5 min at room temperature to obtain a slimy solution. Precipitation buffer (10 mL) poured into the tube to precipitate out proteins and cellular debris. The tube was centrifuged at 13,000g for 10 mints after extensive mixing. Proteins precipitated in the form of while pellet. The supernatant from the previous step was poured into the column and was left to drain by gravity flow. The plasmid DNA gets bound to the column. The column was washed with wash buffer and later 15 mL of elution buffer added to it. The elution tube contained eluted DNA. 10.5 mL of isopropanol was added directly to the eluent to precipitate the DNA and centrifuged at 12,000 g for 40 min at 4°C. Supernatant was carefully discarded, and the pellet washed with 5 mL of 70% ethanol, centrifuged at 12,000 g for 5 min at 4°C. The DNA pellet was air-dried for 15 min and the pellet resuspended in 200 µL of TE buffer.

2.3.15. Plasmid DNA purity and concentration determination

The samples and the control (TE buffer) were micro-spotted on a magnetic cassette as 2 µL. Gen5 software (Take 3 Session) was used to quantify the concentration of the plasmids. DNA purity (A_{260}/A280 1.8-2.0) and concentration (200-500 ng/µL miniprep; 1000-3000 ng/µL maxiprep) was determined on an Epoch Nanodrop spectrophotometer (BioTek) and samples were shipped overnight to Eurofins Genomics

(Louisville, KY) for sequencing. The forward primer for pRab293-F variable-region sequencing was ATC CAC TTT GCC TTT CTC TC for both HC and LC. Plasmid DNA was stored at −20°C.

HC and LC nucleic acid sequence ab1 files from Eurofins were converted to text using SeqVerter software. The HC and LC variable regions were located by searching for leader sequences just before the start of variable region and a short sequence at the start of the constant region. Identification of at least three matching sequences for both HC and LC produced the final nucleotide sequence for each antibody. Nucleotide sequences were converted to amino acid sequence with Expasy Translate and analyzed with EMBOSS Needle. Confirmed HC and LC plasmids were transformed into DH5α cells in a larger preparation, DNA isolated by maxiprep and re-sequenced at Eurofins. The entire cloning procedure is outlined in Figure 2.1.

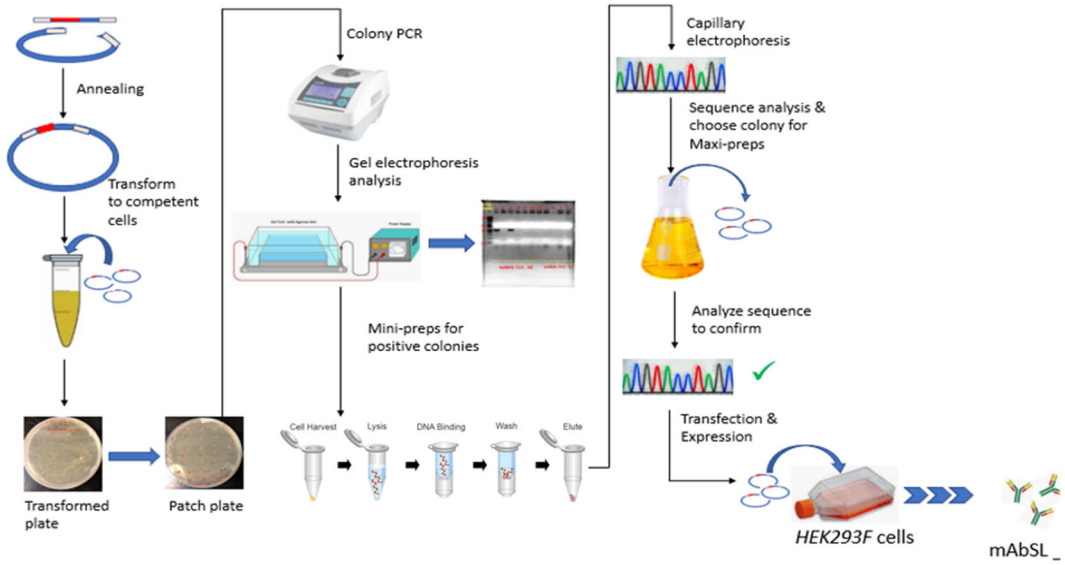

Figure 2.1. Design of cloning and expression of antibodies. Assembled HC & LC DNA fragments from each mAbSL candidate were cloned as described, transformed into DH5α bacterial cells, and grown in agar plates prepared with selective medium. Colonies were chosen and placed in a numbered grid agar plate. Colony PCR was conducted to verify insertion of DNA into vectors. Positive colonies were amplified, and the plasmid

DNA purified by mini-prep. HC & LC plasmids were sequenced at Eurofins (Louisville, KY) and co-transfected into FreeStyle 293F cells.

2.3.16. Re-amplification of mAb HC and LC plasmid into E. coli cells

The desired heavy-chain plasmid (2 µL) and light chain plasmid (2 µL) were each mixed into separate 50 µL of E. coli DH5α competent cells in a 1.5 mL microtube using a sterile tip. The tube was incubated on ice for 30 mins followed by a heat shock at 42°C on water bath for exactly 30 sec and then back on ice for 30 sec. 250 µL of Super Optimal broth with Catabolite Repression (SOC) was added to the mixture and was shaken at 225 rpm at 37 °C for 1 hour. The contents of the vial were added to a 250 mL Erlenmeyer flask which contains 200 mL of LB broth + 200 µL Amp. The flask was incubated 37°C, shaking at 225 rpm for 24 hours.

2.4. Expression and purification of monoclonal antibodies

2.4.1. FreeStyle 293 cell-culture

FreeStyle^{TM} 293 expression system (cat. no. K900001, ThermoFisher Scientific) was used for large scale transfection of 293 human embryonic kidney cells and these cells have the capability of having suspension growth. They have been well adapted to generate high levels of recombinant protein. The cells were grown in a defined, serum-free FreeStyle^{TM} 293 Expression media (ThermoFisher) stored at 4°C. The medium is optimized to support high-density culture, supplemented with GlutaMAX-I. The cells were frozen down and stored in liquid nitrogen in 1 ml cryovial aliquots with 90% FreeStyle^{TM} 293 Expression media and 10% DMSO such that each cryovial contains 1 x 10^6 cells. FreeStyleTM 293 Expression media (17 ml) was pre-warmed in a 125 ml

Erlenmeyer flask to which thawed 1 mL cryovial aliquot was added in a sterile environment. The cells were let grown at 37°C incubator in a humidified atmosphere of 8% CO_2 on a MidSci 19 mm orbital shaker platform at 125 rpm. The cell density was determined using Cellometer cell counter (Nexcelom Bioscience) to ensure healthy growth, good viability, and enough concentration of cells. The cells (20 µL) were mixed with trypan blue dye (20 µL) and the dilution factor was taken into consideration while counting the cells. The cells were passaged when the density was about 2-3 x 10^6 viable cells/ml usually on the third day. The subculturing was done in fresh, pre-warmed medium and cells were diluted to a final density of 0.1-0.2 x 10^6 viable cells/ml in a 250 mL polycarbonate, sterile Erlenmeyer flask with 60 mL total volume of cell. The cells were typically diluted to 10 or 15-fold on day 3. Cells exhibited clumping which did not affect cell growth or viability. It was ensured that clumps were avoided during dilution. Transfection of cells with the plasmid of interest was carried out after 2-3 times of passaging. Viability and mean diameter

2.4.2. Transfection of HC and LC plasmid into FreeStyle 293 cells

Pre-transfection, the cells were split into half and were allowed to grow overnight. Transfection of the cells was performed when the cell density of at least 2 x 10^6 viable cells/ml was achieved. Transfection experiments were performed generally in 30 ml or 120 ml volume using a 125 ml or 500 ml sterile Erlenmeyer flask. The final cell density for transfection was 1 x 10^6 viable cells/ml, amount of plasmid DNA used was 30 µg (1 µg/ml), and 60 µl of 293 fectin™ for 30 µg plasmid (2 µl/µg plasmids). 293 fectin™ is a cation lipid-based transfection reagent that ensures high transfection efficiency. HC and LC plasmids (30 µg) were gently mixed in a pre-warmed OptiMEM to a total volume of

1 ml or 4 ml. 120 µL or 480 µL of 293fectin™ complex was diluted in pre-warmed OptiMEM to a total volume of 1 ml or 4 mL. Incubation was done for 5 mints and was ensured to be not longer than that. The diluted plasmid DNA and 293fectin complex were combined and incubated for 30 mints at room temperature to allow the formation of DNA-293fectin complex. Cell suspension was prepared by adding the needed volume of cell suspension into a sterile, disposable 125 ml or 500 ml Erlenmeyer shaker flasks to which pre-warmed expression medium was added to total the volume to 120 ml. DNA-293fectin complex (8 ml) was added to the flask and was incubated shaking at 37°C in 8% CO_2 condition for 72 hrs. Table 2.3 and 2.4 details the concentration of plasmids, reagents and cells used for the transfection procedure. Figure 2.2 sums the entire expression procedure followed for the generation of monoclonal antibodies.

Table 2.3. List of all the plasmids transfected in 293 F cell with the amount of each reagent used to generate monoclonal AbSL.

Plasmid (1 mL DNA solution for 30 mL volume)						293fectin (1 mL soln for 30 mL vol)	
Date	Plasmid	µg/mL	Expression volume (mL)	plasmid µL for 1 µg/mL	Opti-MEM (µL)	µL 293fectin (2 µl / µg plasmids)	Opti-MEM (µL)
2/18/2019	mAb 113 HC	814	30	25	946	80	920
2/18/2019	mAb 113 LC	681	30	29			
2/18/2019	mAb 108 HC	999	30	20	965	80	920
2/18/2019	mAb 108 LC	1370	30	15			
4/18/2019	mAb 113 HC	814	30	37	919	120	880
4/18/2019	mAb 113 LC	681	30	44			
4/18/2019	mAb 108 LC	999	30	30	948	120	896
4/18/2019	mAb 108 LC	1370	30	22			
5/24/2019	mAb 113 HC	814	30	37	919	120	880
5/24/2019	mAb 113 LC	681	30	44			

5/24/2019	mAb Aβ 513 HC	2784	30	11	964	120	880
5/24/2019	mAb Aβ 513 LC	1192	30	25			
5/24/2019	mAb 545 HC	1222	30	25	916	120	880
5/24/2019	mAb 545 LC	505	30	59			
7/2/2019	mAb 113 HC	1496	120	80	3873	480	3520
7/2/2019	mAb 113 LC	2589	120	46			
7/2/2019	procaspase-1	1000	30	30	933	120	880
12/10/2019	mAb 113 HC	814	30	37	919	120	880
12/10/2019	mAb 113 LC	681	30	44			
12/10/2019	mAb 540 HC	2350	30	13	946	120	880
12/10/2019	mAb 540 LC	736	30	41			
12/10/2019	mAb 511 HC	1789	30	17	968	120	880
12/10/2019	mAb 511 LC	1989	30	15			
2/11/2020	mAb 113 HC	1496	120	80	3873	480	3520
2/11/2020	mAb 113 LC	2589	120	46			
2/28/2020	mAb 502 HC	1015	30	30	942	120	880
2/28/2020	mAb 502 LC	1068	30	28			
2/28/2020	mAb 531 HC	1302	30	23	956	120	880
2/28/2020	mAb 531 HC	1436	30	21			
2/28/2020	mAb 550 HC	2806	30	11	978	120	880
2/28/2020	mAb 550 HC	2686	30	11			
7/24/2020	mAb 113 HC	2016	120	60	3899	480	3520
7/24/2020	mAb 113 LC	2927	120	41			
2/22/2021	mAb 113 HC	2016	120	60	3899	480	3520
2/22/2021	mAb 113 LC	2927	120	41			
2/22/2021	mAb Aβ 513 HC	2010	120	60	3840	480	3520
2/22/2021	mAb Aβ 513 LC	1192	120	101			

10/8/2021	mAb 113 HC	1675	120	72	3887	480	3520
10/8/2021	mAb 113 LC	2927	120	41			
1/27/2022	mAb Aβ 513 HC	2784	120	43	3399	480	3520
1/27/2022	mAb Aβ 513 LC	215	120	558			

Table 2.4. List of expressed mAbSL, volume of cell expression, volume of expression medium used, of cells used and volume of 293 Fectin-plasmid complex used.

Date	mAbSL	Cell/ml	Flask	Tot vol (ml)	Cell vol (mL)	Com-plexes (mL)	EM (mL)	Conc. (mg/mL)	Vol. (mL)	Pro-tein A/G
2/18/2019	113	2.15E+06	125	30	14	2	14			G
2/18/2019	108	2.15E+06	125	30	14	2	14			G
4/18/2019	113	2.00E+06	125	30	15	2	13			G
4/18/2019	108	2.00E+06	125	30	15	2	13			G
5/24/2019	113	2.80E+06	125	30	11	2	17			G
5/24/2019	513	2.80E+06	125	30	11	2	17			G
5/24/2019	545	2.80E+06	125	30	11	2	17			G
7/2/2019	113	2.10E+06	500	120	57	8	55			G
7/2/2019	pro-caspase -1	2.10E+06	125	30	14	2	14			G
12/10/2019	113	3.34E+06	125	30	9	2	19	.164	0.63	G
12/10/2019	540	3.34E+06	125	30	9	2	19	.082	0.7	G
12/10/2019	511	3.34E+06	125	30	9	2	19	0.195	.52	G
2/11/2020	113	2.86E+06	500	120	42	8	70	1.46	0.98	G
2/28/2020	502	2.38E+06	125	30	13	2	15	0.479	0.6	G
2/28/2020	531	2.38E+06	125	30	13	2	15	0.682	0.69	G
2/28/2020	550	2.38E+06	125	30	13	2	15	0.81	0.78	G
7/24/2020	113	4.59E+06	500	120	26	8	86	0.99	0.55	G
2/22/2021	113	4.09E+06	500	120	29	8	83	0.329	0.5	G

2/22/2021	513	4.09E+06	500	120	29	8	83	0.314	0.35	G
10/8/2021	113	2.31E+06	500	120	52	8	60	1.6	0.5	A
1/27/2022	513	2.31E+06	500	120	53	8	59	1.93	0.35	A

2.4.3. High-throughput transfection

Small-scale, high throughput expression was done in a similar manner, but in sterile, 96-deep-well cell plates with a total cell expression volume of 2 mL (MasterBlock, Greiner Bio-One). Expression times were typically 3 days, after which the cell expression volume was centrifuged at 1000g for 5 min and the supernatant (medium) was collected for affinity purification.

Table 2.5. List of all the plasmids transfected in 293 F cells with the amount of each reagent used to generate monoclonal AbSL in a high throughput fashion.

Plasmid (67 µL DNA solution for 2 mL volume)						293fectin (67 µL soln for 2 mL vol)	
Date	**Plasmid**	**µg/mL**	**Exp. vol. (mL)**	**plasmid µL for 1 µg/mL**	**Opti-MEM (µL)**	**µL 293fec-tin (2 µl / µg plasmids)**	**Opti-MEM (µL)**
6/17/2021	mAb 113 HC	2016	2	1	65	4	63
6/17/2021	mAb 113 LC	2927	2	0.7			
6/17/2021	mAb 108 HC	999	2	2	64	4	63
6/17/2021	mAb 108 LC	1370	2	1.5			
6/17/2021	mAb Aβ 513 HC	2010	2	1	64	4	63
6/17/2021	mAb Aβ 513 LC	1192	2	1.7			
6/17/2021	mAb 502 LC	1015	2	1.9	63	4	63

6/17/2021	mAb 502 LC	1068	2	1.8			
6/17/2021	mAb 545 HC	1222	2	1.6	61	4	63
6/17/2021	mAb 545 LC	505	2	3.9			
6/17/2021	mAb 511 HC	1789	2	1.1	65	4	63
6/17/2021	mAb 511 LC	1989	2	1			
6/17/2021	mAb 540 HC	2350	2	0.8	63	4	63
6/17/2021	mAb 540 LC	736	2	2.7			
6/17/2021	mAb 550 HC	2806	2	0.7	66	4	63
6/17/2021	mAb 550 LC	2686	2	0.7			
6/17/2021	mAb 531 LC	1302	2	1.5	64	4	63
6/17/2021	mAb 531 HC	1436	2	1.4			
6/17/2021	mAb 519 LC	2100	2	0.9	64	4	63
6/17/2021	mAb 519 HC	876	2	2.3			

Table 2.6. High-throughput transfection. List of expressed mAbSL, volume of cell expression, volume of expression medium used, of cells used and volume of 293 Fectin-plasmid complex used.

Date	mAbSL	Cell/ml	Tot vol (ml)	Cell vol (mL)	Complexes (µl)	EM (µl)
6/17/2021	113	2.10E+06	2	1	134	866
6/17/2021	108	2.10E+06	2	1	134	866
6/17/2021	513	2.10E+06	2	1	134	866
6/17/2021	502	2.10E+06	2	1	134	866
6/17/2021	545	2.10E+06	2	1	134	866
6/17/2021	511	2.10E+06	2	1	134	866

6/17/2021	540	2.10E+06	2	1	134	866
6/17/2021	550	2.10E+06	2	1	134	866
6/17/2021	531	2.10E+06	2	1	134	866
6/17/2021	519	2.10E+06	2	1	134	866

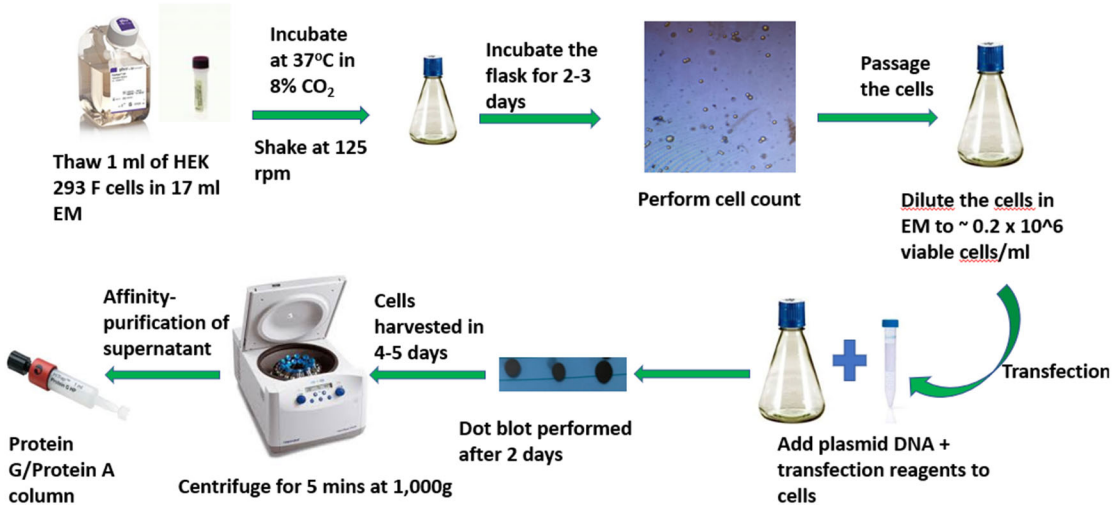

Figure 2.2. Schematic illustration outlining the details of each step followed during 293 F cell-culture, transfection, expression, and purification of monoclonal antibodies.

2.4.4. Collection of supernatants from FreeStyle cells

Cells were harvested to obtain the recombinant protein by centrifuging the entire volume at 1000g for 5 min post-transfection. The pellet was discarded, and the supernatant was collected in three conical tubes which contained the monoclonal antibody.

2.4.5. Dot blot to detect monoclonal antibody

The Whatman nitrocellulose transfer membrane was soaked in MilliQ water for 2 minutes and dried completely. 1.7 µL of the supernatant of the monoclonal antibody sample was spotted as three dots (replicates) along with negative control (BSA sample). The membrane was incubated for 1 hour at room temperature with a blocking buffer (5ml

1X PBS, 100ul of 5% tween, 0.25g milk). It was kept on a 19 mm orbital shaker set at 70 rpm in a cassette container and washed three times for 5 mins each with washing buffer (0.2% tween 20 in 1X PBS). The antibody used was an anti-rabbit IgG Horseradish Peroxidase-conjugated antibody (R& D Systems, Cat #HAF008, Lot# FIN1615011) and was diluted to 1000x in an antibody diluent (5ml 1X PBS, 100ul tween, 0.05g milk). The membrane was incubated with the antibody for 1 hour at persistent shaking and washed three times the same way. Equal volumes of ECL western blot substrate (cat. no. PI-32209, ThermoFisher Scientific) were mixed to make 500 ul solution and the substrate was added to the membrane and vigorously shaken at 120 rpm for 1 min. The membrane was dried and image acquisition on a Bio-Rad ChemiDoc MP gel imager.

2.4.6. Protein A/G affinity column

FreeStyleTM 293F cells were cultured in serum-free 293 Expression Medium in sterile Erlenmeyer flasks under continuous rotation at 125 rpm on a 19 mm orbital shaker at 37°C in a humidified atmosphere of 8% CO2. Cell density and viability were determined with a Cellometer cell counter (Nexcelom Bioscience). 293F cells (1 x 106 cells/ml) were transfected with 1 µg/ml HC and LC plasmids after complex formation in pre-warmed OptiMEM with 293fectin (2 µl/µg plasmids) for 5 min. Small scale, high throughput expression was done in a similar manner, but in sterile, 96-deep-well cell plates with a total cell expression volume of 2 mL (MasterBlock, cat. no. 780271, Greiner Bio-One). Expression times were typically 3 days, after which the cell expression volume was centrifuged at 1000g for 5 min and the supernatant (medium) was collected for affinity purification. Expression medium was loaded with a SuperLoop (cat. no. 18-1113-82, Cytiva) onto a HiTrap Protein G HP (cat. no. 45-000-055, ThermoFisher Scientific)

or MabSelect Prism Protein A (Cytiva) column and washed in 50 mM sodium phosphate pH 7.4 containing 100 mM sodium chloride. Antibodies were eluted with either 0.2 M glycine pH 1.85 (Protein G column) or with 100 mM sodium acetate pH 3.6 (Protein A column). Fractions (2 mL) were collected during the elution phase, immediately neutralized with 0.15 mL 1 M Tris pH 8.5, and concentration determined by UV280 nm absorbance using an extinction coefficient of 1.4 mL mg−1 cm−1. Peak fractions were pooled and concentrated to a final volume of 0.5 ml using an Amicon Ultra-15 centrifugal filter with a 10 kD cutoff (cat. no. UFC9-010-24, ThermoFisher Scientific).

2.5. Site-directed mutagenesis experiments

Phusion™ Site-Directed Mutagenesis Kit is a useful tool to carry out point mutations, insertions, and deletions in a plasmid DNA. The kit utilizes the highly processive Phusion^{TM} Hot Start II DNA Polymerase for amplification of plasmid dsDNA that requires to be mutated. The DNA polymerase ensures high-fidelity exponential amplification and ensures the inhibition of its activity at ambient temperatures to prevent any non-specific product formation prior to the PCR cycle.

2.5.1. Polymerase chain reaction (PCR)

Phosphorylated primers were designed and ordered with the desired mutation. The primers must be phosphorylated at the 5’ end to eliminate a further phosphorylation step before the ligation reaction. It is recommended to use primers purified with reverse-phase HPLC or PAGE. Tm values and determination of optimal annealing temperature are crucial for primer designing. Our primer sequence is less than 20 nucleotides. The annealing temperature of the primer fell between 65°C and 72°C. The total reaction volume used in PCR tubes was taken to be 50 µl. 10 µl of 5X Phusion HF buffer, 1 µl of

10 mM dNTPs, forward primer, and reverse primer diluted to a final concentration of 0.5 µM to the reaction tube. 2 µl plasmid DNA and 0.5 µl of DNA polymerase were added towards the end in the tube. The remaining volume is filled with nuclease free water to make up to 50 µl. DMSO was added to optimize the PCR product. When different annealing temperatures are being tested, make the total solution together with all the reagents being increased to the number of conditions being tested.

Table 2.7. Cycling instructions followed for mutagenesis reaction in the thermal cycler program.

Step	Temperature	Time	Number of cycles
Initial denaturation	98°C	30 s	1
Denaturation Annealing [1] Extension	98°C 65–72°C 72°C	5–10 s 10–30 s 15–30 s/kb	25
Final extension	72°C 4°C	5–0 min Hold	1

5 µl of sample used from the PCR reaction to be tested for agarose gel electrophoresis to verify the formation of PCR amplification. Control plasmid (5 ng/ µl) in TE buffer and 5'-phosphorylated control primers mix were used from the kit for setting control reactions during the troubleshooting process.

2.5.2. Ligation reaction

Digestion of parental methylated DNA was carried out using FastDigest DpnI. 1 µl of FastDigest DpnI enzyme was directly added to the mutagenesis reaction and incubated at 37°C for 15 minutes.

T4 DNA ligase enabled direct ligation (circularization) of mutated PCR products in 5 minutes without any further purification steps required. 10 µl of the ligation reaction mix was prepared. 1-5 µl of PCR product (10-20 ng) was taken after DpnI digestion. 2 µl

of 5X Rapid Ligation Buffer was added from the kit. The remaining volume was adjusted to 9.5 µl with water and mixed. 0.5 µl of T4 DNA ligase was added to the ligation tube and mixed well. The tube was briefly centrifuged and incubated for 5 minutes at room temperature. The product is stored at -20°C.

2.5.3. Transformation of plasmid into E. coli cells and sequencing the product

The transformation and sequencing procedure were followed in the same manner as performed during the cloning procedure of conformationally-selective antibodies as mentioned previously in the method section.

2.6. Aβ enzyme linked immunosorbent assay (ELISA)

2.6.1. Aβ indirect ELISA

Separate tubes of protofibrillar, monomeric, and fibrillar Aβ (50 µL/well) were prepared at a concentration range of 320 nM - 0 nM. The serial dilutions for Aβ were carried out in a coating buffer (0.05 M sodium bicarbonate pH 9.6). The prepared solutions were adsorbed at 4°C on a Nunc (Dhami, Karki, et al. 2022) 96-well MaxiSorp flat-bottom immunoplate for 1 hour or kept overnight. The wells were washed 1**x** (n=3) with phosphate buffer saline pH 7.4 containing 0.05% Tween 20 (PBST) and then blocked with 150 µl blocking buffer (10% milk solution in wash buffer PBST) for 1 hr. All the ELISA steps were performed at room temperature starting from the blocking step and the plate was washed 4x with PBST between each step. Primary antibody (100 µL/well) mAbSL with a final concentration of 0.5 µg/mL (diluted in 5% milk PBST solution) was incubated in the well for an hour. It was followed by the addition of anti-

rabbit IgG horseradish peroxidase (HRP)-conjugated (R&D system) secondary antibody (100 µL/well) in each well for an hour and was diluted in the same buffer as the primary antibody. A 1:1 ratio of 3,3',5,5'-tetramethylbenzidine, and hydrogen peroxide (HRP substrate) was added to each well (100 µL/well) for 5 min. The substrate turned the color of the solution in well as blue. The reaction was stopped using 50 µL/well of 1M H_2SO_4 which changed the color to yellow. The optical density of each well was read on SpectraMax 340 absorbance plate reader (Molecular Devices, Sunnyvale, CA, USA) at 450 nm with a reference reading subtracted at 630 nm. The software SoftMax Pro provides the absorbance measurement of the wells.

2.6.2. Aβ titer ELISA

Titer enzyme-linked immunosorbent assay studies were conducted in a similar manner to indirect ELISA studies but with various dilutions of the serum antibody (AbSL) being used.

2.6.3. Aβ antigen competition ELISA

ELISA is like those described for indirect ELISA. Briefly, Aβ42 protofibrils diluted in coating buffer were applied to a high-binding 96-well ELISA plate (18 ng/well) and allowed to adsorb at 4 °C for 1 h. Separately, serial dilutions of either Aβ42 protofibrils (0-120 nM), monomers (0-1280 nM), or fibrils (0-480 nM) in aCSF were incubated with 0.1 µg/mL monoclonal antibody 4 °C for 1 h. 0.05 mL of each Aβ-antibody mixture was added to the plate wells adsorbed with protofibrils that had been washed, blocked, and washed again. The remaining steps were carried out as described for the indirect ELISA.

2.6.4. Aβ antibody competition sandwich ELISA

The capture antibody used was either affinity-purified AbSL or monoclonal AbSL which was diluted to 0.5 µg/mL in PBS and incubated overnight in a 96-well plate at room temperature. The wells were incubated with 300 µL blocking buffer (PBS containing 1% BSA, 5% sucrose, and 0.05% NaN_3). The steps were washed in between with Phosphate-buffered saline pH 7.4 (1X PBS) containing 0.05% Tween 20. The serial dilutions of Ab 2.1.3 (that recognizes the N-terminus of Aβ) or of Ab9 (that recognizes the C-terminus of Aβ) were performed with concentrations as 500ug/ml, 50ug/ml, and 5ug/ml in separate Eppendorf tubes and the biotinylated Aβ protofibril were added to each tube with a fixed concentration of 20 nM. The antibody (Ab 2.1.3 or Ab9) + biotinylated Aβ protofibril mixture solution (100 µL) was added to each well as a detection antibody and incubated for an hour. HRP-streptavidin conjugate was diluted 200-fold in 1x PBS containing 1% BSA and was incubated in wells for 20 min. The addition of the HRP substrate followed by the stop solution was carried out the same way as indirect ELISA.

2.7. Thioflavin T (ThT) fluorescence measurement

Aβ solutions were assessed by ThT fluorescence as described previously (Nichols, Moss, et al. 2002). SEC Aβ fractions were diluted in aCSF pH 7.8 containing 10 µmol/L ThT. Fluorescence emission scans (460-520 nm) were acquired on a Cary Eclipse fluorescence spectrophotometer using an excitation wavelength of 450 nm. Emission scans were integrated from 470-500 nm to provide a numerical value of ThT relative fluorescence values (RFU).

2.7.1. Aβ monomer aggregation assay (cuvette-based)

Solutions of SEC-purified Aβ42 monomers (10 μM) in 50 mM Tris pH 8.0 containing 100 mM NaCl, 20 μM thioflavin T (ThT), and 0.05% NaN3 were prepared in low-retention microfuge tubes. Triplicate tubes for Aβ42 in the absence or presence of 1 μM mAbSL 113 or Aβ mAb 513 were incubated at 37 °C on an IKA MS 3 mini vortexer at 1000 rpm. Reactions were monitored for ThT fluorescence at 0 h and then at selected time points. 80 μL were removed from each tube and emission scans (460-520 nm) were acquired on a Cary Eclipse fluorescence spectrophotometer using an excitation wavelength of 450 nm. The solution was recovered back into each tube for successive measurements. Numerical ThT values, in relative fluorescence unit values (RFU), were obtained by integration of emission scans from 470-500 nm. ThT buffer controls were included in all experiments and did not display any significant fluorescence. Each reaction was fit to the following 3-parameter sigmoidal equation in SigmaPlot: $y = a / (1 + e^{-(x-x0)/b})$ and parameters x0 and b determined for each reaction. A single time-dependent aggregation curve (± standard error) was constructed for each condition from the regression values. The parameter $t_{1/2}$ was obtained directly from x0, while t_{lag} was obtained from $t_{1/2} – (2/b-1)$. The kinetics analysis was derived from a previous report (Hellstrand et al. 2009).

2.7.2. Aβ protofibril dynamic experiment

Protofibril stability was assessed by quiescent incubation of SEC-isolated Aβ42 protofibrils (10 μM) at 25 °C in the absence or presence of monoclonal antibodies (1, 0.5, and 0.2 μM). The reactions in triplicate were carried out in low-retention tubes in 50 mM Tris pH 8.0 containing 20 μM ThT and 0.05% NaN3. ThT fluorescence was assessed by

withdrawing 80 μL from the upper half of the solution before and after centrifugation at 17,000g for 10 min. Each sample was returned to the respective reaction without disturbing the solution for subsequent measurements. ThT emission scans and quantitation were conducted in the same manner as described in the previous section.

2.8. Atomic force microscopy (AFM)

Aged monomers of Aβ (1-42) were used to make fibrillar aggregation solutions and were diluted to a final concentration of 4-5 μM in water. Mica was cleaved into 11 mm circles and was affixed to 12 mm metal disks. The mica surface was pretreated with 1% 3-amino propyl triethoxysilane (APTES) in 1 mM acetic acid solution for 10 min and air-dried before the application of the sample. The Aβ sample (50 μL) was applied to freshly cut mica, allowed to stand for 15 min, washed with water 3-4 times, air-dried to remove excess water, and stored in a petri-dish with desiccant. Images were taken with Bruker atomic force microscope in Tapping Mode. Height and amplitude analysis was performed using software and the images were flattened.

2.9. Epitope determination of mAbSL on Aβ protofibril

2.9.1. Hydrogen-deuterium exchange/mass spectrometry (HDX-MS)

Continuous HDX labeling of Aβ42 protofibrils and Aβ42 monomer with or without incubation with antibodies (1:1) was performed by taking 150 pmol of the protein and exchanging it in D_2O (85%) at pH 7.4 and 4 °C in 1x PBS buffer for 0, 10, 30, 60, 300, 900, 3600, and 14400, and seconds as previously described (Yan, 2015. The samples were incubated with the antibody (mAb113) for 1 h at 4 °C prior to HDX. Quenching was performed under reducing conditions by adding a solution of 4 M urea with 1% trifluoroacetic acid (TFA) to the reaction vial at a 1:1.5 protein: quench *v/v* ratio. The final

pH was kept at approximately 2.5 to minimize back exchange. The samples were mixed and immediately loaded onto our custom-built HDX platform for desalting, online pepsin digestion, reversed-phase chromatography of peptic fragments, and direct injection into the mass spectrometer for analysis.

The samples were passed over a custom-packed 2 mm x 20 mm immobilized pepsin column at 200 µL/min flow (Chalmers, Busby, et al. 2007). The peptides resulting from digestion were captured by a 2.1 mm x 15 mm ZORBAX Eclipse XDB C8 microtrap column (Agilent, Santa Clara, CA) and desalted at 200 µL/min with H_2O containing 0.1% trifluoroacetic acid for 3 min. The resulting peptides were then separated by a 2.1 mm × 50 mm C_{18} column (2.5-µm Waters XSelect CSH C_{18}) with a 10-min gradient of 5 to 80% acetonitrile in 0.1% formic acid at a flow rate of 100 µL/min delivered by an HPLC pump (Shimadzu Scientific Instruments, Kyoto, Japan). The linear part of the gradient from 1.5 min to 6.5 min raised the acetonitrile content from 15% to 50%, during which time most of the peptides eluted from the C_{18} column. The entire fluidic system, except the pepsin column, was kept in an ice bath to minimize back exchange. Duplicate measurements were carried out for each time point. MS detection was performed on a Thermo LTQ XL Orbitrap (Thermo Fisher Scientific) using the following instrument parameters: spray voltage 4.8 kV, capillary temperature 280°C, capillary voltage 41.5 V, and tube lens 145 V. Data was collected at a mass resolving power of 100,000 at *m/z* 400. Before HDX, overlapping peptides from pepsin digestion were identified by performing data-dependent acquisition (DDA) followed by a targeted analysis with an inclusion list that allowed focused MS fragmentation. The inclusion list helped in improving the identification of low-abundance peptides. In both cases, the six most abundant ions were

selected for collision-induced dissociation (CID). Product-ion spectra were then submitted to PMI-Byonic^{TM} (version 3.8.13; Protein Metrics Inc., CA) for identification and identifications were manually verified. Only verifiable peptides were used for HDX analysis.

The collated peptide list from multiple MS^2 runs and the MS^1 raw files from non-deuterated runs were analyzed by using HDExaminer (version 2.5.1, Sierra Analytics, CA) to generate a total peptide pool containing peptides with good signal intensity and confidence to be reliably used for deuterium labeling analysis. The MS1 raw files for all HDX runs were then input to the software to calculate the centroid masses of isotopic envelopes (m) and deuterium level (*D%*) for the peptide pool as described previously (Zhang and Smith 1993, Yang, Adhikari, et al. 2017). The final deuterium level was adjusted to 95%. The data were not corrected for back exchange because two states (bound and unbound) of the protein complex were compared. The final D% values were exported from HDExaminer onto OriginPro 9.0 (OriginLab, Northampton, MA) for generating HDX kinetic curves.

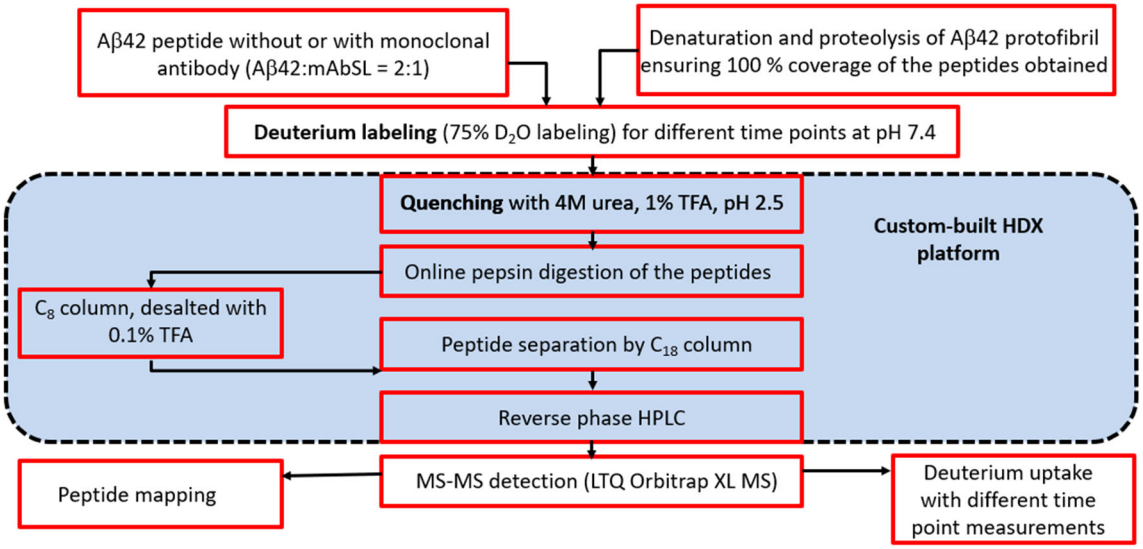

Figure 2.3 HDX-MS experimental workflow. Free Aβ42 protofibril and Aβ42 protofibril bound with monoclonal antibody were diluted in PBS buffered 75% D_2O and incubated for 1, 30, 90, 300, 900, and 3600 secs. Deuterium labeling was quenched by lowering the pH to 2.5 and adding 4 M urea with 1% trifluoroacetic acid to the reaction. The samples were loaded onto a custom-built HDX platform for desalting, online pepsin digestion, reverse-phase chromatography of fragments, and finally injecting into a mass spectrometer. The peptides were analyzed by the HDXExaminer software used for peptide identification. Non-deuterated controls were used for peptide identification.

2.9.2. Fast photochemical oxidation of proteins/mass spectrometry (FPOP-MS)

Previously, FPOP has been used successfully to monitor the time course of Aβ42 aggregation (Li, Rempel, et al. 2016). Gross lab has also successfully applied this technique to study the interactions of an IgG to a globular protein (FcγRIII) (Shi, Liu et al. 2019) using a reporter peptide strategy to compensate for scavengers and to enable normalization and comparison of time-dependent results (Niu, Mackness, et al. 2017).

Two sets of FPOP experiments were performed to complement HDX data. A stock solution of 100 µM YGGFL (Leu-enkephalin) was prepared and used as a reporter peptide for the FPOP time-dependent experiments. Stock solutions of L-methionine (70 mM),

catalase (5 μM), and L-glutamine (200 mM) were prepared. Additionally, the scavenger concentrations were varied for time-dependent experiments by using L-glutamine as a scavenger and varying the concentrations in the reaction mix as 0 mM, 0.5 mM, 2 mM, 5 mM, and 20 mM glutamine in 1X PBS buffer to afford time-dependent measurements. Solutions were prepared starting with a 50-μL sample solution consisting of 9 μL protein solution (either Protofibril alone or protofibril + antibody (1:1)), 2.5 μL reporter peptide, 5 μL glutamine (varying concentrations as indicated above), and 23.5 μL 1X PBS buffer solution to make the volume up to 50 μL. Hydrogen peroxide solution (5 μL of 300 mM H_2O_2) was added to the sample just prior to infusing the solution into the tubing for laser irradiation (FPOP experimental procedures were described in detail previously) (Li, Rempel et al. 2016).

The power of the KrF excimer laser (GAM Laser Inc., Orlando, FL, USA) was adjusted to 21.8 mJ/pulse, and its pulse frequency was set to 7.5 Hz. The width of the laser beam at the intersection with the tubing was 2.2 mm. The flow rate was adjusted to 17 μL/min to ensure a 15% exclusion volume to minimize repeated •OH exposure (double hits). Samples were collected in Eppendorf tubes containing 0.5 μM catalase and 70 mM Met to exhaust the left-over H_2O_2 and to react with the unreacted OH radicals. Additionally, two replicate control samples were prepared and handled in the same manner except no laser-irradiation was used.

To compare the three Aβ42 aggregates, similar FPOP conditions were utilized as described above keeping the L-glutamine (scavenger) concentration in the reaction mix constant at 5 mM. Since the antibody is not present in these samples, there are no additional scavengers present and hence there is no need to do a time-course assay for normalization.

FPOP data analysis and MS^2 conditions are explained in detail in previous publications (Li, Rempel, et al. 2016, Shi, Liu, et al. 2019)

CHAPTER 3: DEVELOPMENT OF A CLASS OF MONOCLONAL ANTIBODIES SPECIFIC FOR Aβ42 PROTOFIBRILS

Amyloid-β peptide (Aβ) antibodies have been an important tool in Alzheimer's disease (AD) research (Masters et al. 2016) since the determination that Aβ was the principal component of neuritic plaques and cerebral deposits in the AD brain (Wong et al. 1985). The first-generation antibodies allowed quantitative measurement of Aβ levels in human tissues and fluids (Seubert et al. 1992) and second-generation C-terminal-selective Aβ antibodies helped resolve the Aβ40/Aβ42 composition in plaques (Gravina et al. 1995). The development of conformation selective Aβ antibodies permitted probing of both soluble (oligomeric) and insoluble (fibrillar) aggregated Aβ species in cells, mouse models, and human tissues and fluids (Georganopoulou et al. 2005, Kayed et al. 2007, Deshpande et al. 2009, Koffie et al. 2009). Currently, conformation selective Aβ antibodies comprise a large group of potential AD therapeutics in clinical trials (Schilling et al. 2018).

It has been well established in vitro that unstructured Aβ monomers (both Aβ40 and Aβ42) will undergo non-covalent self-assembly (Jarrett et al. 1993) to form a polydisperse mixture of structurally-undefined soluble oligomers (Bitan et al. 2003, Kayed et al. 2003, Mittag et al. 2014) and more-defined soluble β-sheet-containing protofibrils (Walsh et al. 1997, Harper et al. 1999, Walsh et al. 1999, Mittag et al. 2014), the latter of which can transition to insoluble β-sheet-rich fibrils (Harper et al. 1997). Fibrils formed in vitro have morphological characteristics like the neuritic plaques observed in the AD brain (Terry et al. 1964, Colvin et al. 2016, Gremer et al. 2017, Yang et al. 2022). While monomeric Aβ appears to be benign, aggregates adopt a biologically

detrimental structure leading to an array of damaging processes in the brain leading to neuronal death (Langer et al. 2011, Benilova et al. 2012, Evangelisti et al. 2016, Katzmarski et al. 2020, Koike et al. 2021). The two predominant forms of circulating Aβ are 40 and 42 amino acids in length. However, the greater aggregation propensity of Aβ42, its presence in the inner core regions of neuritic plaques, the heightened ability to form different oligomeric structures, and the finding that many early-onset AD-causing familial mutations produce a higher Aβ42/Aβ40 ratio have all implicated Aβ42 as a key causative agent in AD (Gu and Guo 2013, Golde 2022, Janelidze et al. 2022, Xu et al. 2022).

While the plaques are the most outstanding Aβ pathological feature, a significant effort over the last 2+ decades have been to understand and target soluble aggregated Aβ species due to their diffusible nature and greater in vitro toxicity (Haass and Selkoe 2007, Lannfelt et al. 2014, Ono and Tsuji 2020). One of these species, protofibrils, which emanate from Aβ monomers and are precursors to fibrils (Harper et al. 1997, Walsh et al. 1997), has been the subject of research for several years. Aβ protofibrils have been described as a non-spherical, filamentous, metastable intermediate (Kodali and Wetzel 2007) and as small, curvilinear aggregates less than 100 nm in length (Walsh et al. 1997, Walsh et al. 1999, Paranjape et al. 2012). Soluble, diffusible protofibrils adopt a β-sheet secondary structure during their formation from random coil monomers (Walsh et al. 1999, Dhami et al. 2022), yet are polydisperse concerning size (Nichols et al. 2015). Aβ protofibrils display a variety of detrimental biological activities including direct neurotoxicity, neuroinflammation, and disruption of cellular processes (Haass and Selkoe 2007, Paranjape et al. 2012, Lannfelt et al. 2014, Yasumoto et al. 2019).

Presently, conformation selective Aβ antibodies are at the forefront of potential AD treatments. While their effectiveness has been vigorously debated, the cumulative data suggests that targeting a particular Aβ conformation has merit. Aducanumab displays selectivity for aggregated Aβ and has been shown to reduce soluble and insoluble Aβ in an AD transgenic mouse model and slow clinical decline in AD patients with mild AD (Sevigny et al. 2016). Initially deemed as not meeting the primary objectives for AD treatment in clinical trials, a follow-up analysis of aducanumab revealed a reduction in the progression of cognitive and functional impairments in patients receiving the highest dose (Kwon et al. 2020). Consequently, aducanumab (Aduhelm™) was granted priority review and approved by the United States Food and Drug Administration (FDA) for the treatment of AD in early-stage patients. Aduhelm™ is now the first potential disease-modifying therapeutic for AD. BAN2401 displays selectivity for Aβ protofibrils and fibrils, reduces Aβ protofibril levels in the brain and CSF of an AD transgenic mouse model, and rescues neurons from Aβ-induced death (Englund et al. 2007, Tucker et al. 2015, Söllvander et al. 2018). BAN2401 (Lecanemab™) continues to meet expectations in Phase 3 trials and has recently received FDA review and successful accelerated approval (van Dyck et al. 2022). Regardless of the therapeutic debate, conformation-selective antibodies remain a ubiquitous and important determinant of various aggregated species in AD brain tissue and fluid samples. The chapter discusses detailed information on the development of a class of novel monoclonal forms of AbSL (mAbSL).

3.1. Isolation and characterization of soluble Aβ42 protofibrils and Aβ42 fibrils

As highlighted before, Aβ42 has a significantly enhanced propensity to aggregate. Synthetic Aβ42 peptide was bought, treated with commercially available hexafluoro isopropanol (HFIP), and vacuum centrifuged to obtain dry aliquots of a thin-filmed Aβ tube. An aliquot of lyophilized Aβ (0.9 mg) was reconstituted in 100 µl of 50 mM NaOH solution, followed by the addition of 900 µl of prefiltered aCSF buffer or TRIS buffer pH 8 to obtain purified Aβ42 protofibrils. Aβ42 was reconstituted in a basic condition to enhance the aggregation pathway of Aβ42 to obtain a better yield of protofibril form. The mixture was incubated at room temperature for 20 minutes, centrifuged at 17,000 g for 10 min and the supernatant was loaded onto the column. The prepared Aβ42 was eluted using Superdex 75 on AKTA fast protein liquid chromatography system at 0.5 mL min^{-1} flowrate and 0.5 mL fractions were collected and placed on ice. Aβ42 protofibrils and monomers were eluted as two distinct peaks. The chromatographic separations showed protofibril peaks in void volume and monomers in the included volume (Figure 3.1A). Aβ42 concentrations were determined by in-line UV absorbance trace using an extinction coefficient of 1450 cm^{-1} M^{-1} at 280 nm. CD data confirms the separation of Aβ42 protofibril and Aβ42 monomer peaks (Figure 3.1B)

Aβ42 protofibril peak eluted between fraction 10 and 20 (5-7 mL) whereas Aβ42 monomer eluted in the range of fraction 25 to 35 (6-8 mL). The buffer used was in accordance with the experiment being worked on. Buffers included were either of the three: aCSF (pH 7.8)/tris (pH 8)/PBS (pH 7.4). It was observed that using aCSF pH 7.8 for 30 min or using PBS pH 7.4 buffer with no incubation time led to more protofibril

production as compared to monomer peak. On the other hand, incubation with TRIS pH 8 buffer for 10 min yielded similar appearing peaks for both Aβ42 species with concentrations being very close to each other. It was also reported that using TRIS buffer at the time of reconstitution increased the productivity of total Aβ42 to a maximum of 64%. There is an expected indispensable loss in the recovery of Aβ42 during the chromatographic separation.

For the preparation of fibril samples for various experiments and assays, an aged monomer was used. Selecting the right buffer with appropriate ionic strength is crucial for the preparation of fibril prep. Carefully examining the aged monomer fractions, it can be concluded that using 50 mM TRIS pH 8 buffer led the monomer to slow down on aggregation even being at 4°C. It could be due to no salt present in the TRIS buffer. Monomer reconstituted in aCSF buffer appeared to aggregate starting in over a week time.

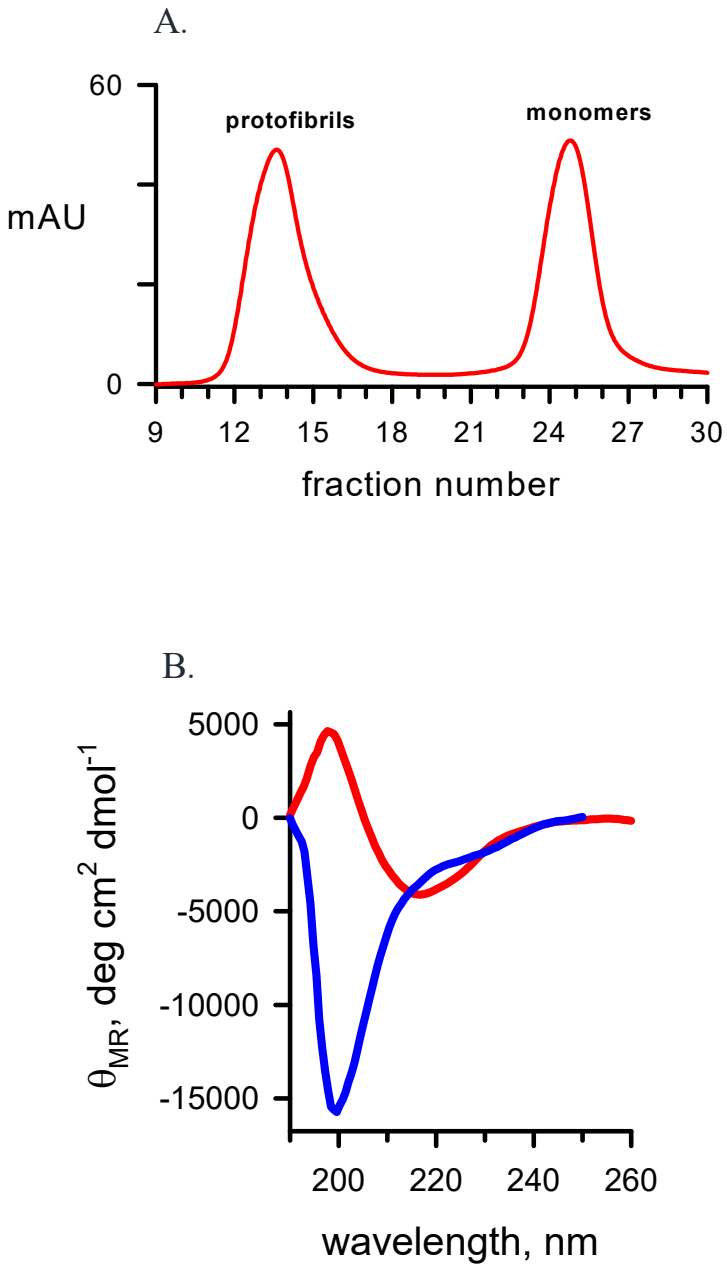

Figure 3.1. Isolation and characterization of Aβ42 by SEC and CD spectra. A. Lyophilized Aβ42 (0.9 mg) was reconstituted in NaOH followed by aCSF/TRIS buffer to a final Aβ42 concentration of 200 µM. The sample after centrifugation was injected into Superdex 75 column, and 0.5 mL fractions were eluted to obtain a UV absorbance trace at 280 nm (red solid line). The first peak obtained was Aβ42 protofibril and the subsequent for Aβ42 monomer (Paranjape, 2012). **B.** SEC-purified two peaks were investigated by CD. CD spectra presented for Superdex 200 isolated Aβ42 monomer

(red, solid line) and for Aβ42 protofibril (blue, solid line). Spectra were represented as mean residue ellipticity (Dhami, Karki, et al. 2022).

3.2. SEC purification of Aβ42 monomers

Previously, the Aβ42 monomer has been purified in Nichols lab with Superdex 75 (Paranjape, Gouwens, et al. 2012, Nichols, Colvin, et al. 2015). For the purification process, the dry Aβ aliquot (0.9 mg) was reconstituted in a solution containing 10 mM NH_4OH and 6 M guanidinium hydrochloride (GuHCl) and then incubated for 10-20 minutes at room temperature. A mild basic condition such as NH_4OH helps retain small species purification which is a monomeric form. GuHCl ensures that Aβ42 does not get misfolded to aggregated structures and remains in a denatured, monomeric form. Superdex 200 column was accidentally used on the AKTA FPLC system one time in August 2019 which yielded heterogeneous chromatographic isolation of Aβ monomer (peak 4) along with two oligomeric peaks (peak 2 and 3) and a void peak 1 (Figure 3.2). Thus, Superdex 200 isolation of Aβ42 displayed four separate peaks in contrast to Superdex 75 isolation of protofibril which portrayed two peaks (Figure 3.1A). The protein concentration determined using BCA assay of the monomer peak from the Superdex 200 column was 0.14 mg/mL. Thioflavin T binding of the peak fraction confirmed that peak 4 is a monomeric species.

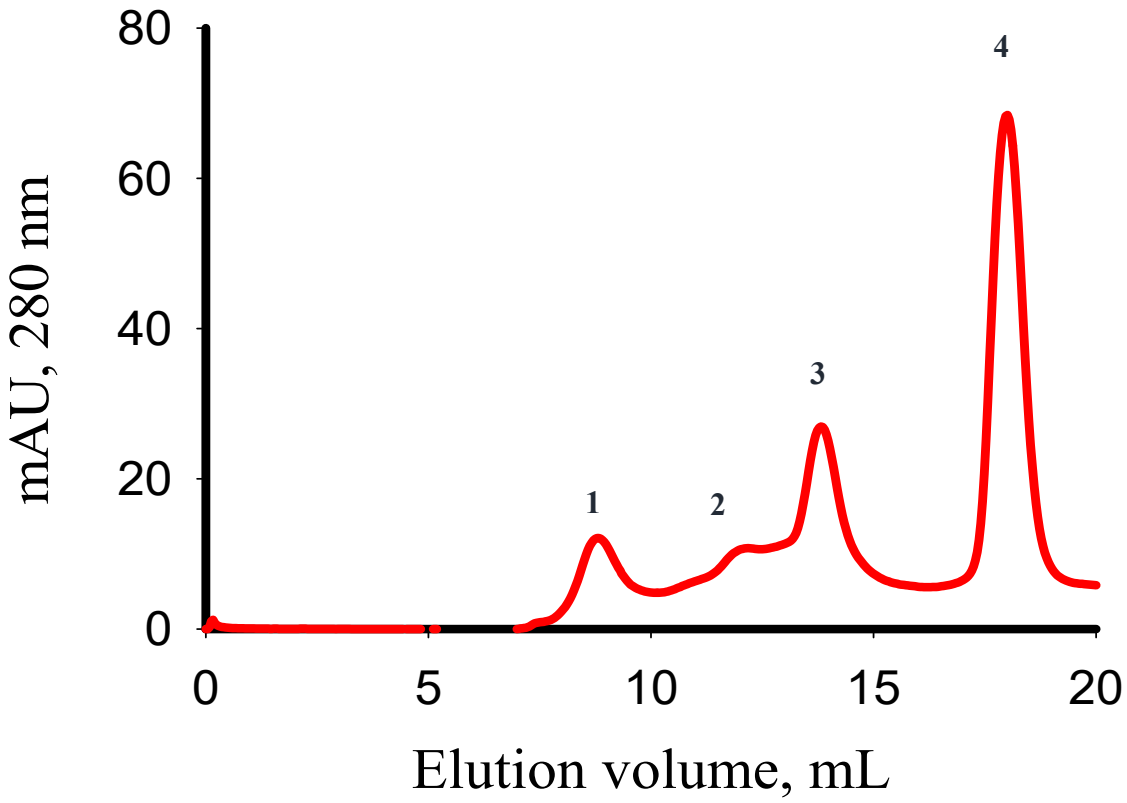

Figure 3.2. SEC purification of Aβ42 using Superdex 200 column. Superdex 200 in line with UV absorbance measurement using AKTA FPLC system. Peak 1 is the void volume, peak 2 and 3 represents oligomer 2 and 3, and peak 3 is the purified monomer. 0.5 mL fractions eluted and stored at 4°C for monomer-based experiments.

The usual monomer fractions were established as fractions 32, 33, and 34 when Superdex 200 was used. Some of the previous purifications in December 2020 revealed that the Aβ42 monomer might be subjected to further cleavage. It was hinted that the monomer never aggregated with thioflavin T fluorescence measurements when used in assays. For such purification preps, monomer fractions 33 and 34 were pooled together and re-purified using Superdex 200 column. The monomer recovered in the fraction range of 35-38. However, the problem was solved when freshly prepared denaturing reagent (GuHCl) was used.

3.3. Production of serum polyclonal antibodies from immunization of a rabbit with Aβ42 protofibrils

In line with the detrimental effect posed by Aβ42 protofibrils, Nichols laboratory isolated and characterized Aβ42 protofibrils. These were shipped to Pacific Immunology (Ramona, CA, USA) for immunization of rabbits with Aβ42 protofibril. Pre-immune serum was obtained from two New Zealand white rabbits (PAC-10079 and PAC-10080) before immunization with 0.1 mg of protofibril in Complete's Freund's Adjuvant. Three more immunizations were performed with 0.1 mg of protofibril in Incomplete Freund's Adjuvant. Five separate bleeds were sent back to UMSL. The bleeds contained high titer antiserum of the polyclonal antibodies termed Antibody St. Louis (AbSL). Rabbits 79/80, 39-40, and 55-56 were separate immunization projects. Nichols lab worked with Pacific Immunology to construct an Aβ protofibril affinity column with Aβ42 protofibril-conjugated resin and the AbSL serum from the column eluted with 0.2 M glycine at low pH. These antibodies were, thus, affinity-purified later in multiple batches and known as apAbSL (Colvin and Roger et al. 2017).

AbSL has been examined in multiple formats by the ELISA technique and is shown to sensitively detect Aβ42 protofibrils. Moreover, the antibody displayed strong affinity and was highly selective for Aβ42 protofibrils over Aβ42 monomer and fibrils even at a lower concentration range of Aβ42 protofibrils (Figure 3.3).

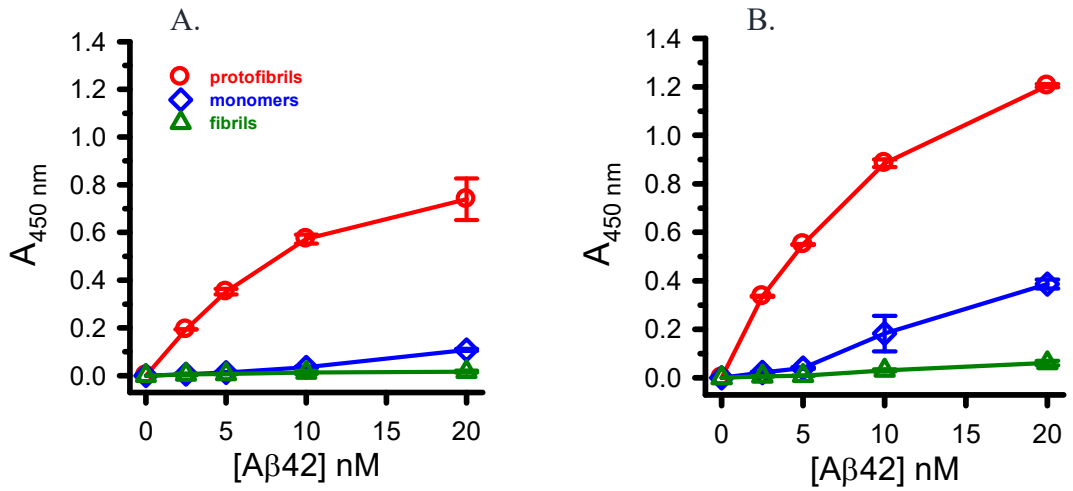

Figure 3.3. AbSL antiserum displays selectivity for Aβ42 protofibrils. 96-well ELISA plates were coated with a concentration range of Aβ42 protofibrils, Aβ42 monomers, and Aβ42 fibrils (2.5-20 nM) and analyzed by indirect ELISA with AbSL anti-serum (1:50,000 dilution). ***A***. Serum from rabbit #55. ***B***. Serum from rabbit #56. Data points (± SEM) represent the average of n=3 trials

The study was initiated by absorbing Aβ42 protofibrils over a 96-well plate with a concentration range of 320 nM -5 nM. Three different incubation times were used to allow the Aβ42 protofibrils to stick to the plate: overnight adsorption, 2h-adsorption, and 1h-adsorbtion (Figure 3.4A). AbSL PAC 55-1 (1:10,000) was used as the primary antibody. It was observed that there is minimal difference in the binding curve between different incubation times for Aβ42 protofibril plating. Therefore, for future indirect ELISA experiments, the plating was generally carried out with 1h incubation. The binding kinetics of many AbSL antibodies were conducted by coating ELISA plates with Aβ42 protofibrils. One such experimental setup is shown in Figure 3.4B, AbSL PAC 39 and PAC 80 (1:5000) were used as primary antibodies. It was noticed that bleed 1 had the lowest affinity as compared to the subsequent bleeds. The observation was held for PAC 39 and 80 (Figure 3.4B). Indirect ELISA on almost all the AbSL antibodies was conducted and curve-fitting on SigmaPlot software yielded K_d and B_{max} for AbSL using

the single rectangular hyperbola equation $y = ax/(b + x)$, $B = (B_{max} * L)/(K_d + L)$. Dissociation constant K_d was calculated for PAC 39, 40, 55, 79, 80, and their respective bleeds. The values ranged between 5 nM to 35 nM with the most efficient binding at 80-1.

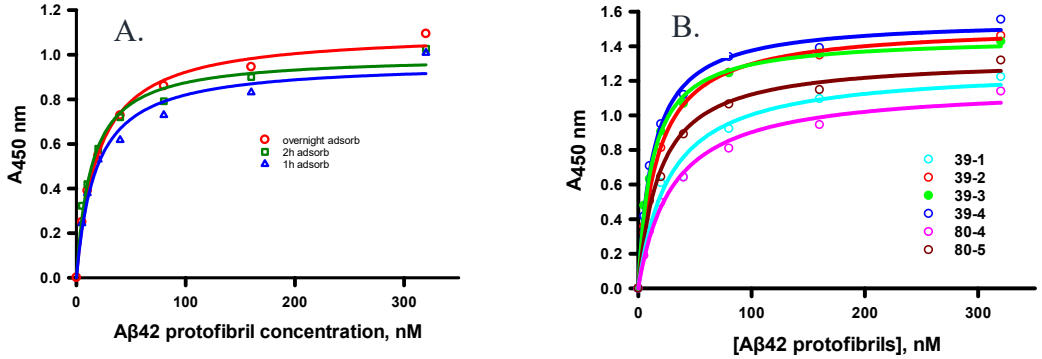

Figure 3.4. AbSL ELISA optimization and recognition of Aβ42 protofibrils with high affinity. ELISA plates were adsorbed with Aβ42 protofibrils at a concentration range of 320 nM-5 nM and analyzed by indirect ELISA. Secondary Ab used was anti-rabbit IgG as **A.** The wells were adsorbed overnight, for 2h and 1h with Aβ42 protofibrils. AbSL antiserum PAC 55-1 (1:10,000 dilution) was used as primary Ab. **B.** AbSL PAC 39 and 80 (1:5000) were used as primary antibodies. Different bleeds were tested for affinity with protofibrils. SigmaPlot curve fitting was done using single rectangular $y = ax/(b + x)$, $B = (B_{max} * L)/(K_d + L)$

After the careful establishment of indirect ELISA protocol, selectivity curves of serum AbSL were generated by plating Aβ42 protofibrils, monomer, and fibrils on 96-well plates with the same concentration range as mentioned before. Figure 3.5 shows the use of PAC 56-1 with two different dilutions of the antibody (1:10,000 and 1:50,000). Higher antibody concentration changes the absorbance values. Titer antibody concentrations can be determined by tweaking the dilution for antibodies as shown here. Thus, AbSL was able to selectively recognize protofibrils as compared to monomers and

fibrils. Several such experiments displayed similar results. There is a significant difference between protofibril and fibril recognition by serum AbSL.

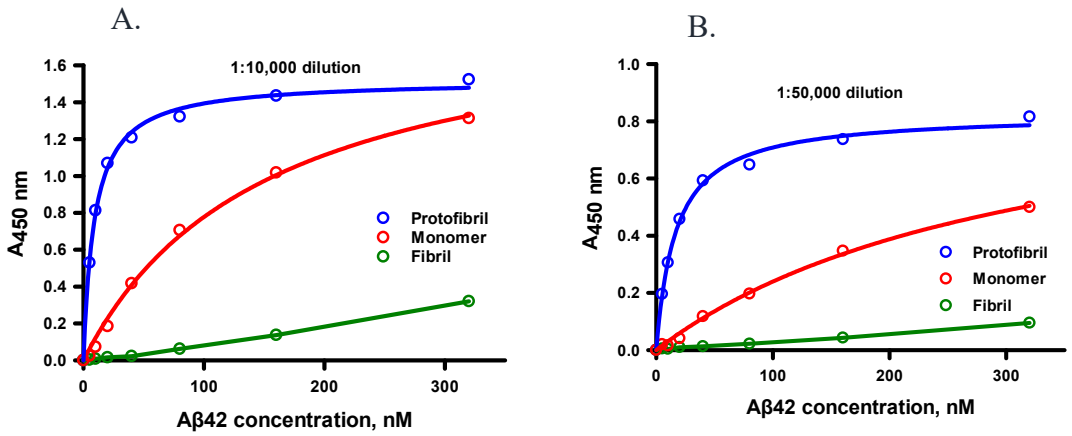

Figure 3.5. AbSL PAC 56-1 selectively recognizes protofibrils over monomers and fibrils. ELISA plates were adsorbed with Aβ42 protofibrils, monomers, and fibrils with a similar concentration range of 320 nM- 5 nM and examined by indirect ELISA. Secondary Ab used was anti-rabbit IgG HRP-conjugated **A.** 1:10,000 dilution of 56-1 used. **B.** 1:50,000 dilution of 56-1 used.

Competition ELISA studies examined the true measure of the dissociation constant (Englund et al. 2007, Jin et al. 2018). The 96-well plates were coated with 80 nM (18 ng/well) Aβ42 protofibrils. Several attempts on competition ELISA were performed to determine the appropriate concentration range of Aβ42 protofibrils to be incubated with AbSL PAC 56-1 (1:10,000 dilution). The concentration range was expanded to obtain a suitable inhibition curve (Figure 3.6A). Semi-log plot was created on Sigma Plot software with a 3-parameter Hill plot. Inhibition ELISA studies yielded a dissociation constant of 5 nM for the interaction of AbSL and Aβ42 protofibril (Figure 3.6B).

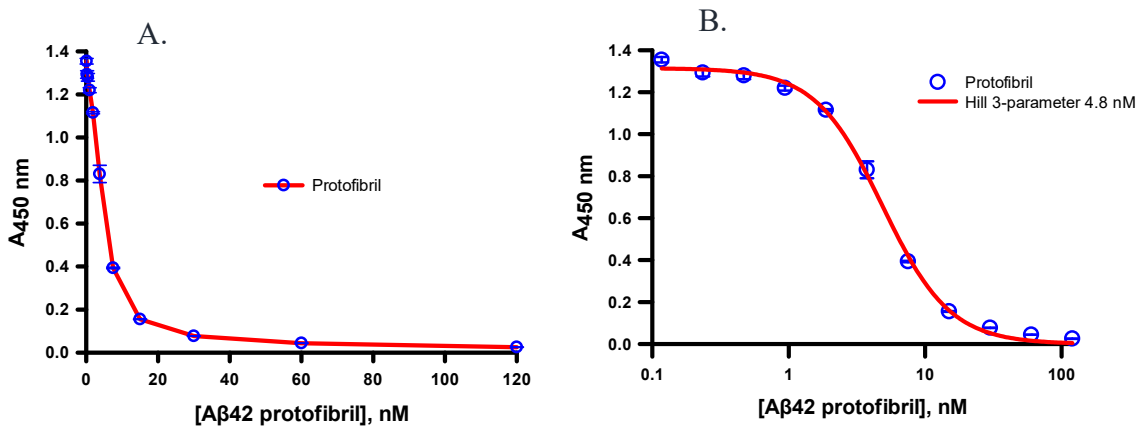

Figure 3.6. Competition ELISA data with a fixed concentration of Aβ42 protofibrils (18 ng/well) coated in the plate. A. The primary antibody AbSL PAC 56-1 (1:10,000) was incubated with an increasing concentration range of 0.12 nM - 120 nM Aβ42 protofibrils in separate tubes for 1 hour. The secondary Ab used was anti-rabbit IgG horseradish peroxidase-conjugate. Data points (± standard error measurements, SEM) represent the average of n=3 trials and **B.** were fit to a 3-parameter Hill plot equation using SigmaPlot software. The curve-fitting of the data provided a Kd value of 4.8 nM.

Serum AbSL antibodies were affinity purified (apAbSL) by other researchers in the Nichols laboratory and this work will be further described in a forthcoming manuscript. A titer indirect ELISA was used to determine suitable concentrations of apAbSL to be used in subsequent experiments (Figure 3.7A). Both serum AbSL and apAbSL (1:10,000 dilution) were tested in an indirect selectivity ELISA with antigen Aβ42 protofibrils and monomers. Although the concentration is not known for the serum AbSL antibody, both serum AbSL and apAbSL displayed similar affinity and selecitivity towards Aβ42 protofibrils and Aβ42 monomers (Figure 3.7B).

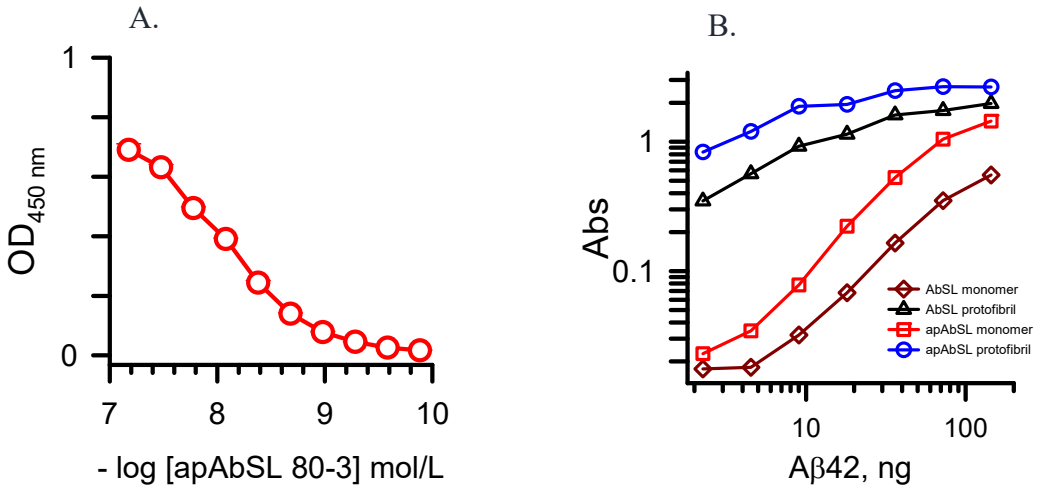

Figure 3.7. Affinity-purified ELISA data. A. Affinity-purified AbSL 80-3 response when varying the AbSL concentration with fixed Aβ42 protofibrils concentration. B. AbSL 80-6 compared with the affinity purified AbSL 80-6. Comparison by indirect ELISA. Stock [apAbSL] is 0.5 mg/mL, diluted by 1:10,000. Dilution for AbSL 80-6 was also kept the same. **B.** Curves for AbSL and apAbSL with Aβ42 protofibrils and monomers compared on a log-log plot (Experiment performed by Nyasha Makoni).

In order to provide some historical context on AbSL antibodies, a study between the Nichols and Combs laboratories revealed interesting insights on Aβ pathology in a 15-month-old APP/PS1 mice when stained with AbSL antiserum. 4G8 antibody which binds to residues 17-24 on Aβ and does not distinguish between aggregated or unaggregated Aβ, was used for comparative studies. Confocal imaging on brain tissues outlined the differentially accessible plaque-like areas by both AbSL and 4G8. Although some degree of colocalization was noticed, AbSL recognized unique regions of Aβ structure that were not stained by 4G8 (Colvin, Rogers, et al. 2017) (Figure 3.8). Furthermore, serum AbSL was used in internalization experiments to detect the engulfment of Aβ42 protofibrils by microglia (Gouwens, Makoni, et al. 2016, Gouwens, Ismail, et al. 2018)

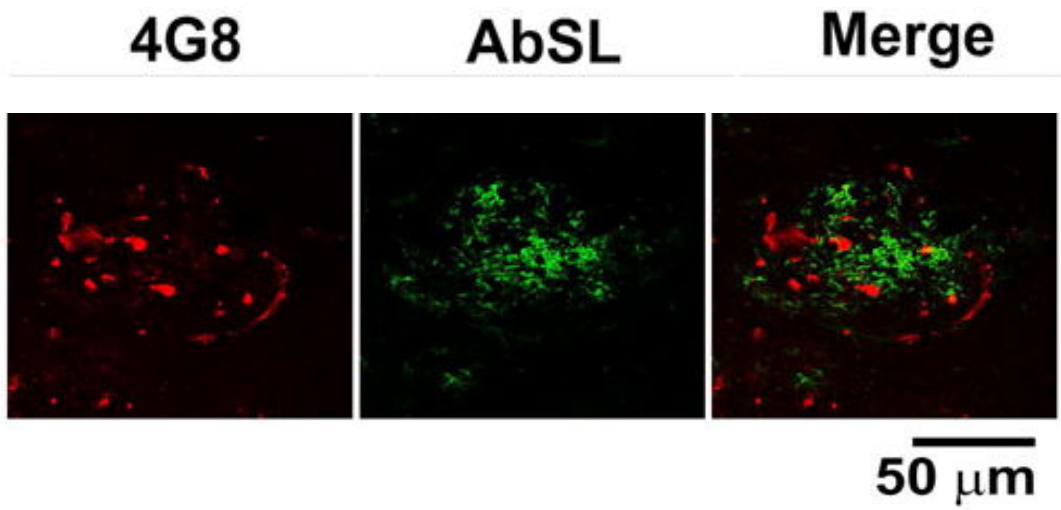

Figure 3.8. Distinct areas of Aβ pathology recognized by AbSL. Brain slices from 15-month-old APP/PS1 mice were stained with 4G8 monoclonal antibody (red) and Aβ protofibril-selective antibody AbSL (green). Little colocalization was seen (Colvin, Rogers, et al. 2017)

3.4. Cloning, expression, purification, and characterization of monoclonal antibodies selective for Aβ42 protofibrils

Due to the interest in Aβ42 protofibrils, which are suggested to cause neurodegeneration in AD (Syvänen et al. 2017), the development of monoclonal antibodies was actively worked on. Our lab prepared and generated Aβ42 protofibrils in aCSF using SEC-purification on Superdex 75 column. To obtain the monoclonal antibodies, SEC-purified Aβ42 protofibrils were mixed with Complete Freund's Adjuvant (CFA), and two New Zealand White rabbits (#55 and #56) were immunized by Pacific Immunology. The second immunization was performed in CFA at 3.5 weeks and the third immunization in Incomplete Freund's Adjuvant (IFA) at 6.5 weeks. Blood was drawn from the rabbits after 1 week of the third immunization. The serum antibodies from the initial bleed of both the rabbits were tested in both titer and indirect ELISA, demonstrated significant selectivity towards Aβ42 protofibrils over Aβ42 monomers and

Aβ42 fibrils and this finding was consistent with our previous observations for the development and characterization of serum AbSL antibody.

The spleens from both rabbits were obtained 5 days after the initial bleed and were delivered to Exon Bio (San Diego, CA) for monoclonal antibody development. Individual B-cells were isolated from spleen lymphocytes using Single Plasma Cell Interrogation (SPIN®) microfluidic technology. This required the use of biotinylated Aβ42 protofibrils. There was a substantial aggregation of Aβ42 protofibril encountered during labeling with sulfo NHS-LC-biotin ester that altered the structure, morphology, and properties of protofibrils. However, NHS-PEG_4-biotin ester worked efficiently as a probe to obtain biotinylated Aβ42 protofibrils (Figure 3.9A). Biotinylated Aβ42 protofibrils were centrifuged to ensure the removal of any fibrillar species formed during the process which was followed by SEC purification. Aβ42 protofibril was predominantly eluted with a little amount of monomer formation (Figure 3.9.B). Testing unlabeled Aβ42 protofibrils and biotinylated Aβ42 protofibrils by coating the plates followed by the addition of streptavidin-HRP conjugate confirmed the success of Aβ42 protofibril biotin labeling (Figure 3.9.C). Serum AbSL antibody #55 recognized biotinylated Aβ42 protofibrils to the same extent as unlabeled protofibrils using indirect ELISA format (Figure 3.9.D). CD analysis on the labeled Aβ42 protofibril confirmed that the labeling procedure did not alter the β-sheet rich secondary structure of protofibril (Figure 3.9.E).

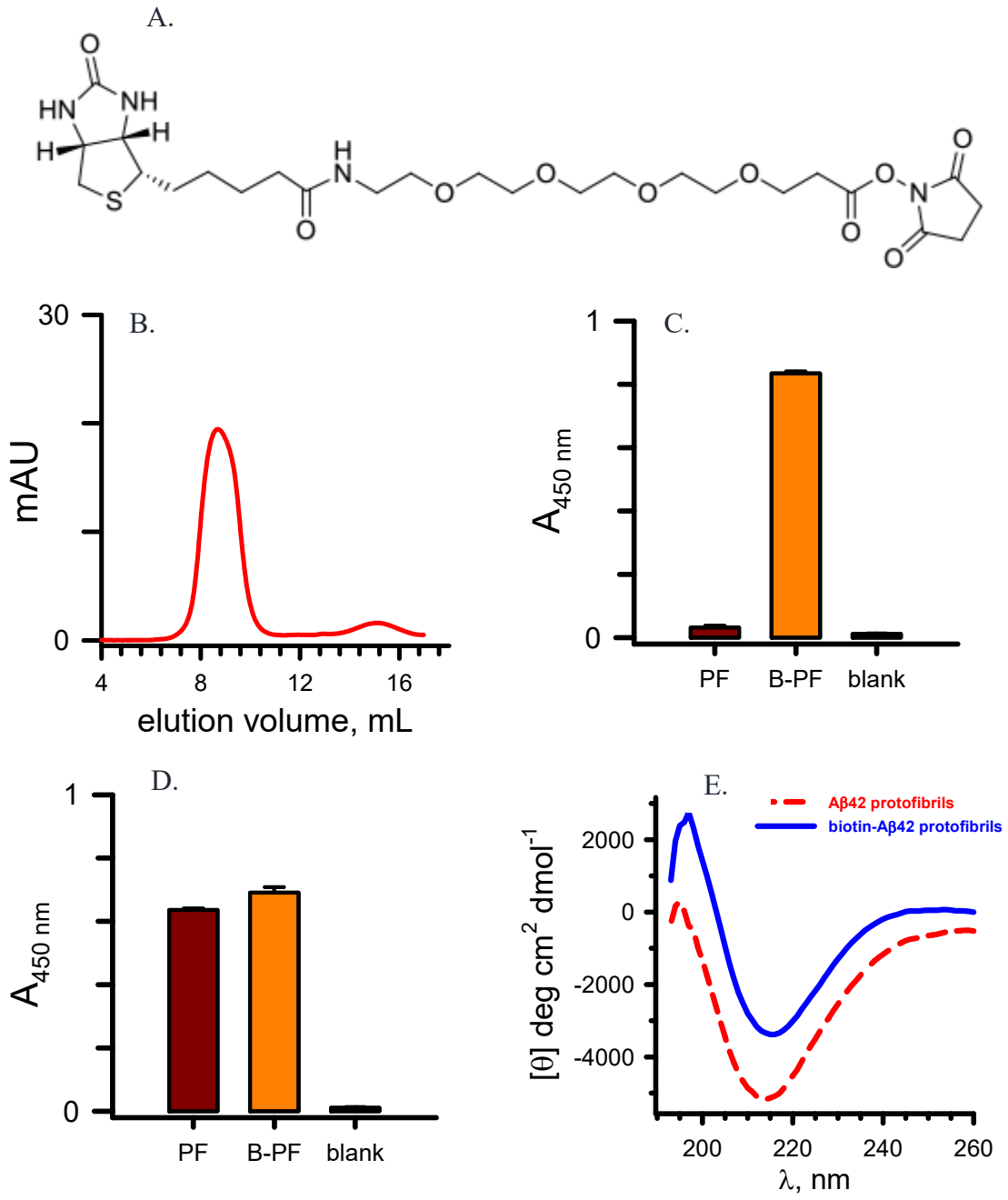

Figure 3.9. Biotinylation of Aβ42 protofibrils does not alter their characteristics. ***A***. NHS-PEG$_4$-Biotin with a molecular weight of 588.67 and spacer arm length of 29 Angstrom. It was used for labeling Aβ42 protofibrils. ***B***. Abs$_{280\ nm}$ trace during Superdex 75 elution of biotinylating mixture. ***C***. Three fractions from the SEC void peak in panel A (8-9.5 mL) were combined (24 μM, 0.11 μg/μL). ELISA plates were coated with unlabeled protofibrils and the SEC-purified protofibril product of the labeling reaction (0.044 μg) followed by incubation with streptavidin-HRP conjugate. The final step of the reaction was Abs$_{450\ nm}$ determination. ***D***. ELISA plates were coated with 0.29 μg

unlabeled (PF) and biotinylated protofibrils (B-PF) and analyzed in an indirect ELISA format. Serum AbSL antibody #55 from Supp Fig 1A was used as the primary antibody (1:5000) and anti-rabbit IgG-HRP as the secondary antibody. ***E***. CD spectra for 24 μM unlabeled (red, dashed line) and biotinylated protofibrils (blue, solid line). For panels B & C, data points (± SEM) represent the average of n=3 trials (Work done by previous lab members)

Exon Bio isolated mRNA for the heavy chain and light chain variable region from single B-cells was PCR-amplified and converted into cDNA by reverse transcription and cloned into pRab293 HC and LC vectors containing the rabbit IgG constant regions. Small-scale transfection of HC and LC into HEK 293 cells was performed. Supernatants were collected from high-throughput expression (small-scale expression) in two separate rounds and sent to our lab for screening for protofibril affinity and selectivity. The first round of evaluation of 41 cell expression supernatants yielded two monoclonal antibodies with notable affinity for protofibrils with mAbSL113 being the topmost candidate for affinity towards protofibril and mAbSL 108 showing a little sensitivity towards protofibril (Figure 3.10.A). Monoclonal antibody (mAbSL113) demonstrated high selectivity using a quick ELISA screen with only one concentration of Aβ42 protofibrils, monomers, and fibrils (Figure 3.10.B).

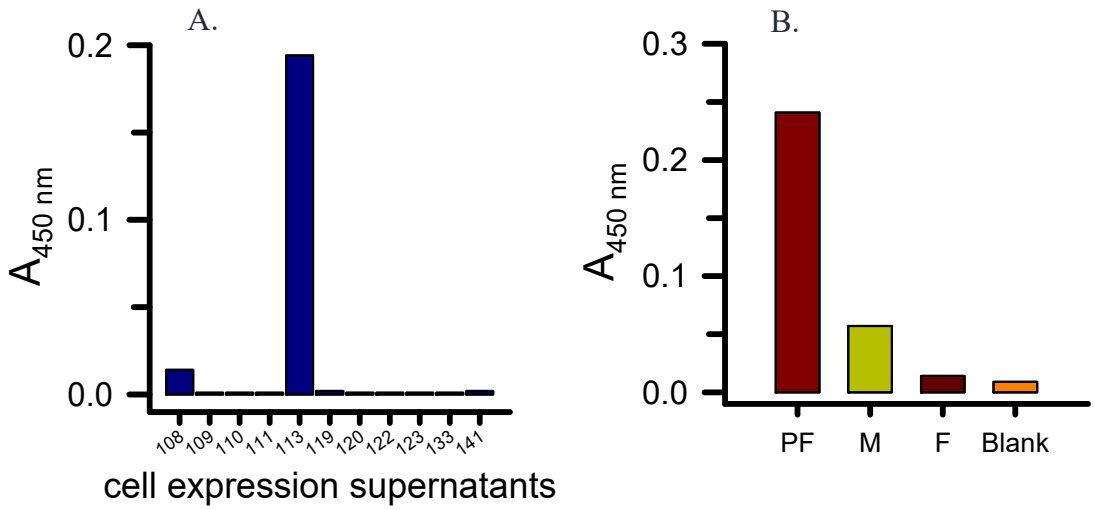

Figure 3.10. Aβ42 protofibril-selective monoclonal antibodies obtained using SPIN® coupled with biotinylated protofibrils. ***A***. The first-round screen of antibody-expressing HEK 293 supernatants. High-binding 96-well plates were coated with Aβ42 protofibrils (1 μg) and probed with the supernatants in an indirect ELISA. 11 of 41 supernatants are shown. ***B***. 96-well plates were coated with Aβ42 protofibrils, Aβ42 monomers, and Aβ42 fibrils (0.5 μg) and probed with supernatant 113 in an indirect ELISA.

Multiple positive hits were recognized in the second round of screening 36 cell-expression supernatants that were evaluated by ELISA to determine affinity to Aβ42 protofibrils (Figure 3.11.A). The selectivity comparisons of the top cell supernatant candidates were drawn with Aβ42 protofibrils, monomers, and fibrils. Furthermore, 2 non-conformational selective Aβ antibodies (Aβ mAb) were identified to be used as controls (Figure 3.11.B). The higher binding candidates were organized by the number showing the raw data (Figure 3.11.C). The data were normalized to the protofibril binding (Figure 3.11.D). The assay allowed the antibodies to be distinguished based on relative affinity and selectivity.

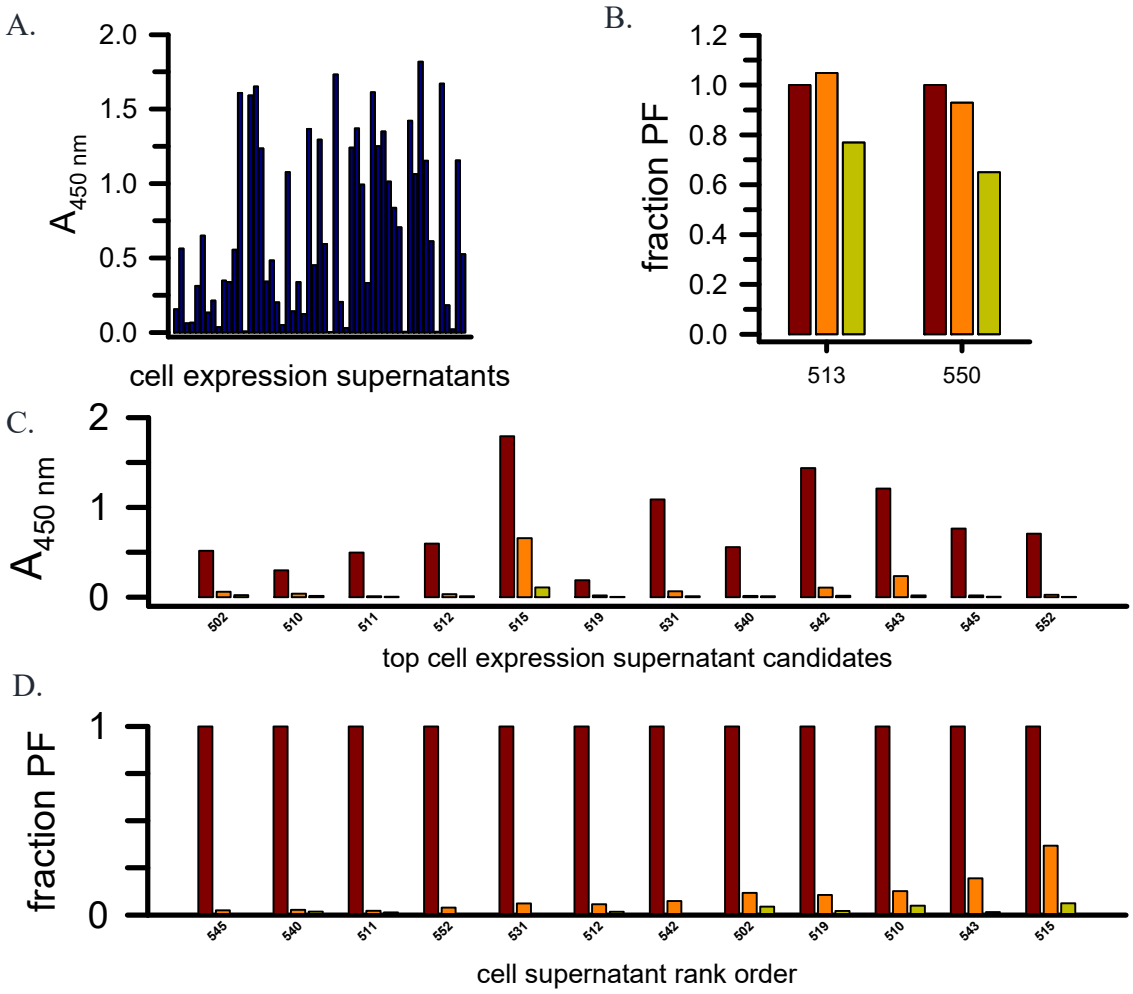

Figure 3.11. The second-round screen of 36 antibody-expressing HEK 293 supernatants. Plates were coated with Aβ42 protofibrils, Aβ42 monomers, and Aβ42 fibrils (0.45 μg) and probed with the supernatants in an indirect ELISA. ***A***. Only Aβ42 protofibril binding is shown for clarity. ***B***. ELISA absorbance data for two of the non-conformation-selective Aβ antibody-expressing HEK 293 supernatants. ***C***. Raw ELISA absorbance data for both affinity and selectivity of second-round antibody candidates. ***D***. The ELISA data was normalized to the protofibril response to demonstrate the rank order protofibril selectivity. (Figure created by Dr. Nichols)

3.4.1. Cloning of HC and LC

Exon Bio sent us the assembled fragment and linearized vector for the positive-monoclonal antibody hits. The assembled fragment contains the HC and LC variable region DNA fragments of the monoclonal antibody clones. The linearized vector has an integration of constant region for rabbit IgG and ampicillin resistant gene. CMV

promoter and the constant region of either HC or LC and terminator on vectors are overlapped with the assembled fragments to make the cloning simpler (Figure 3.12)

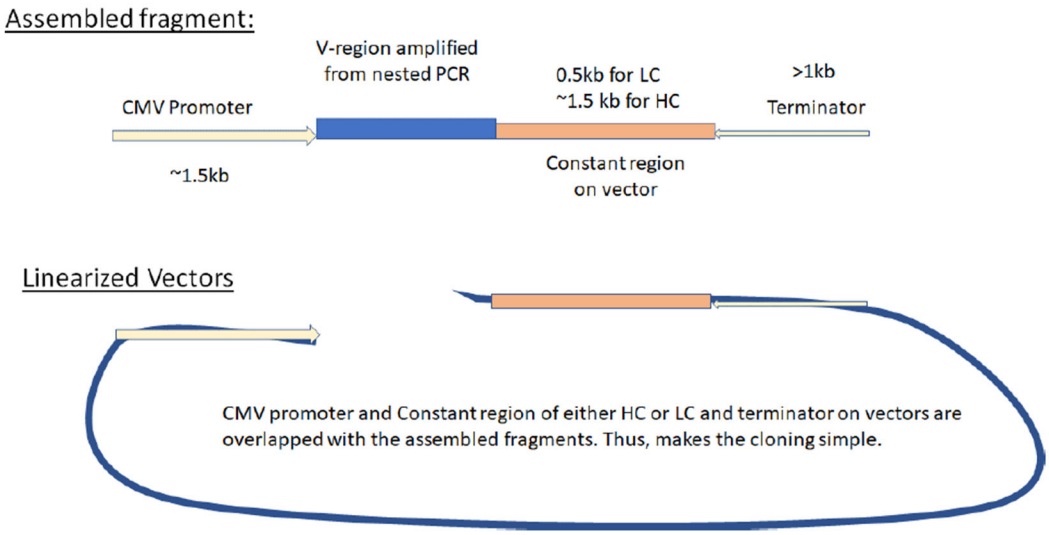

Figure 3.12. Details of assembled fragment and linearized vector sent by Exon Bio to be used for cloning of positive monoclonal antibody hits.

The cloning procedure has been outlined in the Methods chapter in much detail. This procedure was carried out for each monoclonal antibody separately. Essentially, the assembled DNA fragment bearing the V-region was annealed fully to the linearized pRab293 vector for both heavy-chain and light-chain separately using a PCR thermocycler. The vector used for the heavy chain of 10 assembled fragments was pRab293H2 and for the light-chain of 10 assembled fragments was pRab293L3.

The plasmid (2 µL) for HC and LC was transformed to DH5-α competent cells (50 µL) by heat shock in separate tubes, spread to ampicillin treated agar plate and the transformation plate each for HC and LC was incubated for 24 hours at 37°C (Figure 3.13A). The bacterial colonies were transferred to a gridded patch plate where single bacterial colonies were grown for 24 hours at 37°C with well-organized, separated, and

marked colonies (Figure 3.13B). This is followed by colony PCR on numerous colonies using forward primer, pRab293-F (atccactttgcctttctctc); reverse primer, RabIgH-R3 (accgtggagctgggtgtgt) for HC and RabIgK-R9 (tggtgggaagatgaggacag) for LC and PCR Master Mix provided. The gel electrophoresis of screening each colony to verify the insertion of the DNA fragment into the vector was ensured with positive inserts at the 0.5 kb mark (Figure 3.14).

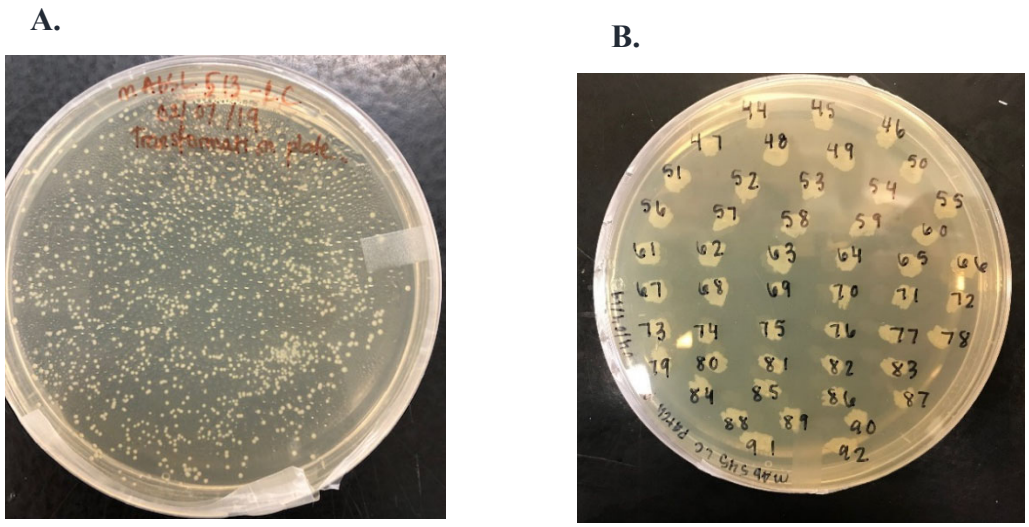

Figure 3.13. Cloning of the variable region for mAbSL 512 HC and LC antibodies was carried out as described. ***A***. Bacterial growth on agar-LB plates after cloning and transformation. ***B***. Preparation of a gridded patch plate using single colonies from the growth plate.

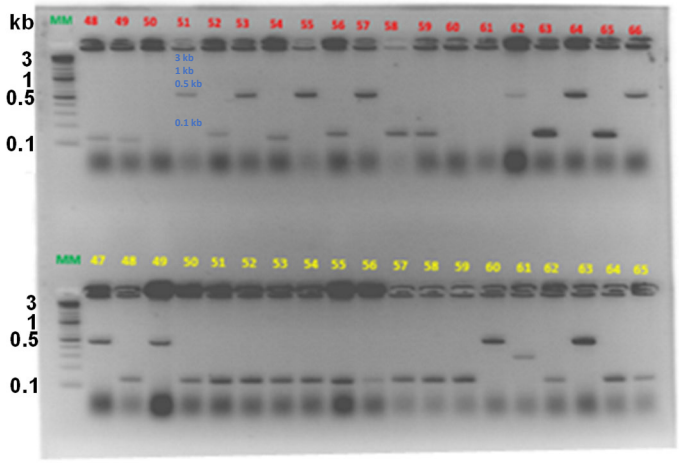

Figure 3.14. Agarose gel electrophoresis after colony PCR of patch plate colonies. Molecular weight markers are in kilobases (kb). The amplified DNA for plasmids containing the inserted variable region was observed at 0.5 kb, while amplified DNA for plasmids lacking the insert was found at just above 0.1 kb. HC positives were observed in colonies 51, 53, 55, 57, 62, 64, and 66. LC positives were observed in colonies 47, 49, 60, and 63.

Small-scale purification (mini-prep) of plasmid DNA was performed after recognizing three confirmed insertions of respective variable regions for each antibody HC and LC. The concentration of the obtained plasmid was determined using Nanodrop analysis. The purified DNA was sequenced at Eurofins Genomics using capillary electrophoresis. After the consistent sequence is confirmed from at least 3 bacterial colonies, large-scale purification of the plasmid is conducted using Maxi-prep protocol with similar steps involved in mini-prep. The purified plasmid is brought into 200 µL TE buffer and concentration is determined for it.

Sequence analysis identified amino acid residues within both the HC and LC that consistently differed between the Aβ protofibril-selective mAbSL antibodies and the non-selective Aβ mAbs. Overall, the LC variable-region protein sequences contained high identity with all determined to be 124 amino acids in length. Identity and similarity

scores ranged from 89.5-95.2 and 92.7-97.6, respectively when compared to the non-selective Aβ mAb 513 (Table 3.1). Despite the high sequence identity, several areas of dispersity were found at residues 28, 44, 58, 102-104, and 107-108. The HC variable region sequences also had high homology but displayed more heterogeneity than the LC (identity 66.2-95.7 and similarity 71.7-97.1). The length of the HC variable-region sequences differed by 1 or 2 residues (137, n=1; 138, n=4; 139, n=5). Due to this occurrence, some gaps had to be considered to perform sequence alignment. Multiple areas of HC dispersity were found at residues 35-37, 58-59, and 103-109. The biggest sequence outlier, mAbSL 108, has considerable differences with the other mAbSL antibodies, and displays a lower affinity for protofibrils, yet still retains some selectivity for protofibrils over other Aβ species. A deeper and more specific analysis of the sequences showed locations of particular interest that may play a role in conferring mAbSL selectivity for Aβ protofibrils. For the HC, 5 residues were identified in the HC and 1 in the LC that was consistent in the non-selective Aβ mAbs, but different in the Aβ protofibril-selective mAbSL antibodies (Table 3.2). Interestingly and uniquely, mAbSL 502 matches 5 of the 6 residues common to the non-selective Aβ mAbs and only has the Ser at residue 35, yet still displays selectivity for protofibrils.

Table 3.1. Sequence identities between mAbSL and Aβ mAb antibodies

Heavy chain	Identity	Similarity	Gaps
Aβ mAb 550	95.7	97.1	0
mAbSL 502	95.7	97.1	0
mAbSL 519	90.6	91.4	0
mAbSL 545	90.6	90.6	0
mAbSL 113	84.9	87.8	1
mAbSL 540	82.7	84.9	1
mAbSL 531	82	84.2	2
mAbSL 108	66.2	71.7	13

Light chain			
mAbSL 545	95.2	97.6	0
mAbSL 519	94.4	97.6	0
mAbSL 502	94.4	96.8	0
Aβ mAb 550	92.7	95.2	0
mAbSL 113	91.9	96.0	0
mAbSL 531	91.9	95.2	0
mAbSL 540	91.1	95.2	0
mAbSL 108	89.5	92.7	0

Table 3.2. Notable amino acid differences between mAbSL and Aβ mAb antibodies.

Residue	Aβ mAbs	mAbSLs
HC 35	Arg	Ser, Thr
37	Ser	Tyr
45	Pro	Ala
104	Ile	Glu, Thr, Gln
105	Gly	Ser, Thr
LC 102	Gly	Ser, Ala

3.4.2. Cell-culture and transfection of 293 F cells with heavy-chain and light-chain plasmid

FreeStyle™ 293 mammalian expression system (293 human embryonic kidney cells) was used for large-scale transfection of cloned HC and LC plasmid because these cells have the capability of having suspension growth. They have been well adapted to generate high levels of recombinant protein. The cells were grown in a defined, serum-free FreeStyle™ 293 Expression media stored at 4°C. The medium is optimized to support high-density culture, supplemented with GlutaMAX-I.

At the time of cell culture, an aliquot of 293 F cells was grown in an expression medium and incubated at 37°C in 8% CO_2 at continuous rotation for 2-3 days. Cell counting was performed on at regular basis to ensure healthy growth, good viability, and

enough concentration of cells. The cells were passaged and diluted to 0.2×10^6 viable cells/ml on every third day. Transfection was done using the plasmid DNA and 293 fectin reagent either at a large-scale (120 mL total volume) or a small-scale (30 mL total volume). The cell suspension was prepared by adding the needed volume of cell suspension into a sterile Erlenmeyer shaker flask to which a pre-warmed expression medium was added. DNA-293fectin complex (8 ml) was added to the flask and was incubated shaking at 37°C in 8% CO_2 condition for 72 hrs.

A dot blot was performed after 2 days of transfection confirming the presence of the mAbs. Cells were harvested in 4-5 days by centrifuging for 5 minutes at 1000g. Pellet was discarded, and the supernatant removed which contained the monoclonal antibody (Figure 3.15)

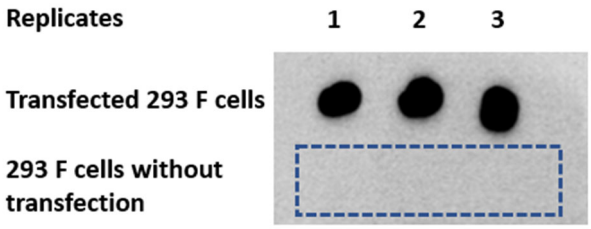

Figure 3.15. Expression of mAbSL antibodies confirmed by dot blot of 293 F cell expression supernatant. Freestyle 293 F cells were co-transfected by HC and LC plasmids from mAbSL 113 (1 µg/mL). The medium was collected from the growing cells and tested. The supernatant after spinning at 1000 g for 5 min was dotted in triplicate onto the membrane and blocked for 1 hour, followed by secondary antibody anti-rabbit IgG Horseradish peroxidase (1:1000 dilution). ECL substrate was applied and imaged using a gel imager.

3.4.3. Expression and affinity purification of secreted monoclonal antibodies

The mAbSL antibodies are secreted directly into the medium making recovery via centrifugation possible. The secreted antibody was loaded to a Protein G column for initial affinity purification work. The equilibrium/wash buffer used was PBS pH 7.4 and the elution buffer was 0.2 M glycine, pH 1.85. Later, the Protein A affinity column (MabSelect Prism A) was used for large-scale transfection and protein A ligand generally binds to the Fc region of an immunoglobulin. The equilibrium/wash buffer used was 50 mM sodium phosphate, 100 mM sodium chloride pH 7.4 and the elution buffer was 100 mM sodium acetate, pH 3.6. The peak fractions were pooled and concentrated using a spin column to usually a final volume of 0.5 ml. Typical yields of the purified antibodies ranged from 10-30 mg/L. The concentrations obtained for all the transfections are provided in Table 3.7. The cloning, purification, and sequencing of the HC and LC plasmid pairs for the 8 antibodies permitted their expression, purification, and characterization of multiple mAbSL and Aβ mAb monoclonal antibodies (Figure 3.16). Each antibody showed varying degrees of selectivity for Aβ42 protofibrils compared to Aβ42 monomers (Figure 3.17)

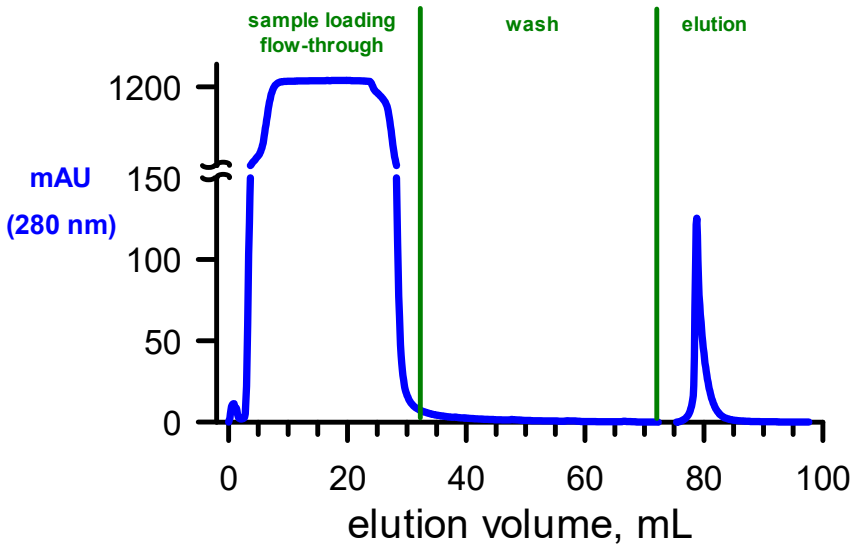

Figure 3.16. Purification of mAbSL antibodies. FreeStyle 293 cells were co-transfected with mAbSL HC and LC plasmids. The transfected cells were centrifuged for 10 min at 5000 g and the supernatant was affinity purified on a Protein G column. Antibody elution was monitored by UV absorbance at 280 nm. The Elution buffer used was 0.2 M glycine, pH 1.86 into 2 mL fractions and were neutralized with 300 µL in 1M Tris-HCl. Eluted fractions were pooled together and concentrated using spin filters. The concentration was determined by measuring absorbance at 280 nm.

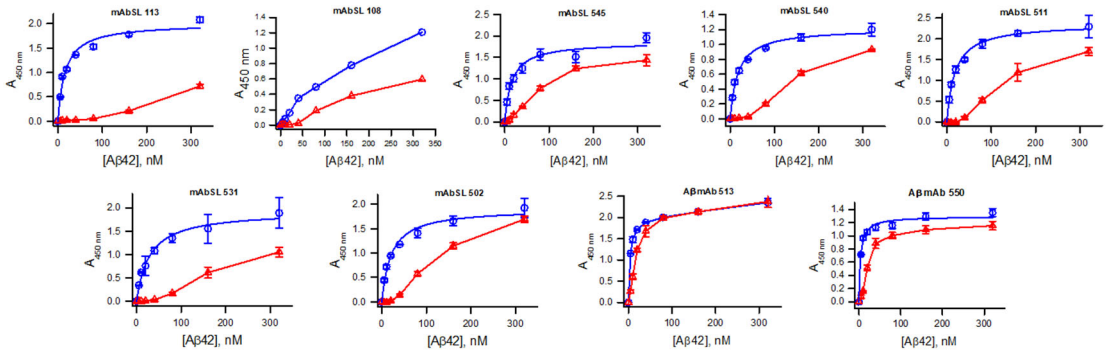

Figure 3.17. mAbSL and Aβ mAb antibodies expressed in-house display different Aβ42 protofibril selectivity. Monoclonal antibodies were assessed for selectivity with an indirect ELISA after expression in FreeStyle 293-F cells and affinity purification. Microplate wells were coated with a concentration range (5-320 nM, 1-72 ng) of SEC-

purified Aβ42 protofibrils (blue circles) or Aβ42 monomers (red triangles) and probed with each monoclonal primary antibody. The concentration used for each primary antibody was 0.5 μg/mL, except for mAbSL 108, which was used at 17 ug/mL. Completion of the ELISA provided the final $A_{450\ nm}$ values. Data points (± SEM) represent the average of n=3 trials. (Supervised Antanisha Parks on these experiments)

3.4.4. Monoclonal antibodies offer great selectivity towards protofibrils

Several ELISA studies were performed on the generated monoclonal antibodies. Indirect ELISA studies were carried out on recombinantly expressed antibodies mAbSL 511, mAbSL 113, mAbSL 540, and mAbSL 545. Curve-fitting using a single rectangular hyperbola, y=ax/(b+c) yielded Kd as 23 nM, 16 nM, 21 nM, and 9 nM respectively (Figure 3.18A). One of the mAbSL antibodies with the highest affinity and selectivity for Aβ protofibrils was mAbSL 113. Dose-dependent mAbSL binding in a titer ELISA to 80 nM (18 ng/well) Aβ42 protofibrils showed a significant interaction even at 0.5 nM mAbSL 113 (Fig 3.18B). A considerably less affinity was displayed by mAbSL 108 for Aβ42 protofibrils with no significant interaction below 10 nM antibody. To better assess the selectivity of mAbSL 113, a competition ELISA was employed whereupon solution Aβ42 protofibrils, Aβ42 monomers, and Aβ42 fibrils competed with Aβ42 protofibrils coated on wells. Nonlinear curve-fitting of the data provided affinity values in terms of the dissociation constant (K_d). A K_D of 7 nM was determined for mAbSL 113 binding to Aβ42 protofibrils and a KD of 602 nM for mAbSL 113 binding to Aβ42 monomers (Fig 3.18C). This represented nearly 2 orders of magnitude preference of mAbSL 113 for Aβ42 protofibrils relative to monomers. In a separate competition ELISA comparing protofibrils and fibrils, KD values of 2 nM and 153 nM were determined for mAbSL 113 binding to Aβ42 protofibrils and fibrils, respectively (Fig 3.18D).

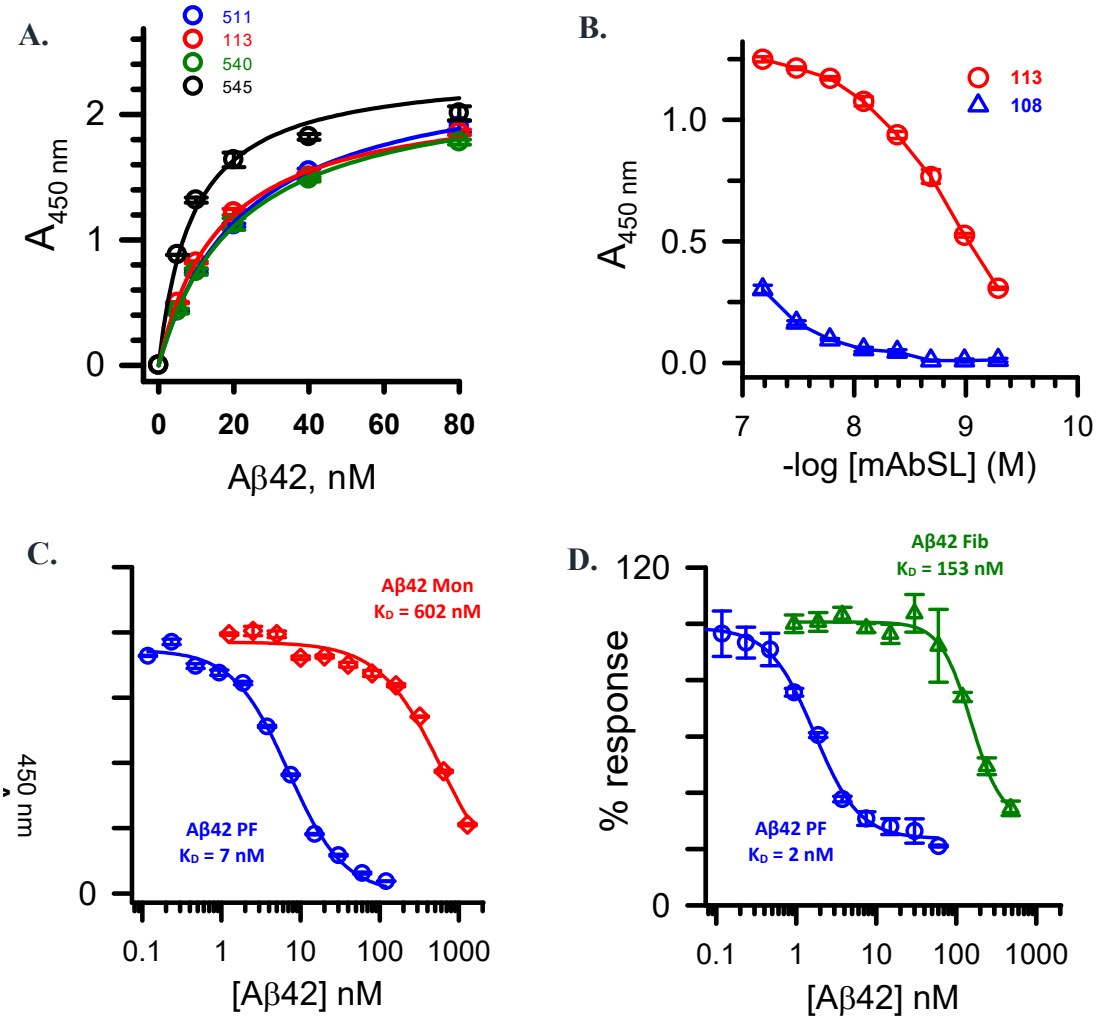

Figure 3.18. ELISA reveals affinities of mAbSL 113 for Aβ42 species. ***A***. Aβ42 protofibril-selective expressed mAbSL preferentially binds to Aβ42 protofibril as assessed by indirect ELISA. Absorbance trace A_{280} nm obtained by plating ELISA plated with Aβ42 protofibril in the concentration range of 80 nM -5 nM. Each data point is the average ± standard error for three independent measurements. Curve-fitting of the data was performed using Sigma Plot. Data points (± standard error measurements, SEM) represent the average of n=3 trials and were fit to a 3-parameter Hill plot equation using SigmaPlot software. The curve-fitting of the data provided K_d value shown in the plot. ***B***. Different ELISA formats (titer, indirect) were used to assess mAbSL antibodies. 96-well ELISA plates were coated with Aβ42 protofibrils (18 ng/well) and probed with a concentration range of affinity-purified mAbSL 113 (red circles) or mAbSL 108 (blue triangles) antibodies. Competition experiments were conducted as described in the Methods between solution Aβ42 protofibrils, Aβ42 monomers, and Aβ42 fibrils and Aβ42 protofibrils coated on wells. ***C***. Solutions containing mAbSL 113 (1 µg/mL) and a concentration range of Aβ42 protofibrils (0.12-120 nM) and Aβ42 monomers (1.25-1280 nM) were incubated for 1 h prior to application to the protofibril-coated wells (18

ng/well). An indirect ELISA yielded the final $A_{450\ nm}$ values. Data points (± standard error measurements, SEM) represent the average of n=3 trials and were fit to a 3-parameter Hill plot equation using SigmaPlot software. The curve-fitting of the data provided K_d value shown in the plot. ***D***. In a separate competition experiment, solutions containing mAbSL 113 (0.1 μg/mL) and a concentration range of Aβ42 protofibrils (0.06-60 nM) and Aβ42 fibrils (0.94-480 nM) were incubated as in panel A and applied to protofibril-coated wells (18 ng/well). The final ELISA $A_{450\ nm}$ values for each species were normalized to the lowest concentration of each competitor (highest $A_{450\ nm}$) and presented as % response. Data points (± SEM) represent the average of n=3 trials for both panels. Data were fitted with a 4-parameter Hill equation using SigmaPlot software, which provided K_D values shown in the graphs.

3.4.5. High-throughput transfection using deep-well plate

The expression of all mAbSLs in high-throughput transfection with 2 mL cell expression volume. The supernatants were directly assessed without affinity chromatographic purification of the secreted antibodies. High-throughput expression of mAbSLs and Aβ mAbs in deep-well plates provided a rapid method for evaluating the expression and conducting characterization studies before purification. Indirect selectivity ELISA studies using cell-free supernatants obtained from the expression wells demonstrated varying degrees of selectivity for Aβ42 protofibrils over monomers by the 8 different mAbSLs and no conformational selectivity by the 2 Aβ mAbs (Figure 3.19A,B).

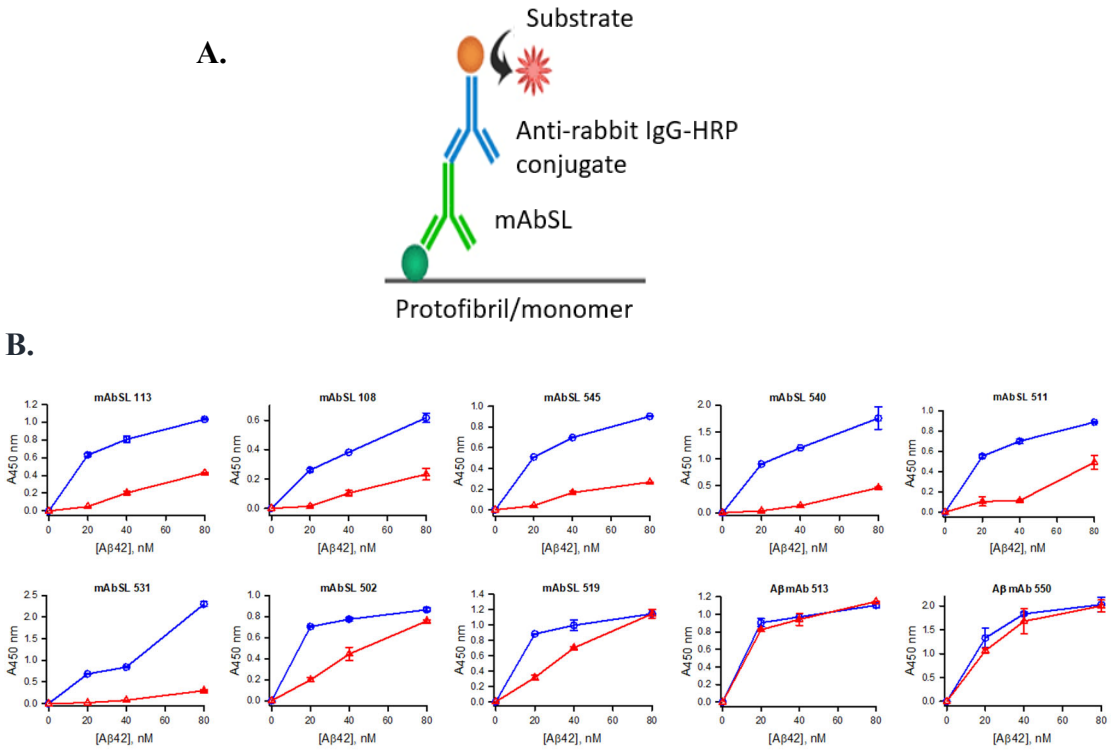

Figure 3.19. High-throughput expression permitted rapid assessment of multiple mAbSL antibodies. A. Schematic of ELISA arrangement**. B.** Small-scale expressions were performed in FreeStyle 293-F cells using a deep-well cell culture plate (2 mL volume). After 3 days of expression, cell-free supernatants were directly assessed for selectivity with an indirect ELISA. Microplate wells were coated with 20, 40, and 80 nM (0.1 mL) of SEC-purified Aβ42 protofibrils (blue circles) and Aβ42 monomers (red triangles) for 1 h followed by application of 0.1 mL cell-free supernatants containing mAbSLs or Aβ mAbs. Completion of the ELISA provided the final $A_{450\ nm}$ values. Data points (± SEM) represent the average of n=2 trials. (Supervised Ryan Domalewski and Gabriel Riggio on these experiments)

3.5. Conclusion

It has been challenging to discover conformational-selective monoclonal antibodies that preferentially bind to Aβ42 protofibril over monomers and fibrils. The task is tedious to perform because of the transient nature of Aβ42 protofibril and the structural polymorphism displayed (Bonito-Oliva, Schedin-Weiss, et al. 2019). The findings presented in this chapter describes the success in the development, cloning, sequencing, expressing, and purifying of a novel class of Aβ conformation-selective

monoclonal antibody which confers selectivity and access for soluble Aβ-protofibrils named Antibody St. Louis (mAbSL). Polyclonal serum antibody (AbSL) and monoclonal antibody (mAbSL) display significant selectivity towards protofibrils and lower affinity towards Aβ monomers and fibrils. Thus, it can be concluded that mAbSL can discern differences between Aβ protofibril structure and Aβ fibril structure with greater sensitivity than other conformational selective antibodies in the field such as BAN2401 and Aducanumab. AbSL recognizes Aβ forms in AD mice brains that may not be easily detected by conventional Aβ antibodies (Colvin, Rogers, et al. 2017).

The information provided includes new developmental methods and expanded antibody analysis. Aβ protofibril selectivity has been ascertained by adopting ELISA strategies including indirect ELISA and antigen competition ELISA format. We have also successfully expressed and characterized 8 mAbSL antibodies in a high-throughput fashion using 2 mL deep-well cell culture plates. The procedure involving smaller volume yielded sufficient antibodies for ELISA testing. Aβ mAb 513 and 550 were identified as non-selective monoclonal candidates.

Cloning and sequencing of the HC and LC variable regions from multiple mAbSL and Aβ mAb antibodies provided new insights into variable-region amino acid residues that may impart selectivity for one Aβ conformation over another. Cloning and sequence analysis of the mAbSL and Aβ mAb HC and LC variable regions yielded insights into potential regions or residues on the mAbSL antibody that are involved in conformational recognition. There are many combinations of amino acid residues that antibodies utilize for contact sites, but there was some consistency observed for the mAbSL antibodies in the sequence comparison with the non-conformation selective Aβ mAbs. There are few

published reports containing conformation-selective antibody sequence information. A crystal structure of the gantenerumab Fab fragment in complex with Aβ1-11 (PDB 5CSZ) included the gantenerumab HC and LC sequences (Bohrmann et al. 2012). Sequence alignment and comparison with the mAbSL 113 variable regions gave surprising results. Even though gantenerumab is a human antibody and mAbSL 113 is derived from rabbits, there was a high degree of identity and similarity. The HC sequences had 57% identity and 66% similarity with 16 gaps, while the LC sequences had 50% identity and 69% similarity with 10 gaps.

Conformation-selective antibodies that target Aβ have been a significant area of research for many years. Polyclonal antibodies M93/M94 and A11 display significant selectivity for Aβ-derived diffusible ligands (ADDLs) (Lambert et al. 2001) and Aβ oligomers respectively (Kayed et al. 2003). A11 has been used to detect oligomers in brain tissue from AD mouse models (Lesne et al. 2006, Deshpande et al. 2009). Monoclonal antibody NAB61 preferentially recognizes a conformational epitope present in oligomeric Aβ structures (Lee et al. 2006) and was instrumental in elucidating a halo of oligomeric Aβ surrounding plaques in an AD mouse model (Koffie et al. 2009). BIIB037 is a human monoclonal antibody that binds fibrillar Aβ42 with high affinity but does not bind soluble Aβ40 (Goure et al. 2014).

Human monoclonal antibody BiiB037 and the humanized form, aducanumab, display a much greater affinity for aggregated Aβ than for soluble (monomeric) Aβ, reduces soluble and insoluble Aβ in an AD transgenic mouse model, and slows clinical decline in AD patients with mild AD (Goure et al. 2014, Sevigny et al. 2016). Monoclonal antibody mAb158 displays selectivity for Aβ protofibrils and fibrils

(Englund et al. 2007) and its humanized form, BAN2401, reduces Aβ protofibrils in the brain and CSF of an AD transgenic mouse model (Tucker et al. 2015), and rescues neurons from Aβ-induced death (Söllvander et al. 2018). Another humanized monoclonal antibody, gantenerumab, also displays high-affinity binding to aggregated Aβ (Bohrmann et al. 2012, Goure et al. 2014). Thus, achievements have been made to obtain antibodies that are selective for either aggregated or monomeric Aβ. However, the development of antibodies with selectivity between aggregated forms of Aβ (e.g., oligomers, protofibrils, fibrils) has been far less reported. The findings in this report demonstrate the ability of the mAbSL antibody to differentiate between Aβ42 protofibrils and fibrils.

There is both vigorous debate and promise for conformation-selective antibodies in AD therapeutics. Aducanumab was initially deemed as not meeting the primary objectives for AD treatment in clinical trials, but follow-up analysis revealed a reduction in the progression of cognitive and functional impairments in patients receiving the highest dose (Kwon et al. 2020). Based on these results, aducanumab (Aduhelm^{TM}) was approved by the United States Food and Drug Administration (FDA) as the first potentially disease-modifying therapeutic for AD. BAN2401 (Lecanemab) continues to meet expectations in clinical trials (Kwon et al. 2020, McDade et al. 2022, van Dyck et al. 2022), and is likely to seek FDA approval in the coming year. The enthusiasm is tempered somewhat by the modest effects on disease progression (Walsh et al. 2022).

Binding constants obtained for conformation selective Aβ antibodies provide information regarding selectivity between distinct Aβ species. Using an inhibition ELISA, mAb158/BAN2401 (Lecanemab) yielded IC50 values of 6-7 nM for Aβ42 protofibrils and 1200-1400 nM for LMW Aβ42 (monomer) (Englund et al. 2007). As

reported above, mAbSL 113 had KD values in the low nM range (2-9 nM) for Aβ42 protofibrils, 150 nM for Aβ42 fibrils, and 600 nM for Aβ42 monomers in a similar type of binding assay. The apparent affinity (EC50) of aducanumab for aggregated Aβ42 was reported to be 0.1 nM, with no binding observed to monomeric Aβ40 at concentrations up to 1 μM. Aducanumab did bind to bona fide human Aβ fibrils (Sevigny et al. 2016). Equilibrium binding studies using surface plasmon resonance produced binding constants for gantenerumab binding to Aβ fibrils, oligomers, and monomers of 0.6, 1.2, and 1.7 nM respectively (Bohrmann et al. 2012).

Lecenamab (BAN 2401) is an investigational humanized monoclonal antibody that binds to neutralize and eliminate soluble, toxic Aβ aggregates. A recent study demonstrated statistically significant results from a large global Phase 3 confirmatory clarity AD clinical trials. The anti-Aβ protofibril selective antibody had a positive effect on disease pathology and slowed down the progression of the disease. This groundbreaking study with a clinically meaningful impact on cognition and function ensures the effectiveness of therapeutic drugs targeting the early stages of AD. AbSL, a protofibril-selective antibody discerned the differences between conformationally-distinguishable species such as protofibrils, fibrils and monomers.

The newly developed class of antibodies has potential diagnostic and therapeutic utility in AD tissue and patients, and we believe targeting Aβ42 has beneficial effects. The effectiveness and utility of AbSL would ameliorate the current loopholes in AD.

CHAPTER 4: PROPERTIES OF MONOCLONAL PROTOFIBRIL-SELECTIVE ANTIBODY

Studying the effects of the expressed conformational-sensitive antibodies on monomer aggregation and protofibril transition to fibrils is crucial for understanding how monoclonal antibody affects the molecular mechanism of aggregation of amyloid protein and for the exploration of therapeutic aspects of monoclonal in AD. It is critical to understand the impact of mAbSL on Aβ42 monomer folding to form an aggregated assembly. These aberrant soluble assemblies have been known to cause marked degeneration of the neurons and their synapses and thus offer a compelling approach to target the misfolded soluble structures (Huang and Liu 2020, Ono and Tsuji 2020).

A detailed experimental plan was carried out to evaluate the effect of a selective and a non-selective monoclonal antibody on Aβ42 aggregation. Going forward, we aimed to use a selective mAbSL (mAbSL 113) and a non-selective antibody (mAb Aβ 513) to carefully draw differences in the impact of both the antibodies on Aβ42 monomer aggregation and Aβ42 protofibril dynamics. Monoclonal AbSL 113 was one of the first clones to display a highly selective nature towards Aβ42 protofibrils immunogen as compared to Aβ42 monomers and Aβ42 fibrils (Figure 4.1A). In other words, mAbSL 113 is a sequence-independent antibody and it recognizes a secondary or quaternary structure on Aβ42 protofibrils. Monoclonal Ab Aβ 513, on the other hand, exhibited the same reactivity profiles with Aβ42 monomers, protofibrils, and fibrils (Figure 4.1 B). We hoped that working simultaneously with both the characterized antibodies will help us

resolve the mechanism of both a sequence-specific antibody and a non-sequence-specific antibody and will yield us molecular-level insights on the role of monoclonal antibodies in the clearance of Aβ42.

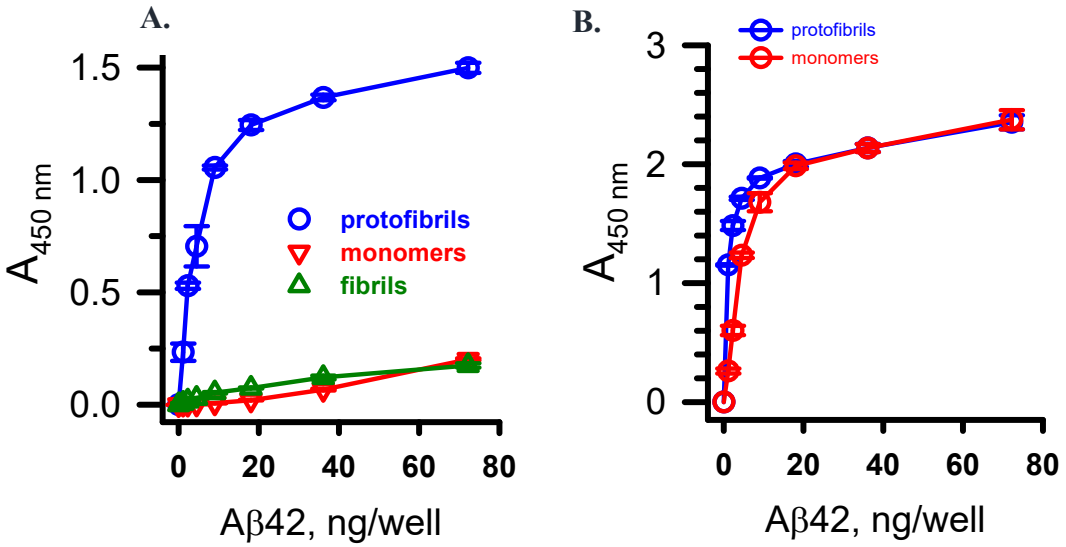

Figure 4.1. Indirect ELISA with a protofibril-selective antibody and a non-selective antibody. A. Microplate wells were coated with a concentration range (5-80 nM, 1-72 ng/well) of Aβ42 protofibrils (blue circles), Aβ42 monomers (red down triangles), and Aβ42 fibrils (green up triangles) and probed with mAbSL 113 (1 µg/mL). **B.** The same experimental set-up for panel B was used to assess mAb Aβ 513 (0.5 µg/mL) selectivity for Aβ42 protofibrils (blue circles) and Aβ42 monomers (red triangles), A similar. Data points (± SEM) represent the average of n=3 trials for all three panels.

The kinetics of Aβ42 monomer aggregation was monitored spectroscopically using thioflavin T fluorescent dye. Thioflavin T (ThT) is a well-known measure of β-pleated sheet content and provides a great way to examine the aggregation advancement of Aβ42. Thus, it is evident that the dye does not associate with solvent exposed monomeric Aβ42 and thus no fluorescence is observed in the presence of monomer (Levine III 1993). The assay is based on variations of the fluorescence confronted on binding with the aggregated amyloid protein. ThT fluorescence was determined by

placing 80 uL of the solution in a quartz cuvette. Fluorescence emission scans (460-520 nm) were acquired on a Cary Eclipse fluorescence spectrophotometer using an excitation wavelength of 450 nm. Emission scans will be integrated from 470-500 nm to obtain ThT relative fluorescence values (RFU).

4.1. Monoclonal antibody inhibits Aβ42 monomer aggregation

Several attempts were made to optimize the conditions necessary to mimic SEC-purified Aβ42 monomer aggregation in the lab. The parameters which were constantly modified included temperature modifications, quiescent or shaking conditions with changes in the speed of the shaker used, buffer system used, the concentration of Aβ42 monomers and thioflavin T dye.

4.1.1. Concentration-dependent effect of selective monoclonal antibody

After successful optimization in a cuvette-based assay, the solution of SEC-purified Aβ42 monomer (5 μM) was incubated quiescently at 37°C in a water bath in the presence or absence of mAbSL 113 for a 15-hour time. The assay was performed in a siliconized tube with two different concentrations of the antibody being 0.5 μM (Aβ42 monomer: mAbSL 113=10:1) and 0.05 μM (Aβ42 monomer: mAbSL 113=100:1). The concentration-dependent inhibition of the conformational-selective antibody was observed with increase in $t_{1/2}$ values with elevated concentration of antibody (Figure 4.2).

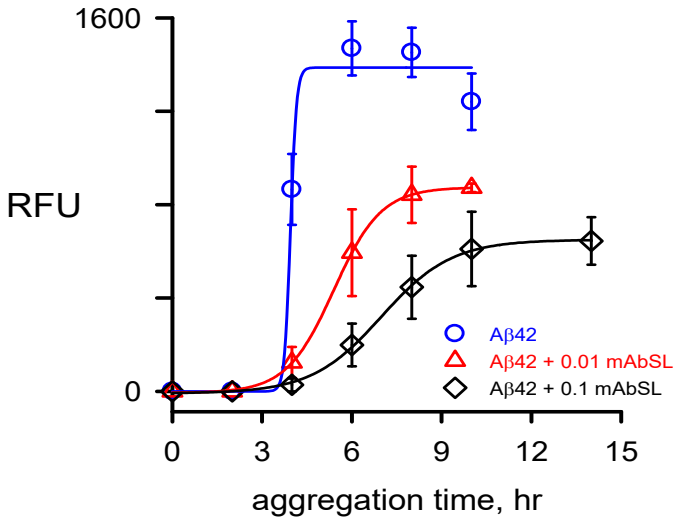

Figure 4.2. AbSL monoclonal antibody inhibits Aβ aggregation at sub-stoichiometric ratios. Solutions of SEC-purified Aβ42 monomer (5 μM) were incubated quiescently at 37 °C (water bath) in low-retention tubes in the absence (circles) or presence of monoclonal AbSL (mAbSL) antibody at 0.01 (triangle) and 0.1 (diamonds) molar ratios to Aβ42. Thioflavin T (ThT) (10 μM) was included in the solution as well as NaN_3 (0.05%) to prevent microbial growth. At selected time points, ThT fluorescence was determined by placing 80 μL of the solution in a quartz cuvette and taking emission scans from 460-520 nm with an excitation wavelength of 450 nm. Numeric values were obtained by integration of the emission curves from 470-500 nm. The cuvette samples were recovered back into their respective tubes and incubated further. Data points and error bars represent the average and standard error for n=3 replicate tubes at each time point for each aggregation solution. Curve fitting was done as described and yielded $t_{1/2}$ values of 3.9 h, 5.4 h, and 6.5 h for Aβ42 alone, Aβ42 + 0.01 mAbSL, and Aβ42 + 0.1 mAbSL respectively.

It is of great interest to carefully examine the impact of our antibodies on Aβ42 aggregation kinetics. Thus, the Aβ42 monomer concentration was increased to 10 μM for the next set of experiments with the monoclonal antibody. The kinetics of Aβ42 monomer aggregation was conducted by incubation with 1 μM concentration of the monoclonal AbSL 113 with constant shaking at 1000 rpm in a low-retention tube (n=3). The buffer system used for the experiment was 50 mM TRIS pH 8.0 buffer with 30 mM salt concentration. The kinetic data were fitted to a 4-parameter sigmoid equation to

determine kinetic parameters $t_{1/2}$ (time at half completion of the aggregation process) and t_{lag} (lag time) (Hellstrand et al. 2009). Aβ42 monomer aggregation in the absence of an antibody yielded a $t_{1/2}$ value of 3.8 h and a t_{lag} of 2.9 h (Figure 4.3). The dotted curves represent the error in Aβ42 monomer aggregation (Figure 4.3). The inclusion of mAbSL 113 at a sub-stoichiometric concentration had a striking and unique effect on Aβ42 monomer aggregation. Although the data could not fit with a conventional equation, a nucleation and growth phase were noted that correlated temporally with aggregation in the absence of antibody (Figure 4.3). However, the aggregation progress was significantly and rapidly suppressed between 5-6 hours and failed to yield any detectable aggregates over time. The effect of mAbSL 113 on Aβ42 monomer aggregation kinetics suggested that the antibody was binding to aggregates soon after nucleation, thus preventing further growth.

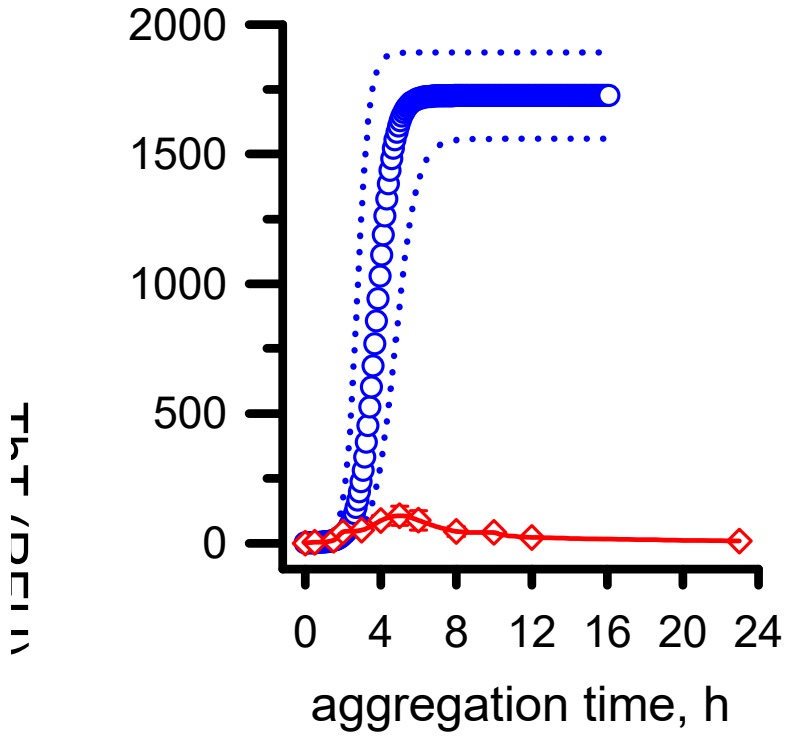

Figure 4.3. mAbSL monoclonal antibody inhibits Aβ aggregation at sub-stoichiometric ratios. Solutions of SEC-purified Aβ42 monomer (10 μM) were incubated by shaking at 1000 rpm 37°C in low-retention tubes in the absence (black curve) or presence of monoclonal AbSL (mAbSL) antibody 113 at 0.1 (red). Thioflavin T (ThT) (20 μM) was included in the solution. 50 mM TRIS pH 8.0 buffer was used with 30 mM salt concentration. At selected time points, ThT fluorescence was determined by placing 80 μL of the solution in a quartz cuvette and taking emission scans from 460-520 nm with an excitation wavelength of 450 nm. Numeric values are presented as relative fluorescence units (RFU) and were obtained by integration of the emission curves from 470-500 nm. The cuvette samples were recovered back into their respective tubes and incubated further. Data points and error bars represent the average and standard error for n=3 replicate tubes at each time point for each aggregation solution. Curve fitting was done using SigmaPlot. The dotted line represents the standard error in the aggregation data of the Aβ42 monomer in the data obtained. (Graph created in collaboration with Dr. Nichols)

4.1.2. Effect of a non-selective monoclonal antibody

The reaction kinetics of Aβ42 monomer aggregation was performed similarly with the non-selective monoclonal antibody candidate mAb Aβ 513. The same reaction conditions were used to monitor the assay. The impact of Aβ mAb 513 (1:10 antibody-

Aβ ratio) on Aβ42 monomer aggregation kinetics was very different, in that nucleation and elongation was both inhibited through a more conventional mechanism. $t_{1/2}$ increased from 2.2 h to 3.8 h in the presence of antibody, and the t_{lag} was extended from 1.1 h to 2.8 h (Figure 4.4). The maximum ThT fluorescence was significantly reduced from 5400 to 1200 in the presence of the mAb Aβ 513. The inhibitory effect of the non-conformation-selective mAb suggested a mechanism whereby Aβ42 monomers are immediately bound upon incubation, effectively lowering the Aβ42 concentration and lengthening the lag phase. The maximum aggregation dwindled as compared to of Aβ42 monomer alone (Figure 4.4).

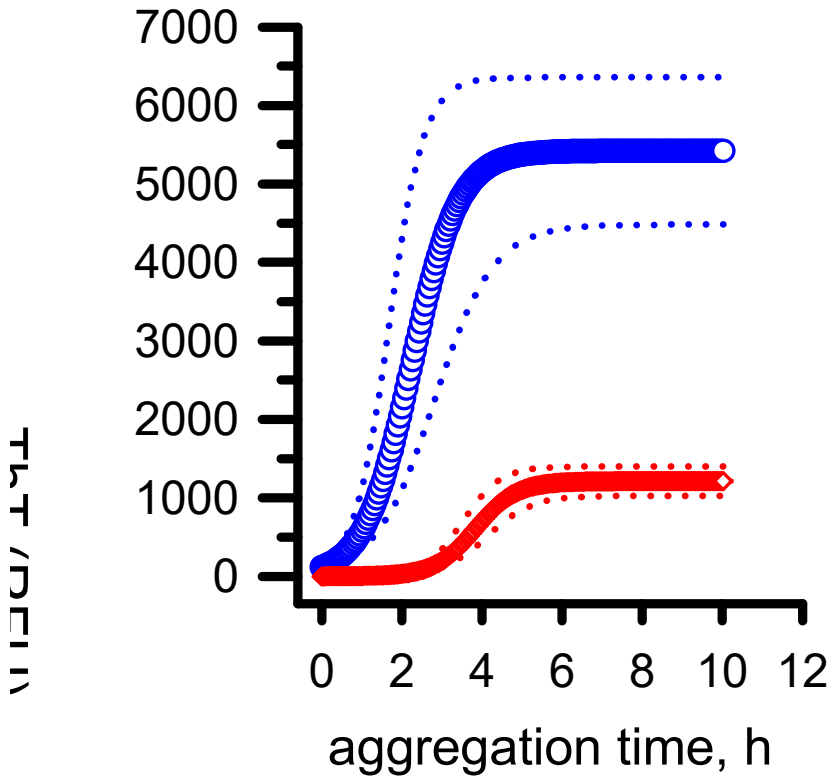

Figure 4.4. mAb Aβ monoclonal antibody inhibits Aβ aggregation at sub-stoichiometric ratios. Solutions of SEC-purified Aβ42 monomer (10 μM) were

incubated shaking at A. 1000 rpm (left panel) B. 750 rpm (right panel) 37°C in low-retention tubes in the absence (black curve) or presence of monoclonal AbSL (mAbSL) antibody at 0.1 (red) mAb Aβ 513. Thioflavin T (ThT) (20 μM) was included in the solution. 50 mM TRIS pH 8.0 buffer was used with 30 mM salt concentration. At selected time points, ThT fluorescence was determined by placing 80 μL of the solution in a quartz cuvette and taking emission scans from 460-520 nm with an excitation wavelength of 450 nm. Numeric values were obtained by integration of the emission curves from 470-500 nm. The cuvette samples were recovered back into their respective tubes and incubated further. Data points and error bars represent the average and standard error for n=3 replicate tubes at each time point for each aggregation solution. Curve fitting was done using a 3-parameter sigmoidal curve on SigmaPlot. The dotted line represents the standard error in the aggregation data of the Aβ42 monomer in the data obtained. (Figure created in collaboration with Dr. Nichols).

4.2. Monoclonal antibody interacts with Aβ42 protofibrils

Studies by many groups have shown that the rate of protofibril formation and the time over which protofibrils persist is strongly influenced by Aβ primary sequence (Walsh et al., 1997; Nilsberth et al., 2001). We were interested in observing the steady-state level of protofibrils governed by the interaction of our monoclonal antibody with protofibrils and conversion to fibrils. Studies were conducted to demonstrate how mAbSL affects the progress of protofibril, by dissociation or by conversion to fibril formation. Previous studies have shown two different modes of Aβ40 protofibril growth: protofibril elongation by monomer addition and protofibril association by itself. The two modes resolved by varying salt concentrations were confirmed by MALS and AFM studies (Nichols et al., 2002). It was interesting to look at the influence conformational-selective antibodies have on Aβ42 protofibril. Closely examining the formation of the complex helped us infer necessary information on how mAbSL inhibits the deleterious effects of Aβ42.

We were curious to know the impact of both selective and non-selective antibodies on Aβ42 protofibril dynamics (dissociation or further assembly) in vitro.

Quiescent incubation of SEC-purified Aβ42 protofibrils (10 μM) in the absence and presence of mAbSL 113 and Aβ mAb 513 separately (n=3) was carried out at room temperature in low-retention tubes with 50 mM TRIS pH 8 as a buffer for 3 days. The ThT fluorescence signal for each reaction tube was measured two times each day: the first time before spinning the tube (pre-spin) and the second time after the sample was spun at 17,000 g for 10 minutes (post-spin). The fluorescence measurement in the Aβ42 protofibrils reaction tube by itself had a slight change in reading from consecutive days. There was minimal difference in RFU measurements between pre-spin and post-spin readings due to their stability and did not undergo either dissociation or further assembly to an insoluble species (Figure 4.5).

In the presence of mAbSL 113 or Aβ mAb 513 at a 1:10 antibody: Aβ molar ratio, the Aβ42 protofibrils immediately formed an insoluble complex in the solution that could be removed from the solution by centrifugation. Nearly 93% and 78% of the Aβ42 protofibrils were found in an insoluble complex within 30 min of incubation with mAbSL 113 or Aβ mAb 513, respectively. After 2-3 days of incubation with both antibodies, the Aβ42 protofibrils were completely removed from the solution by centrifugation (Figure 4.5).

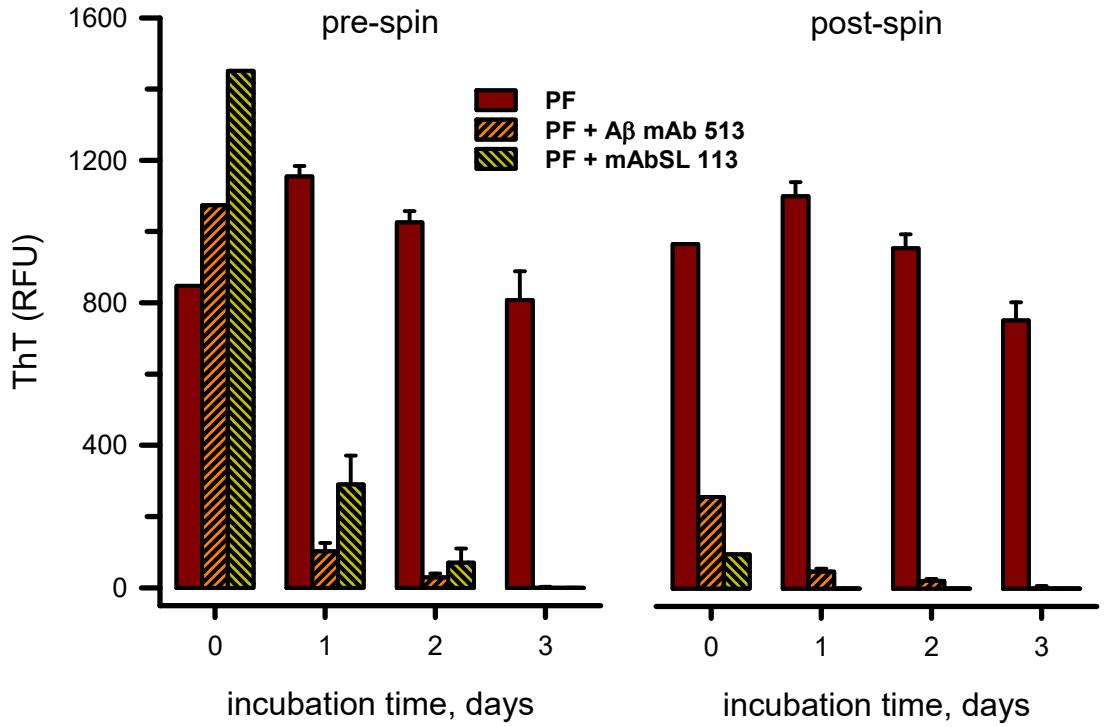

Figure 4.5. Protofibril dynamics in the presence of mAbSL monoclonal antibody at the 10-fold difference. Solutions of SEC-isolated Aβ42 protofibrils (10 μM) and ThT (20 μM) were incubated quiescently at 25 °C in the absence or presence of mAbSL 113 or Aβ mAb 513 at varying antibody concentrations (0.2, 0.5, or 1 μM). Solutions were assessed by ThT fluorescence and reported as relative fluorescence units (RFU). ***A***. Solutions of Aβ42 protofibrils in the absence (solid red bar) or presence of mAbSL 113 (orange hatched bar) or Aβ mAb 513 (yellow hatched bar) at a 1:10 mAb: Aβ42 ratio. ThT data is shown before, or following, centrifugation at 17,000*g* for 10 min. (Figure credits: Dr. Nichols)

In an extended time course of incubation, SEC-isolated Aβ42 protofibrils became less soluble over time (Figure 4.6). However, the inclusion of mAbSL 113 and Aβ mAb 513 1:20 antibody: protofibril ratio fastened this process. The lower stoichiometric ratio allowed observation of differing effects between the conformational-selective mAbSL 113 and the nonconformational-selective Aβ mAb 513 antibodies (Figure 4.6). At early time points (0-6 days), mAbSL 113 was much more effective than Aβ mAb 513 at altering protofibril stability and triggering conversion to an insoluble complex. Even at

this low antibody: protofibril ratio, mAbSL 113 rapidly caused deposition of Aβ42 protofibrils just 30 min after inclusion in the solution (Figure 4.6). Further lowering of the antibody: protofibril ratio to 1:50 yielded a similar difference between the effects of the two antibodies, with mAbSL 113 still exerting a significant impact on protofibril dynamics (Figure 4.6). The deposition time course with the inclusion of Aβ mAb 513 was closer to that of Aβ42 protofibrils alone.

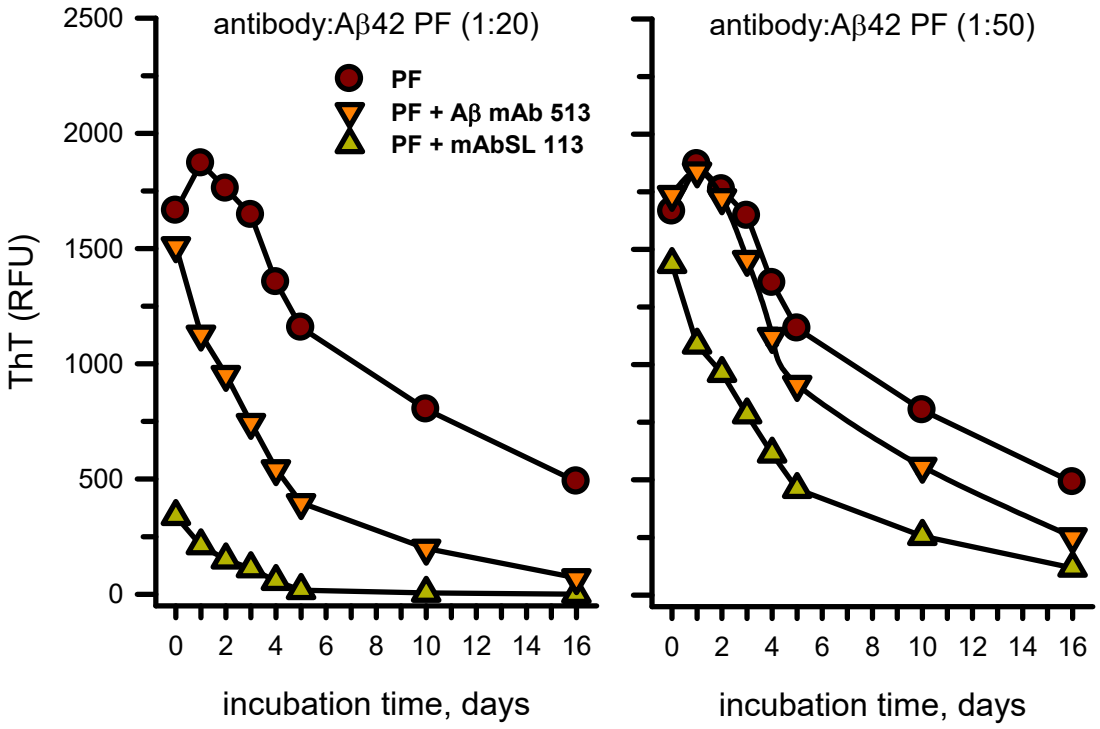

Figure 4.6. Protofibril dynamics in the presence of mAbSL monoclonal antibody. Solutions of SEC-isolated Aβ42 protofibrils (10 μM) and ThT (20 μM) were incubated quiescently at 25 °C in the absence or presence of mAbSL 113 or Aβ mAb 513 at varying antibody concentrations (0.2, 0.5, or 1 μM). Solutions were assessed by ThT fluorescence and reported as relative fluorescence units (RFU). Solutions of Aβ42 protofibrils in the absence (dark red circles) or presence of mAbSL 113 (orange down triangles) or Aβ mAb 513 (yellow up triangles) at 1:20 and 1:50 mAb: Aβ42 ratios. All panel B data is following centrifugation at 17,000*g* for 10 min (post-spin). Data bars (± SEM) for all measurements represent the average of n=3 trials. All panel B error bars are smaller than the symbols and not visible. (Figure credits: Dr. Nichols)

4.3. Aβ42 protofibrils and monoclonal antibody complex imaged using atomic force microscopy

Atomic force microscopy (AFM) is a great tool to study the topography of conformationally-distinct structures such as Aβ42 protofibrils and fibril structures. I have worked quite a bit on using AFM on the pellets observed from the protofibril dynamics section. High-resolution images of Aβ42 fibrils were gathered to be used as a control (Figure 4.7).

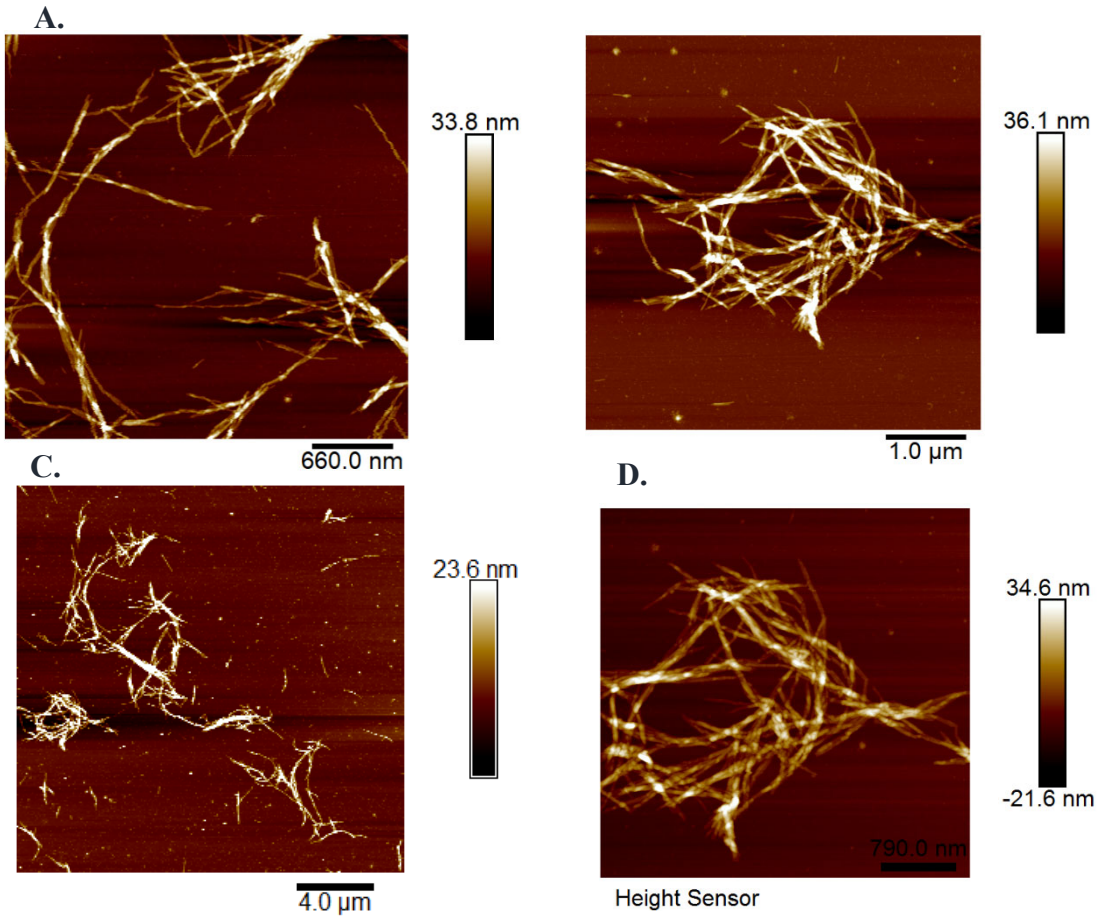

Figure 4.7. Images of Aβ42 fibrils (5 µM). A solution of Aβ42 (10 µM) was prepared and applied to the mica bead. All 4 panels show the insoluble fibrillar structure. The length ranges from 12-20 nm.

Images for Aβ42 protofibrils from Aβ42 protofibril dynamic experiment described in Figure 4.5 were taken using AFM. Images are shown in Figure 4.8 and the image analysis has been summarized in Table 4.1.

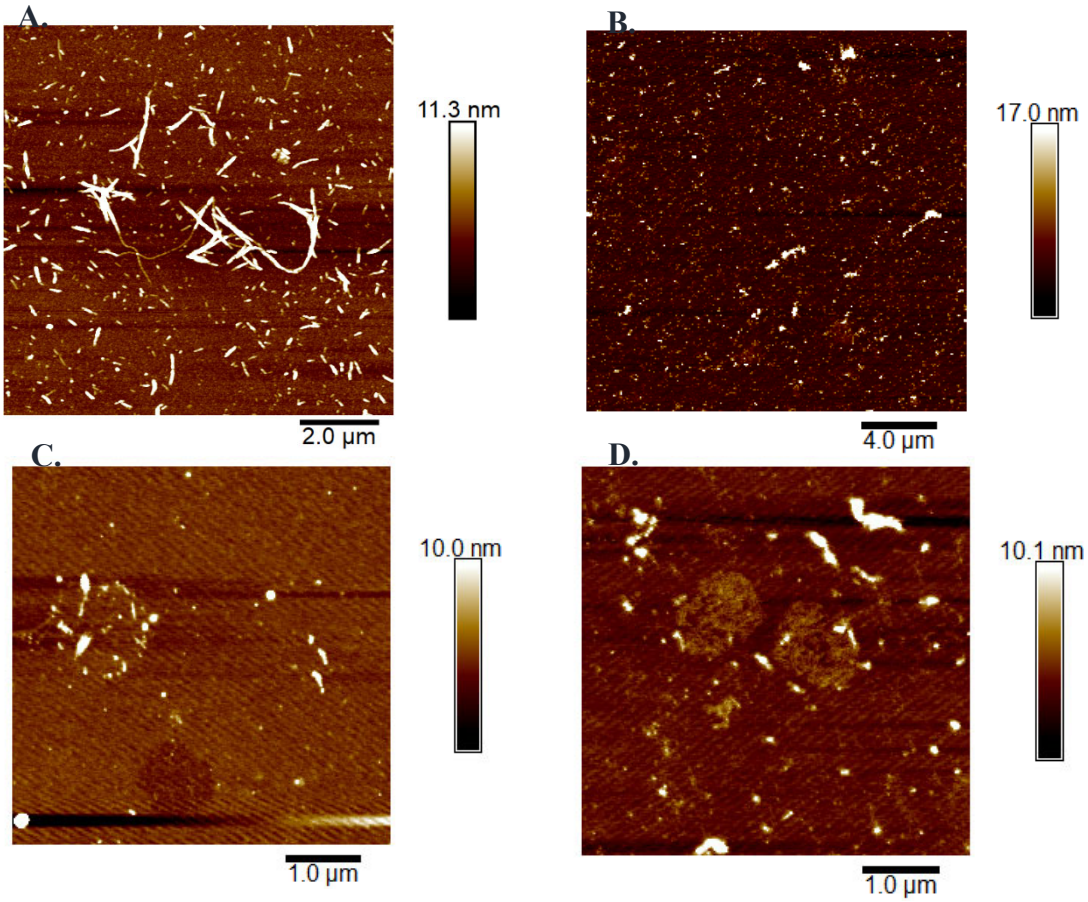

Figure 4.8. Morphological differences between Aβ42 fibrils and Aβ42 protofibril samples from protofibril dynamics. The samples were reconstituted in sterile water and applied on freshly cut mica beads with **A.** Aged Aβ42 monomer (fibril) **B.** Protofibril sample **C.** Aβ42 protofibril+mAbSL 113 **D.** Aβ42 protofibril+mAb Aβ 513

B.

Table 4.1. Height, length, and width analysis of Aβ42 fibrils and samples from Aβ42 protofibril dynamics (Aβ42 protofibril in the presence and absence of antibodies)

	Height analysis (nm) **(Mean height±SD)**	**Length analysis (µm)** **(Mean length±SD)**	**Width analysis (µm)** **(Mean width)**
Aβ42 fibril	20.3±2.8	1.5±0.2	0.2
Aβ42 protofibrils	17.1±2.7	0.23±0.02	0.13
Aβ42 protofibrils with mAbSL 113	12.4±1.6	0.3±0.02	0.15
Aβ42 protofibrils with mAb Aβ 513	16.5±2.9	0.5±0.1	0.18

4.4. Conclusion

The research study has strengthened the experimental mechanism to study the Aβ monomer aggregation pathway and the transition to insoluble fibril with the intermediates as oligomeric and soluble protofibril species. The conditions that influence the rate of oligomerization have been identified and optimized. Elucidating the mechanistic features of the conformational-selective and non-selective monoclonal antibodies is vital. It was evident from the experiments shown in this chapter that the conformational-selective monoclonal antibody (mAbSL 113) has a strong concentration-dependent inhibitory effect on Aβ42 monomer aggregation. mAbSL 113 exerted complete inhibition even at a 10-fold less concentration than Aβ42 monomer concentration. The conformational-

selective antibodies in the field have been previously studied to work at higher concentrations (Lannfelt, Möller, et al. 2014). Bonito-Oliva et al. generated monoclonal antibodies to a nucleobindin 1 (NUCB1)-human islet amyloid polypeptide (hIAPP) protofibril complex that recognized both hIAPP and Aβ protofibrils (Bonito-Oliva et al. 2019). The antibodies were selective for Aβ42 protofibrils over Aβ40 monomer and exhibited a concentration-dependent inhibitory effect on Aβ42 monomer aggregation with significant inhibition (40-70%) at equimolar antibody: Aβ42 ratios (Bonito-Oliva et al. 2019). Crenezumab, a humanized monoclonal antibody that targets the mid-Aβ region (residues 12-23), binds Aβ monomers, oligomers, and fibrils with similar affinities (Adolfsson et al. 2012, Goure et al. 2014). Crenezumab prevented Aβ42 monomer aggregation, and disassembled preformed Aβ42 aggregates, at a 1:10 sub-stoichiometric molar ratio (Adolfsson et al. 2012). This level of potent Aβ42 monomer aggregation inhibition was observed by the protofibril-selective mAbSL 113 antibodies. However, the pattern of inhibition by mAbSL 113 was suggestive of a mechanism in which soluble Aβ42 protofibrils were formed, rapidly bound by antibody, and their further assembly was suppressed.

The mechanism of inhibition of a non-selective antibody at 10-fold less concentration than Aβ42 monomer is significantly different from the conformational-sensitive antibody. The presence of mAb Aβ 513 with Aβ42 monomer affects the lag phase and strongly diminishes the aggregation kinetics, thereby promoting reduced fibril formation.

Considering the non-selective antibody mAb Aβ 513, it probably recognizes a sequence rather than a conformation. It binds to soluble Aβ42 protofibrils at a similar

extent the way it does with Aβ42 unstructured monomers and insoluble Aβ42 fibrils. Time-course aggregation effect of mAb Aβ 513 was characterized on soluble Aβ42 protofibrils and is shown to inhibit the aggregation of Aβ42 monomer to a significant extent.

Protofibrils represent a transient soluble intermediate in Aβ fibrillogenesis. Once removed from residual Aβ monomer, they are quite stable (Coalier et al. 2013), but can continue to further assemble into larger insoluble fibrillar structures (Walsh et al. 1999, Nichols et al. 2002). If one is to consider conformation-selective antibodies as potential therapeutics, it is of interest to know how the antibody binding impacts the antigen structure or properties. The presence of conformational-selective antibody, mAbSL 113, directly with Aβ42 protofibrils displayed functional binding of the antibody to Aβ42 protofibrils converting it to an insoluble pellet which was observed as early as 24 hours by naked eyes. The images obtained of the pellet generated in the presence of conformationally-selective antibodies suggest the inhibition of amyloid aggregation to mature fibrils occurs through the active binding of antibodies to soluble pre-fibrillar misfolded structures. There is a strong possibility of these monoclonal conformationally-selective antibodies acting as rescue agents preventing the conversion of intermediate structures formed during Aβ42 aggregation to mature fibrils in brain samples. Further analysis of the interaction of mAbSL on brain extracts from mouse models and from the human sample would suggest that mAbSL 113 would block the conversion of protofibrils to fibrils and remove protofibrils by either antibody-mediated processes or direct deposition of insoluble non-fibrillar antibody-protofibril complexes.

Additional antibodies obtained during the same selection process (Aβ mAbs) were not selective for a particular Aβ conformation and served as important controls for comparing differences between conformation-selective and non-conformation-selective antibodies.

Observation with a non-selective conformational antibody, mAb Aβ 513, ensured complex formation with Aβ42 protofibrils without altering the structure. The sequence-independent monoclonal antibody exhibited strong binding to Aβ42 protofibrils and the images confirmed that the insoluble pellet formed is nowhere near to fibril structure. It can be elucidated that the mechanism of Aβ42 aggregation inhibition of conformational-selective antibodies is through functional binding of intermediate soluble Aβ42 species and preventing their saturation to form insoluble fibrils.

The conformational-selective antibody binds preferentially to Aβ42 protofibrils, ultimately, preventing the formation of mature fibrils.

The biological consequences of Aβ protofibrils have been well-documented and the list of deleterious effects is expansive and very diverse (Huang and Liu 2020, Ono and Tsuji 2020). Iwatsubo and colleagues demonstrated that injection of Aβ42 protofibrils into the neocortex and hippocampus of A7 mice at 8 months led to increased levels of formic acid extracted insoluble Aβ42 when analyzed 4 months later. Our findings have shown that Aβ42 protofibrils activate both TLRs and the NLRP3 inflammasome, and Aβ42 protofibrils, but not Aβ42 monomers or fibrils, readily interact with (Paranjape et al. 2013), and are rapidly taken up by (Gouwens et al. 2016), microglia. Following internalization by microglia, Aβ42 protofibrils can be trafficked into microvesicles and released from the cell (Gouwens et al. 2018. The cumulative

research over many years provides a myriad of reasons to target distinct conformations of aggregated Aβ, including protofibrils. Our panel of conformational-sensitive antibodies have a high affinity towards target Aβ42 protofibrils over natively folded monomers and insoluble plaque-forming fibrils. The reactivity of the characterized monoclonal antibodies is quite convincing. Thus, the use of passive immunization of our expressed and purified antibodies as therapeutic and diagnostic tools can be a valuable resource in the field of AD.

CHAPTER 5: EPITOPE MAPPING OF Aβ42 PROTOFIBRILS

Aβ is amphipathic in nature with the N-terminal segment cleaved from the hydrophilic extracellular domain of APP and the transmembrane C-terminal region comprises primarily of hydrophobic amino acids (Selkoe 2004, Touchette, Williams et al. 2010). The middle region of Aβ (residues 17-20) contributes prominently to the formation of β-sheet structure (Williams, Portelius, et al. 2004). Solid-state NMR (Tycko 2015, Xiao, Ma et al. 2015, Colvin, Silvers, et al. 2016, Wälti, Ravotti, et al. 2016) and cryo-electron microscopy (Gremer, Schölzel, et al. 2017, Close et al. 2019) studies on Aβ40 and Aβ42 confirmed the presence of well-organized hydrophobic and non-polar inner core with an open, disordered orientation of N-terminal region which does not significantly form part of the β-sheet secondary structure (Au, Ostrovsky, et al. 2019).

Aβ42 fibrillar structures obtained from AD patients correspond to be made of two identical S-shaped protofilaments. Two different categories of filaments were captured. Type I filaments were obtained from sporadic AD patients with the presence of many dense plaque cores in the brain regions. Type II filaments were estimated in individuals with familial AD, PD, DLB, and FTD and these cases had abundant diffuse Aβ deposits (Yang et al. 2022). Type I filaments extend from residue 9 to 42 and type II filaments from residue 12 to 42 in the ordered core of S-shaped protofilaments (Figure 5.1). The finding directly correlates with the disordered structure from residue 9 or 11 at the N-terminal region. However, partial reproducibility is noticed with in vitro filaments as compared to structures from human AD patients.

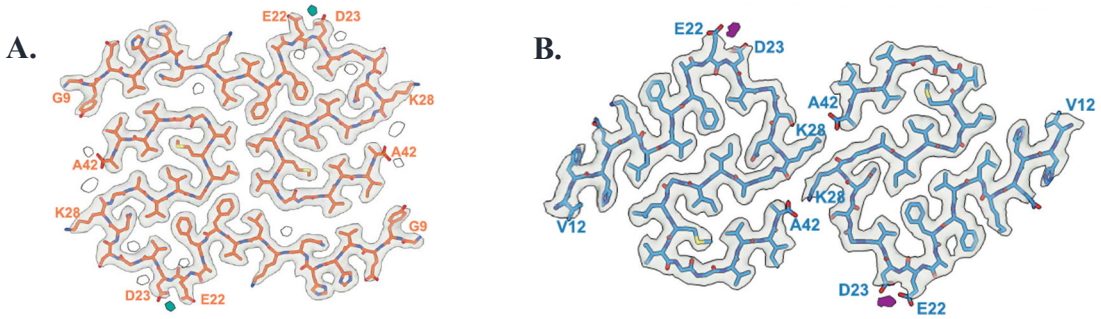

Figure 5.1. Cryo-EM density maps and atomic models of A. Type I, **B.** Type II filaments found in AD brain. The ordered core consists of two identical S-shaped protofilaments of type I (orange) and type II (blue). The residues that form part of the S-shaped domain are highlighted (Yang et al. 2022).

The atomic resolution structure of the Aβ42 fibril core has been studied by Colvin et al. consisting of dimer molecules in an S-shaped amyloid fold as shown in Figure 5.2. This arrangement offers a hydrophobic core to fibril, and it can serve us as being the structure that relates to protofibril structure. The Wetzel group identified structural differences between Aβ40 protofibrils and mature fibrils using HDX-MS coupled with online proteolysis (Kheterpal et al. 2006). It was revealed that the internal fragment is protected from deuterium exchange in fibrils as compared to protofibrils whereas there are similarities in N-terminal and C-terminal segments in both protofibrils and fibrils (Kheterpal et al. 2006). FPOP-MS is used to compare the changes in solvent accessibility between antigen alone and antigen-Ab complex by quantitating the extent of oxidation of the side chains by OH radicals by photolysis of H_2O_2 (Zhang et al. 2017; Jones et al. 2011). The Gross laboratory showed how using FPOP-MS can yield residue level information when the kinetics of oligomerization of Aβ42 is monitored and conveyed which regions were majorly involved during the β-sheet structure formation as aggregation progresses (Li et al. 2016). Competition ELISA studies with AbSL targeted the involvement of the N-terminal region of protofibril (Colvin et al. 2017). Antibodies

are an important tool in studying protofibril structure and aggregation. There is a lack of accurate epitope mapping analysis in the conformation-selective antibodies previously employed in the field (Saper et al. 2009). Hence, the characterization of the specificity of the binding site of mAbSL on the protofibril structure will help us get down to sub-regional and residue-level information.

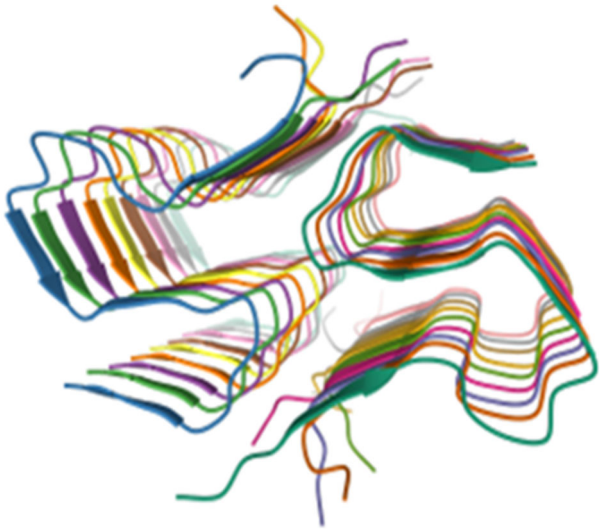

Figure 5.2. Atomic resolution structure of monomorphic Aβ42 amyloid fibrils (PDB ID 5KK3) (Colvin et al. 2016)

5.1. Antibody competition study of a monoclonal antibody with antibodies Ab5 and Ab 2.1.3

Antibody competition ELISA has been elucidated in the method section. 96-well plates were firstly coated with 100 µL of mAbSL 113 (0.5 µg/mL). An Aβ42 C-terminal non-selective antibody, Ab 2.1.3, and an Aβ42 N-terminal non-selective antibody, Ab 5, were used as two competing antibodies with mAbSL (Figure 5.3). Three separate tubes were prepared with different amounts of both Ab 2.1.3 and Ab9: 0.005 µg, 0.05 µg, and 0.5 µg. Each tube was incubated with 20 nM biotinylated protofibrils. The mixed

solutions were applied to the wells, followed by streptavidin HRP conjugate and the addition of HRP substrates.

Ab 2.1.3 and Ab 5 are Aβ42 non-selective antibodies. The N-terminal specific antibody, Ab 5 showed significant inhibition of binding between Aβ42 protofibrils and mAbSL 113 as the concentration of Ab 5 was increased (Figure 5.3 B). This indicates that as the concentration of competitor antibody was increased, the accessibility of Aβ42 protofibrils to mAbSL 113 on the plate was lost to a great extent. There was a considerable drop in the absorbance with an equimolar amount of Ab 5 and mAbSL and a complete inhibition of binding when Ab 5 was 10-fold more in concentration than mAbSL. The data suggests the involvement of the N-terminal region in the interaction of conformation-specific antibody mAbSL 113 and Aβ42 protofibril. However, for the C-terminal specific antibody, Ab 2.1.3, a gradual decrease in absorbance was observed (Figure 5.3 B). The decline in the interaction of mAbSL with protofibril was statistically significant. The effect observed was lower as compared to the N-terminal binding antibody. It can be established that the epitope for mAbSL Aβ42 protofibril is associated with the C-terminal region as well.

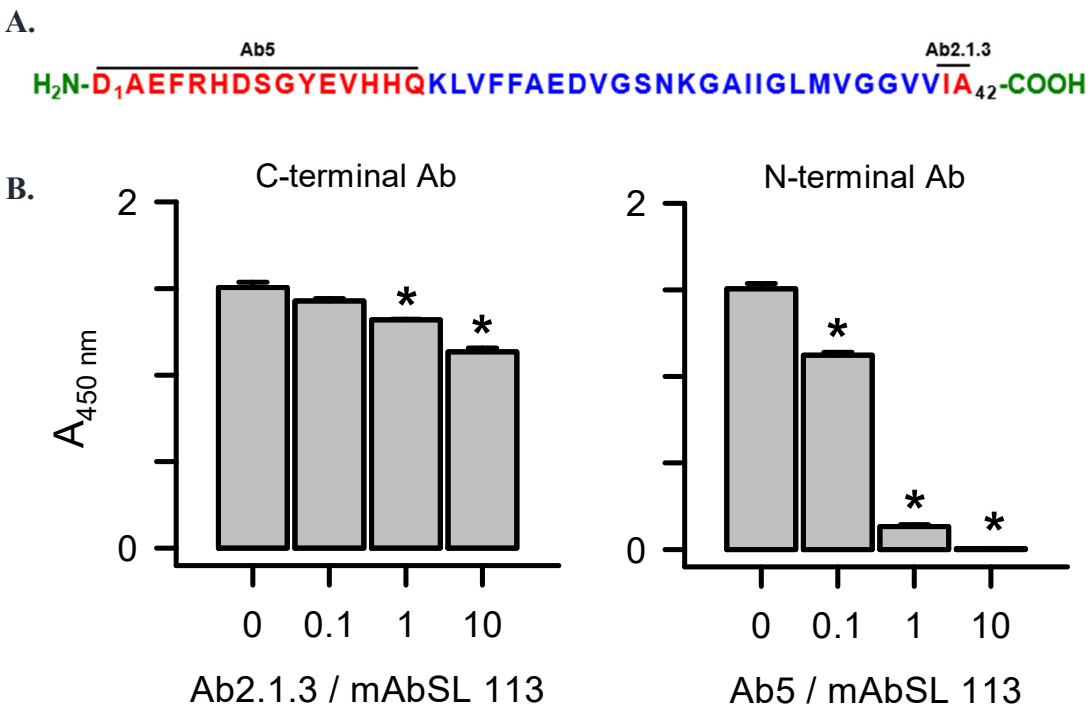

Figure 5.3. Probing the mAbSL epitope on Aβ42 protofibrils with an antibody competition ELISA. Solutions of biotinylated Aβ42 protofibrils that had been incubated with 3 concentrations of a C-terminal specific (Ab2.1.3) or an N-terminal specific antibody (Ab5) were applied to wells coated with mAbSL 113. Streptavidin-HRP conjugate was added, followed by HRP colorimetric substrates. The final concentrations were 0.5 µg/mL mAbSL 113; 20 nM protofibrils; and 0.05-5 µg/mL Ab2.1.3 or Ab5. Statistical analysis: 2-tailed paired T-test, p values <0.5 considered significant. (Experiment performed by Thao Pham and figure created in collaboration with Dr. Nichols)

5.2. Hydrogen-deuterium exchange-mass spectrometry

The elucidation of the interaction of monoclonal AbSL with Aβ42 protofibrils is crucial for understanding the mechanism of action of mAbSL. Undoubtedly, the high-resolution techniques for epitope-mapping studies that provide the maximum degree of structural details of the interactions are NMR spectroscopy and Cryo-Electron microscopy. However, these powerful techniques are quite expensive, labor-intensive, and have low throughput. Hydrogen-deuterium exchange mass spectrometry has emerged as a great tool for epitope-mapping experiments that provide thorough detail about the

binding interactions involved. The technique measures the rate of exchange for protein backbone amide-hydrogen with the heavier isotope deuterium. The kinetics of the exchange is influenced by hydrogen bonding and solvent exposure of the protein. The solvent accessibility and rate of hydrogen-deuterium exchange decrease when the antigen protein either adopts a conformational fold or the protein engages with an antibody, thus, providing structural details of the local environment around the protein. Proteolytic digestion of the interaction using mass spectrometry yields the regions of the peptide involved in antibody interaction. HDX-MS technique utilizes a low concentration of protein sample and has a relatively fast turnaround and is cost-effective. The methodology integrates online custom-based instrumentation, data collection of the protein sample, and software for data analysis. It is a suitable technique and has the potential to study complex proteins such as Aβ42.

5.2.1. Differential uptake of deuterium by conformationally distinct Aβ42 species

Mass spectrometry-based hydrogen-deuterium exchange (HDX) was performed by our collaborators from Washington University to analyze the differences in the hydrogen bonding pattern of Aβ42 monomer, protofibril, and fibril**.** Previously, Gross lab has utilized various conditions to reduce and denature proteins before their incubation with the antibody to yield the epitope.

By online type XIII-pepsin digestion, 19 overlapping peptides of Aβ42 (100% coverage) were obtained (Figure 5.3). Aβ42 monomer is a relatively small protein and is easy to denature and digest quickly under normal conditions. However, proteolysis of recalcitrant and tightly bound aggregates of Aβ42 required more concentration of

denaturant or a longer quenching time. Since these are non-specific proteases, they produce overlapping peptides, but the enzyme pepsin has a strong cleavage propensity at C-terminus to Phe4, Phe19, and Leu34. Hence, peptides cleaved after these residues had much higher intensities and were easy to analyze after HDX analysis. Therefore, improved peptide separation and identification by MS-MS was ensured to cover the entire Aβ42 sequence. Thus, Dr. Saketh Chemuru has been able to successfully identify and optimize conditions suitable for Aβ42 protofibril denaturation.

Figure 5.4. Amino acid sequence and pepsin digestion of Aβ42 protofibrils. SEC-purified Aβ42 protofibrils (250 pmol) were treated with 4 M urea + 1% TFA quench followed by incomplete digestion on an immobilized pepsin column. Peptides were trapped, desalted by a C8 column, and eluted from a C18 column with water-acetonitrile. MS-MS was conducted using an LTQ-Orbitrap XL mass spectrometer to identify the above peptides (blue arrows). A total of 19 peptides were identified using MS-MS analysis.

Continuous HDX labeling of Aβ42 protofibrils (43 μM), monomers (19 μM), and fibrils (46 μM) were performed by taking 200 pmol of the protein and exchanging it in D_2O (75%) at pH 7.4 and 4 °C in 1x PBS buffer for 0, 10, 30, 90, 300, 900, 3600, and 14400 secs in duplicates as previously described (Yan, Grant, et al. 2015). The final volume of the samples in D_2O was kept at 100 μL.

Significant structural changes were observed based on deuterium uptake percentages of the three Aβ42 species throughout the entire sequence of Aβ42 (Figure 5.4). However, the region with residues 1-16 displayed similar deuterium uptake profiles for Aβ42 monomer, protofibril, and fibril samples. It is indicative that the protein structure is structured and highly ordered for protofibril and fibril except at the N-terminal region. The

protofibrils and fibrils differ in terms of their HDX protection indicating that protofibrils adopt an intermediate β-sheet network throughout the entire length of Aβ42. The largest differences in HD exchange between the protofibril and fibril samples were observed in the middle domain (20-34) indicating more involvement of C-terminal residues (38-42) towards the β-sheet structure in the protofibril sample. As expected, the deuterium uptake profile of the protofibrils and fibrils progressively shows a significant reduction at all labeling time points in the incorporation of deuterium as we move towards the middle and C-terminal region of the protein. This highlights rigidity and low solvent exposure and provides key aspects about local-conformational dynamics which is probably due to an extended β-sheet network with a tightly bound core containing stronger H-bond interactions. The deuterium incorporation remains lowest for fully formed Aβ42 fibrils among all three species throughout the course of the experiment. The result is in concordance with other previous HDX-MS studies on Aβ42 fibrils and protofibrils, indicating the robust highly ordered structure of both species. There appeared minimal role of the N-terminus (1-14) as part of the fibril/protofibril structure. It is hard to measure the exact β-sheet network of the aggregates without knowing the back exchange present in the system. In contrast, the percent deuterium incorporation of individual peptides for Aβ42 monomer curves showed a steep graph that confirms high conformational flexibility and maximum solvent exposure due to the more disordered and random structure of the monomer. Aβ42 monomers are expected to be more susceptible and accessible to deuterium exchange than Aβ42 protofibril and fibril. Thus, these experiments revealed distinct changes in the local conformational dynamics of all three Aβ42 species. The data matches the expected trends. It confirms the presence of a well-organized hydrophobic and

non-polar inner core in Aβ42 and a more disordered structure of the N-terminal region which does not form part of the β-sheet secondary structure.

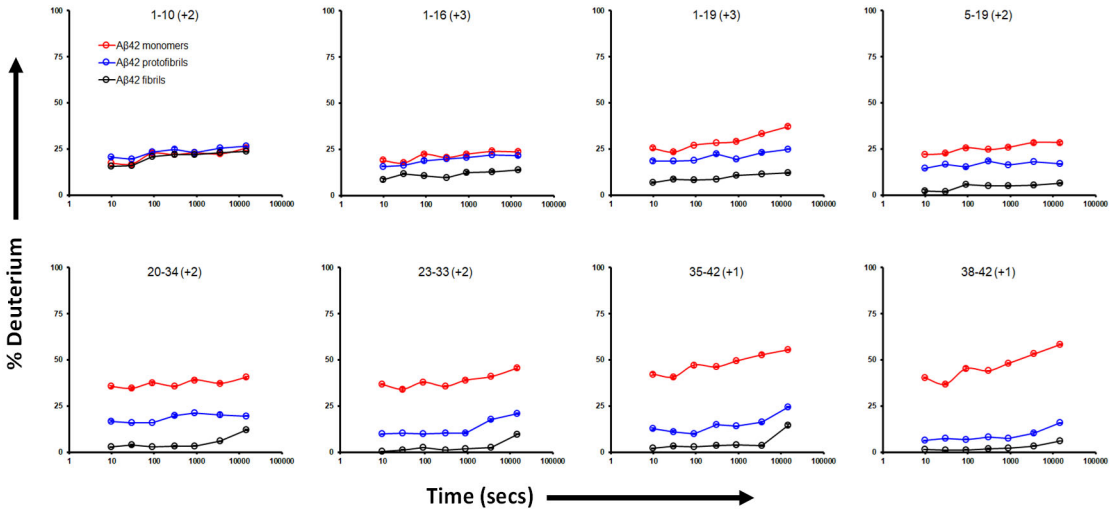

Figure 5.5. HDX-MS plots for peptides obtained from Aβ42 species. Aβ42 protofibrils, monomers, and fibrils were diluted into a 75% deuterated water solution (D2O) for 4 h. At selective time points, samples were removed and subjected to pepsin-catalyzed proteolysis. 2D incorporation was determined by MS for the Aβ peptide fragments. Time courses of deuteration for monomers (red), protofibrils (blue), and fibrils (black) incubated under the same conditions. 8 of 10 peptide fragments are shown. Each data point is the average of n=2 measurements and standard error bars are shown. (Work in collaboration with Saketh Chemuru and figure credits to Dr. Nichols)

5.2.2. Conformational epitope of selective monoclonal antibody on Aβ protofibrils involves N-and C-terminal region

Epitope mapping is crucial for understanding the mechanism of action of monoclonal antibodies on Aβ42 protofibril. Closely studying the deuterium incorporation profiles of Aβ42 protofibrils in the presence and absence of mAbSL 113, provided us with a clear glimpse of the regions involved during the binding interaction.

To measure the antibody binding site, 70 µL of Aβ42 protofibrils sample was incubated with 250 µL of mABSL113 antibody (Aβ42: antibody = 2:1). The samples were

incubated with the antibody (mAb113) for 1 h at 4 °C before HDX. A 6-time point HDX experiment was conducted in duplicates by exchanging the samples with D2O (75%) at pH 7.4 and 4 °C in 1x PBS buffer for 0, 30, 90, 300, 900, and 3600 secs.

HDX-MS data in the presence and absence of mAbSL 113 revealed local effects caused by binding. The antibody showed a clear reduction in deuterium incorporation for N-terminal residues and C-terminal residues emphasizing active binding at the N-terminal 1-10 region and minor interactions in the peptide 39-42 (Figure 5.5). The deuterium uptake curves might look close to each other for N-terminal and C-terminal domains, but the time points measurement was statistically significant using a 2-tailed paired T-test with p-value < 0.5. It is highly likely that the antibody has two binding domains at the two extreme ends of the protofibril structure and the protofibril might be a β-loop structure with the two ends next to each other. In contrast, the middle region was determined to have overlapping data points in the bound and unbound states indicating essentially identical deuterium uptake for all labeling time points in bound and unbound state. The local structure of the corresponding region was not highly impacted by complex formation. This firmly confirmed that the mAbSL conformational epitope on Aβ42 protofibril resides in a structural motif involving both N- and C- terminal regions. It suggests the presence of the head-to-tail arrangement of the N-terminal being adjacent to the C-terminal in precursor Aβ42 protofibril as determined by a similar arrangement in Aβ42 fibril formed in vitro (Colvin, Silvers, et al. 2016). Thus, HDX-MS revealed conformational dynamics of Aβ42 protofibrils in the presence and absence of mAbSL 113.

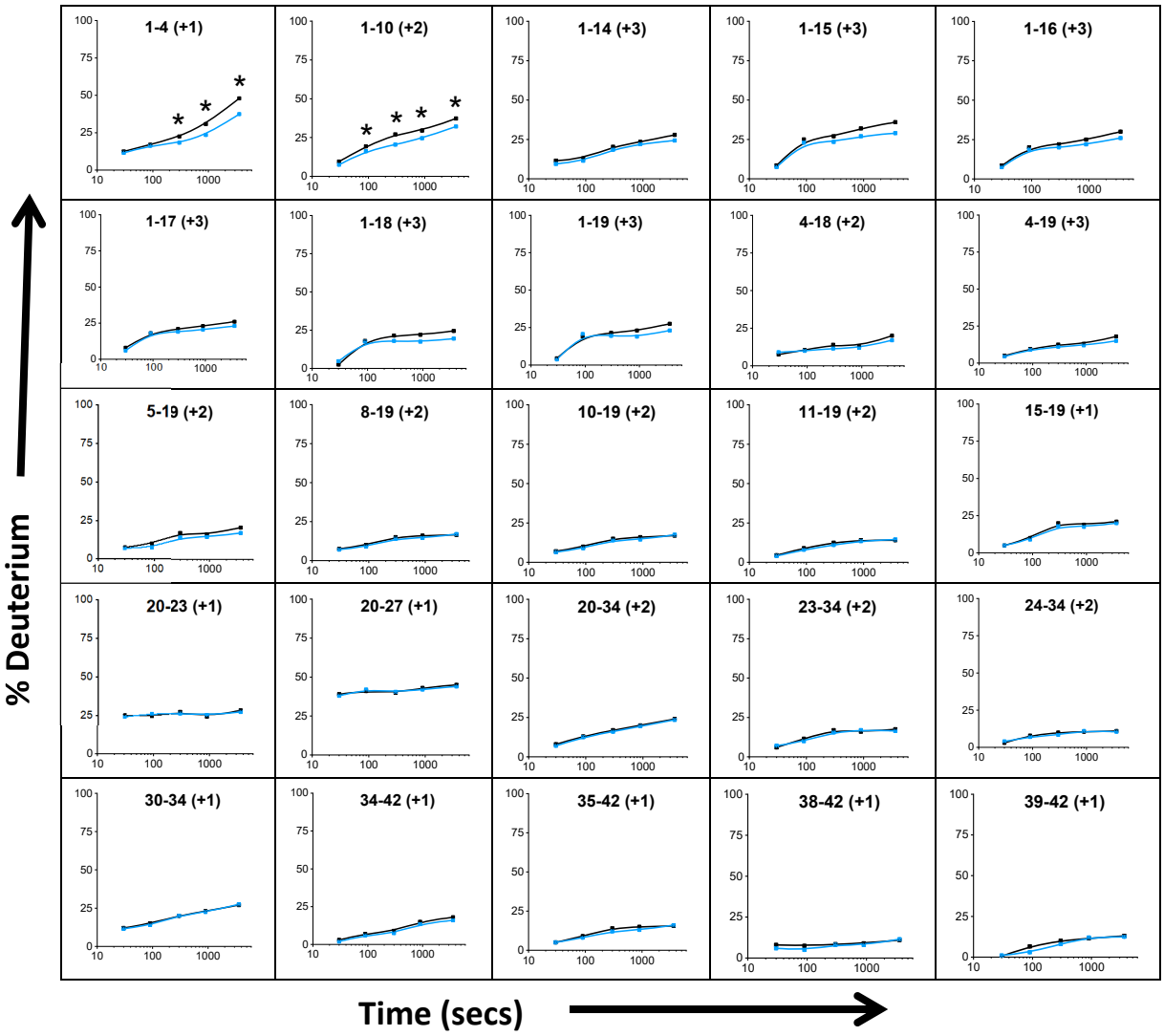

Figure 5.6. HDX-MS epitope mapping. The protofibril sample and antibody mAb113 were mixed at a 2:1 w/w ratio and incubated at 4 °C for 1 h immediately prior to HDX. The deuterium incorporation graphs for a variety of peptides (with the charged state) as a function of exposure time in both the presence (blue) and absence (black) of antibody are indicated here. Statistical analysis was done using a 2-tailed paired T-test with p values < 0.5 considered significant. (Work in collaboration with Saketh Chemuru and figure credits to Dr. Nichols)

5.3. Fast photochemical oxidation of proteins-mass spectrometry

Gross lab has pioneered the development of the FPOP technique, which utilizes photolysis of hydrogen peroxide to generate OH free radical. The free radical can oxidize at least 14 of 20 amino acid side chains to produce detectable products. The modifications on the side chains are quite stable and irreversible. The method efficiently provided residue-level information to probe the binding interface between an antigen and an antibody.

5.3.1. FPOP also shows an intermediate structure of Aβ42 protofibrils

FPOP footprinting was performed to outline the conformational differences between the three conformationally distinct SEC-purified Aβ42 samples (monomers, protofibrils, and fibrils).

FPOP methodology used a single scavenger concentration (L-glutamine= 5mM). The oxidation percentage of FPOP amenable residues in Aβ42 after MS^2 fragmentation of LysN-digested peptides is represented in Figure 5.6. Barring the two N-terminal residues Phe 4 and His 6, there was a significant difference in the oxidation levels for the residues between the three distinct Aβ42 samples. The result strongly supports the HDX findings that the fibril structure exhibited significant protection from oxidation in the middle and C-terminal regions. As expected, the amino acid residues in Aβ42 protofibrils maintained the intermediate modification percentage between monomer and fibrils, strongly supporting the HDX-MS data. The C-terminal residues Met 35, and Ile 41 showed considerable differences in oxidation between protofibrils and fibrils revealing the highly ordered structure of fibrils as compared to soluble protofibrils. Interestingly, HDX-MS and FPOP data strengthen the observation that the C-terminal domain of the Aβ42

monomer has a better deuterium uptake profile and oxidation percentage respectively than the N-terminal region, claiming the signification conformational breathing in Aβ42 monomer random coil structure, which considerably reduced as the monomers progress towards aggregation pathway. The exposed hydrophobic residues get buried in the core as the monomer gets aggregated into β-sheet rich structures. Met 35 was identified as the most oxidized residue in all three Aβ42 species.

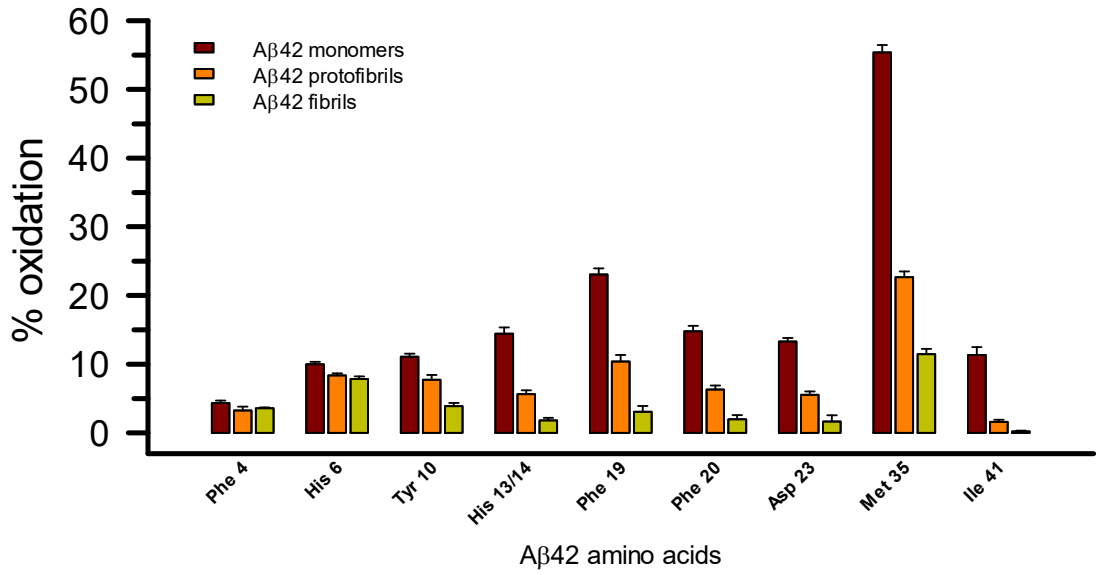

Figure 5.7. FPOP-MS of Aβ42 species. The extent of FPOP modification of 9 residues in Aβ42 peptide sequences was determined for Aβ42 monomers, protofibrils, and fibrils. The oxidation data is plotted as a % of a reporter peptide with increasing L-Gln (scavenger) concentration. Each data bar is the average ± std error of n=3 measurements (Work in collaboration with Saketh Chemuru and figure credits to Dr. Nichols)

5.3.2. FPOP shows an involvement of N-and C-terminus in the epitope mapping of Aβ protofibrils

FPOP kinetic plots were obtained of LysN-digested peptides of Aβ42 protofibrils in unbound and bound states with mAbSL 113. The lifetime of •OH is tunable and is

predominantly controlled by the radical scavenger concentration (Niu, Mackness, et al. 2017). In the bound state, there is a presence of a big protein (antibody) which inherently acts as a scavenger of •OH. Hence, to accurately normalize the unbound and bound states' FPOP modification data, the antibody accounts were taken in for some loss in the oxidation of Aβ42 residues. Hence, normalization of the values was required by using a reporter peptide system.

The fraction of leu-enkephalin modified at each glutamine concentration was plotted vs the corresponding fraction modified for each LysN-digested peptide of Aβ42 on the y-axis.

The non-overlapping nature of the curves in peptides 1-15 and 28-42 indicate that there is solvent exposure change in these regions based on antibody binding (Figure 5.7). FPOP was significantly reduced for residues F4, H6 (N-terminal), and M35, and V40/I41 (C-terminal) in the antibody-bound Aβ42 protofibrils compared to protofibrils alone. Antibody binding was not observed in the Aβ42 peptide middle region (Y10, H13/14, L17, F19/20, and D23/V24).

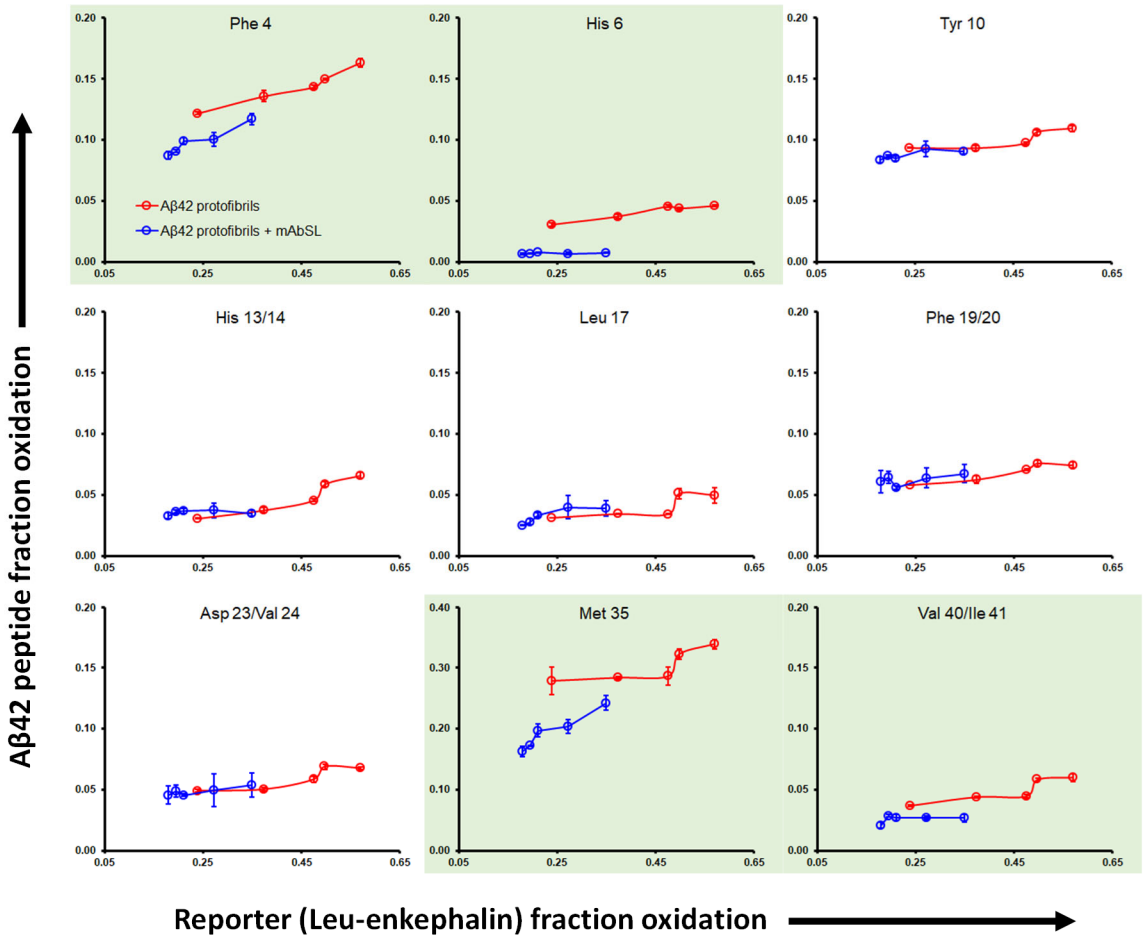

Figure 5.8. FPOP epitope mapping. FPOP modification of Aβ42 protofibrils in the absence or presence of mAbSL 113 antibodies. The 9 residues span the Aβ42 peptide sequence. The oxidation data is plotted as a fraction modified of Aβ peptide versus a reporter peptide because of increasing L-Gln (scavenger) concentration. Each data point is the average ± standard error for n=3 measurements. The data revealed a conformational epitope that incorporates N- and C-terminal residues. (Work in collaboration with Saketh Chemuru and figure credits to Dr. Nichols)

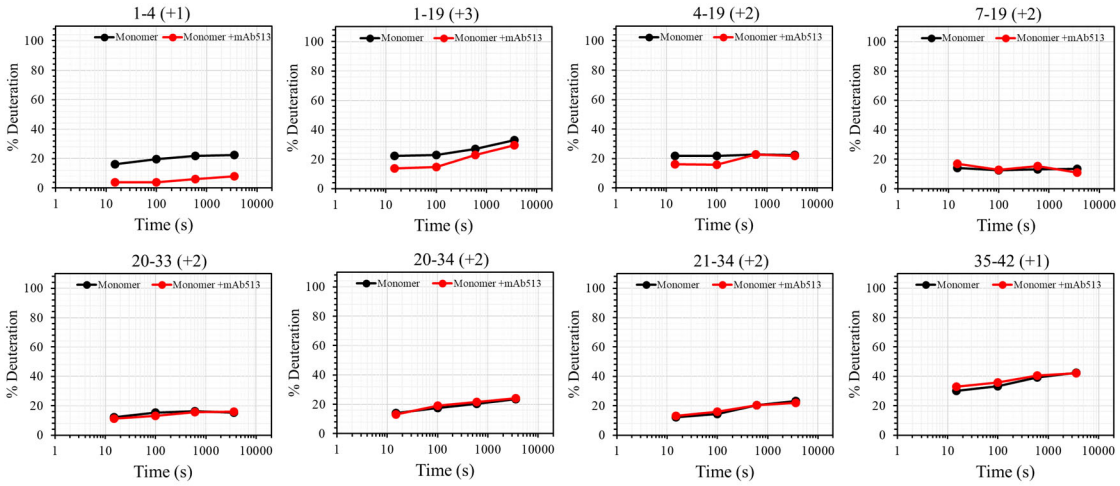

Figure 5.9. HDX epitope mapping for a non-selective antibody. Preliminary HDX-MS epitope mapping for mAb Aβ 513 antibody and Aβ42 monomers. Deuteration was determined for Aβ42 peptide fragments representing the N-terminal, middle, and C-terminal regions of Aβ42, 8 of which are shown. Antibody binding (decreased HDX) was observed in both the N- and C-terminal regions. Each data point is the average of n=2 measurements and standard error bars are shown but obscured within the diameter of the symbols. Statistical analysis was done using a 2-tailed paired T-test with p values < 0.5 considered significant.

5.4. Conclusion

Currently, conformation-selective antibodies are the primary tool for identifying Aβ species in a variety of AD tissue samples. However, little is known typically about the antigen structure, the conformation motif that is recognized by the antibody, and the location of the binding site (epitope). An informative and more productive strategy is to understand what, where, and how the antibody is binding to the target. This information will not only allow better interpretation of important tissue and fluid analysis but also yield structural insights about the antigen. This chapter significantly contributed to determining that Aβ42 protofibrils possess a conformational epitope for mAbSL and that this epitope has a specific structure distinct from monomers and fibrils. Furthermore, it was confirmed that the epitope lies in the N- and C-terminal regions of Aβ42.

Epitope-mapping approach accurately determined the main antigenic sites revealing distinct changes in local conformational dynamics when the antibody is bound to the antigen.

The meticulous characterization of conformational-specific antibodies and investigation of the specificity of these antibodies is quintessential (Saper et al. 2009). There has not been much progress in studying the interaction and binding of the antibodies targeting the protofibril structure (Söllvander et al. 2018). The knowledge of where the antibody binds to the protofibril structure is critical for understanding the mechanism of how Aβ changes from monomer to soluble protofibril form and then finally to insoluble fibril. Ultimately, efforts to decrease protofibrils using antibodies may slow or reverse the progression of AD and potentially assist in preventing neuronal damage.

The research plan explored the epitope of mAbSL and the binding affinity of the interaction. It provided us with insights into the residues involved in the interaction with the antibody. This methodology helped nail down the changes in protein flexibility and conformation when bound to the selective monoclonal antibody compared to a non-selective antibody to determine the binding sites on Aβ42 protofibril. Conclusively, the experimentation designed for this aim determined the conformational epitope of the mAbSL on the Aβ42 protofibrils.

Structural knowledge of Aβ42 filaments may lead to the strategic development of better animal and in vitro models for studying the disease, inhibitors for Aβ42 fibril assembly, and imaging agents with enhanced sensitivity and specificity.

CHAPTER 6. CONVERSION OF A SELECTIVE ANTIBODY TO A NON-SELECTIVE ANTIBODY

A class of monoclonal Aβ42 protofibril-selective antibodies have been expressed and identified. Two non-selective antibodies that were not selective for recognizing one conformational form of Aβ over other were found to be mAb Aβ 513 and 550. Carefully analyzing the difference in the sequences of conformational-selective and non-selective antibodies led to the identification of specific residues in the heavy-chain and light-chain variable regions. The study aimed to predict the HC and LC residues that confer conformational selectivity to Aβ antibodies.

Sequence analysis in HC and LC variable region: Heavy chain variable regions have 138 or 139 amino acid residues whereas the light chain variable region sequences are 124 in length. There were 17 differences found between Aβ-protofibril selective antibody (mAbSL 113) and non-selective antibody (mAb Aβ 513 or 550) in the heavy-chain amino acid sequence. However, 14 of those substitutions determined in mAb Aβ 513 were present in other protofibril selective antibodies. Most probably these 14 residues did not participate in providing selectivity to Aβ-protofibrils. The 3 remaining amino acid substitutions within mAbSL 113 HC most likely were involved in contributing significantly to conferring selectivity (Table 6.1). Similarly, examining LC variable region amino acid sequences highlighted 10 amino acid residues (out of 124 residues in LC) that differentiated mAbSL 113 to mAb Aβ 513 or mAb Aβ 550. 3 residues were chosen on similar grounds (Table 6.1)

Figure 6.1. Key amino acid differences between conformational-selective Aβ antibody and Aβ non-selective antibody. The differences are represented as selective antibody mAbSL 113 non-selective monoclonal antibody mAb Aβ 513 or mAbSL 550.

Heavy chain	Light chain
Glycine (G) → Arginine (R)	Serine (S) → Asparagine (N)
Aspartic acid (D) → Serine (S)	Asparagine (N) → Lysine (K)
Proline (P) → Isoleucine (I)	Alanine (A) → Glycine (G)

We aimed to introduce single- and double-point mutations into Aβ-protofibril selective antibody mAbSL 113 HC and LC and evaluate the effect of these introduced changes on Aβ selectivity (Figure 6.2). Site-directed mutagenesis required various steps. The single point mutation we focused on was substitution of mAbSL HC amino acid residue glycine to arginine. The mutation chosen in the nucleic acid sequence was from GGC to CGC (Figure 6.3). Two attempts were made to design our primers.

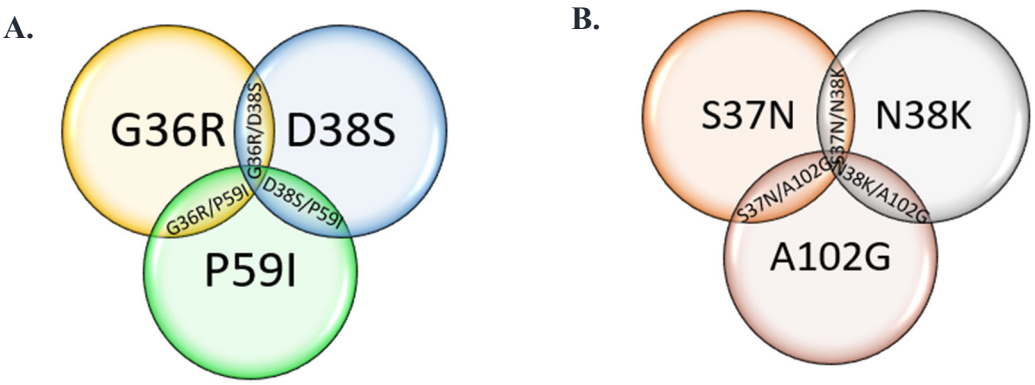

Figure 6.2. Proposed single or double amino acid substitutions in mAbSL 113 through site-directed mutagenesis studies. **A.** Heavy-chain mutations **B.** Light chain-mutations proposed.

Amino acid residue	33	34	35	36	37	38	39
113	F	S	S	G	Y	D	M
113 G36R	F	S	S	R	Y	D	M

NA base	97	98	99	100	101	102	103	104	105	106	107	108	109	110	111	112	113	114	115	116	117
113	T	T	C	A	G	T	A	G	C	G	G	C	T	A	C	G	A	C	A	T	G
113 G36R	T	T	C	A	G	T	A	G	C	C	G	C	T	A	C	G	A	C	A	T	G

Figure 6.3. Introduction of a single nucleotide mutation in mAbSL 113 HC

Our expedition with using Thermo Scientific™ Phusion ™ site-directed mutagenesis kit involved mAbSL HC plasmid subjected to denaturation, annealing with 5'-phosphorylayed primers, extension, ligation by T4 DNA ligase and transformation into DH5α E. coli cells. Mini-prep purification followed by analysis of sequence obtained from the mutated plasmid (Figure 6.4).

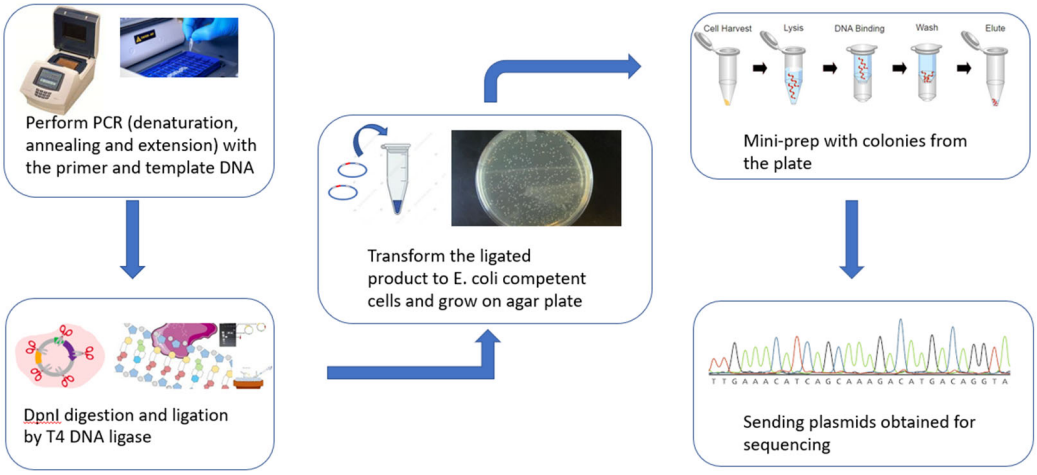

Figure 6.4. Steps involved in site-directed mutagenesis.

All the steps were performed as mentioned in the method section using primer 1 (Figure 6.5) but the mutant plasmid was not of the right sequence. The primer bands were observed in the gel analysis of the PCR product indicating that the intact primers might have dimerized because of being self-complementary to each other and PCR product was not formed (Figure 6.6A and 6.6C). The mutant colonies were also analysed and there was no signal observed in mutant colonies (Figure 6.6B and 6.6D). Tweaking the temperature and other conditions also did not help.

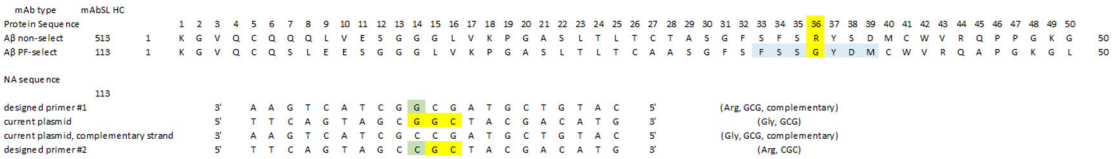

Figure 6.5. Design of Primer 1 shown.

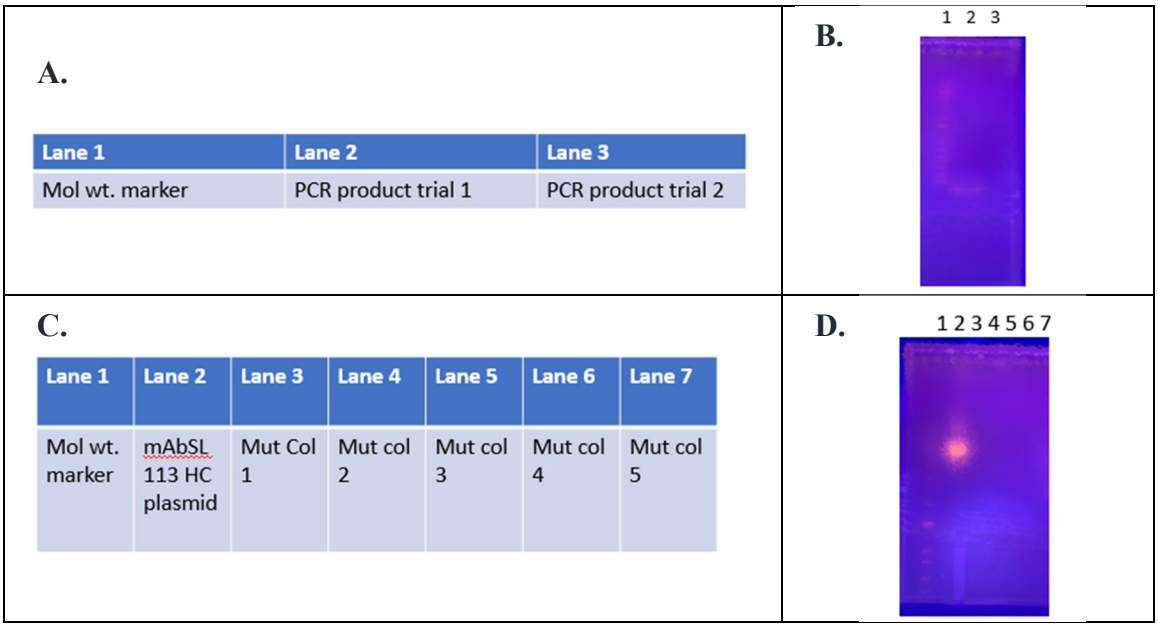

Figure 6.6. DNA gel analysis using Primer 1 design. A. Lane-wise information of the PCR product introduced during gel electrophoresis. B. Only primer bands observed in lane 2 and 3. C. Lane-wise information of the plasmids analyzed with different colonies after performing all the steps of site-directed mutagenesis. D. The bright band represents plasmid band from mAbSL HC (positive control). No successful mutation observed.

The troubleshooting was performed to take a look at each step of site-directed mutagenesis technique. Firstly, primer design was modified to make the primers not complementary to each other (Figure 6.7A) and the reagents used in the PCR reaction were optimized several times to ensure the formation of the plasmid (Figure 6.7B). The annealing temperature of 65°C provided the best results. Two bands appeared without including DMSO and a single product appeared after including 1.5% DMSO. This indicates that DMSO prevented non-specific binding (Figure 6.7C).

A.

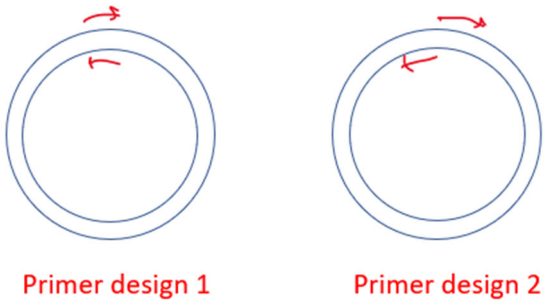

B.

Lane 1	Lane 2	Lane 3	Lane 4	Lane 5	Lane 6
Mol. Wt. marker	R1 (65°C)	R1 with DMSO (65°C)	R2 (66°C)	R2 with DMSO (66°C)	Control

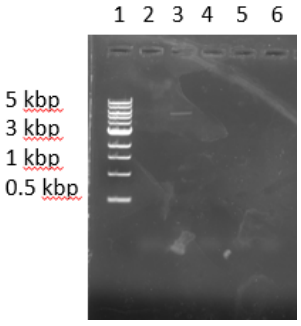

C.

	1 tube (ul)	Samples without DMSO (ul) Three tubes	Samples with DMSO
Nuclease free water, H2O		79.5	50
5X Phusion buffer	10	30	20
10 mM dNTPs	1	3	2
Forward primer	5	15	10
Reverse primer	5	15	10
Template DNA (mAbSL 113 HC plasmid)		2+2+2 (R1+R2+C)	2+2 (R1'+R2')
Phusion Hot Start DNA Polymerase (new)	0.5	1.5	1
DMSO (Dr. Chubiz lab)	1.5	-	3

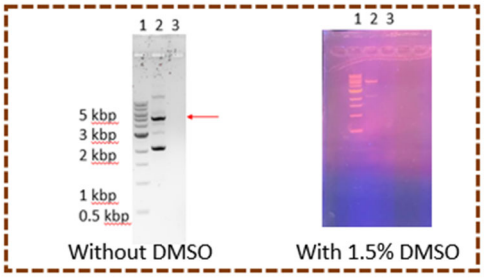

Figure 6.7. Successful PCR product formation with the use of primer 2. **A.** Schematic representation of both the primer design. **B.** Two different annealing temperatures used for PCR reaction of the primer with the product with and without

including DMSO. PCR product formed with annealing temperature 65°. **C.** The optimized reagents used for performing PCR.

Transformation step was probed using Phusion control reaction where LB-ampicillin agar plate had X-gal and IPTG which produces blue and white colonies. The efficient transformation was ensured with more blue colonies being formed. Transformation with both Topshot and DH5α E. coli cells was carried out. Better results with topshot cells were observed (Figure 6.8). Water was also used as a control and there was no bacterial growth observed for the transformation plate with water added to the cells. However, later bacterial growth with DH5α E. coli cells took place.

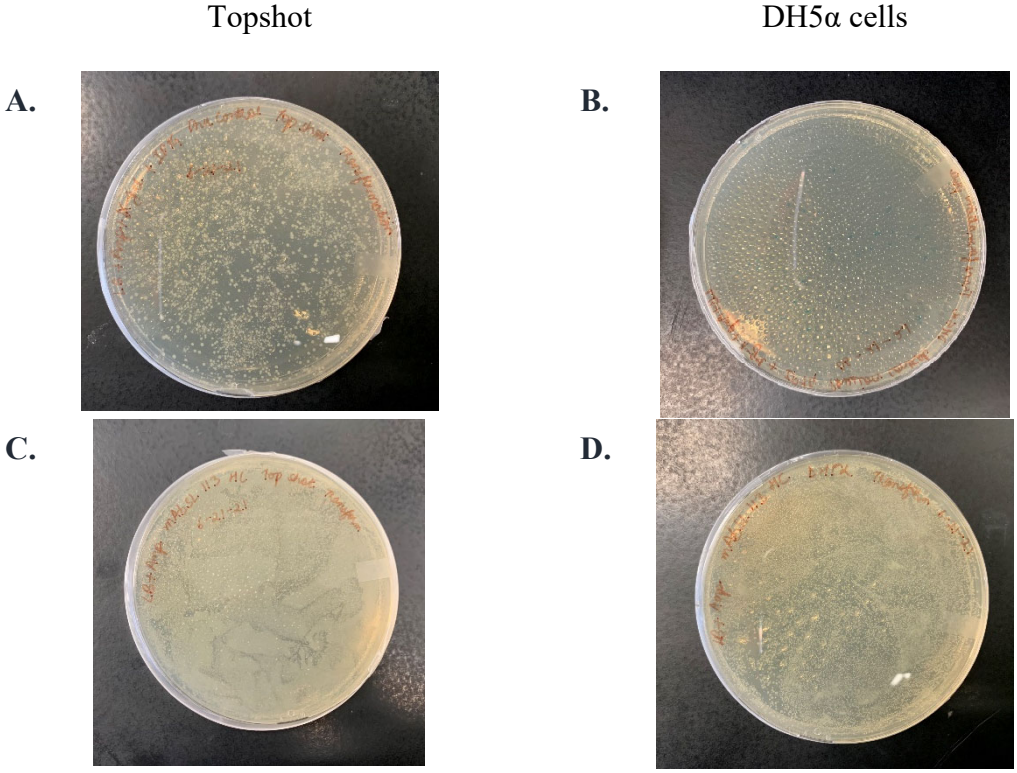

E. 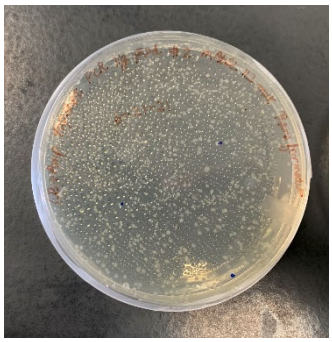 **F.** 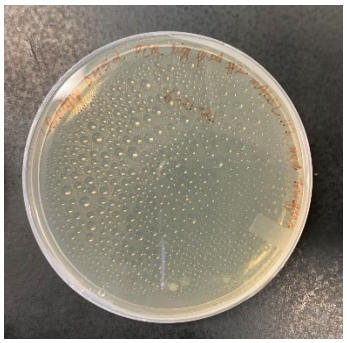

Figure 6.8. Transformation step was evaluated using Topshot cells (A,C,E) and DH5α cells (B,D,F). A. Control reaction using LB-ampicillin agar-plate that has X-gal and IPTG produced white and blue colonies. Transformation efficiency ensured. B. Bacterial colony growth in both the cells using mAbSL HC plasmid as a positive control. Massive colony growth ensured in both the type of cells. C. Transformation performed with PCR product ensured colony growth with Topshot cells.

Conclusion: It is an ongoing work to convert a selective monoclonal antibody by introducing mutations in the HC variable region of the plasmid. However, no conclusive result has been obtained. The future studies after successful site-directed mutagenesis to engineer the point mutations will involve cloning, expression and ELISA evaluation of the engineered antibody. The knowledge of the key residues in HC and LC of the conformational-selective antibodies that are instrumental in conformational selectivity of Aβ protofibrils will help us in extrapolation of structural details about Aβ protofibril. The epitope determination study will strengthen the extracted information through these studies.

CONCLUSION

The fulcrum of driving AD pathology onset has been conspicuously attributed towards the central role played by Aβ aggregation and the soluble oligomers have a pivotal role in exacerbating the disease progression (Bemporad and Chiti 2012). The hallmarks of AD, Aβ plaques, can be clearly visible in brain samples, whereas soluble oligomeric assemblies, polydisperse in size, are obscured. The mechanism of these aberrant oligomeric assemblies has been widely studied. However, the structure of these diffused toxic counterparts of Aβ still remain elusive (Tomic et al. 2009).

Monoclonal antibodies have emerged as a versatile tool for research, diagnostic and disease mitigation. These have been instrumental in detection of pathological hallmarks in AD. The research work has helped determine structural aspects of Aβ protofibril that influence conformation-selective antibodies and strengthened molecular level insights on the soluble Aβ protofibrils. Determination of conformational motifs and antibody residues involved for the soluble Aβ protofibril species has great success towards diagnostics and therapeutics aspects of AD and other neurodegenerative diseases. Conformational epitope for monoclonal antibody on Aβ protofibril structure has been established in our study. Structural studies correlate the core structure of Aβ protofibril to plaque bound Aβ fibrillar structure. Effect of mAbSL on amyloid nucleation and fibrillation is a novel area to be investigated due to the potential diagnostic and therapeutic uses in AD patients. Knowledge of Aβ42 protofibril structure may lead to potential development of treatment targeting the species.

The proposed project mapped the conformational epitope of mAbSL 113 on the protofibril by employing various techniques such as antibody competition ELISA and hydrogen-deuterium exchange mass spectrometry.

Aβ42 protofibrils are important therapeutic targets identified and are well-known in the progression of AD. The antibodies used in the project established and identified the key regions to be targeted on the Aβ42 aggregation pathway. It helped gain in-depth knowledge about the structural changes of these inflammatory species involved in the pathogenesis of AD.

BIBLIOGRAPHY

1. Ajit, D., M. L. Udan, G. Paranjape and M. R. Nichols (2009). "Amyloid-beta (1-42) fibrillar precursors are optimal for inducing tumor necrosis factor-alpha production in the THP-1 human monocytic cell line." Biochemistry **48**(38): 9011-9021.
2. Andreasen, N. and K. Blennow (2002). "Beta-amyloid (Abeta) protein in cerebrospinal fluid as a biomarker for Alzheimer's disease." Peptides **23**(7): 1205-1214.
3. Au, D. F., D. Ostrovsky, R. Fu and L. Vugmeyster (2019). "Solid-state NMR reveals a comprehensive view of the dynamics of the flexible, disordered N-terminal domain of amyloid-β fibrils." Journal of Biological Chemistry **294**(15): 5840-5853.
4. Baldassarre, M., C. M. Baronio, L. A. Morozova-Roche and A. Barth (2017). "Amyloid β-peptides 1-40 and 1-42 form oligomers with mixed β-sheets." Chem Sci **8**(12): 8247-8254.
5. Bateman, R. J., C. Xiong, T. L. Benzinger, A. M. Fagan, A. Goate, N. C. Fox, D. S. Marcus, N. J. Cairns, X. Xie, T. M. Blazey, D. M. Holtzman, A. Santacruz, V. Buckles, A. Oliver, K. Moulder, P. S. Aisen, B. Ghetti, W. E. Klunk, E. McDade, R. N. Martins, C. L. Masters, R. Mayeux, J. M. Ringman, M. N. Rossor, P. R. Schofield, R. A. Sperling, S. Salloway and J. C. Morris (2012). "Clinical and biomarker changes in dominantly inherited Alzheimer's disease." N Engl J Med **367**(9): 795-804.
6. Bekris, L. M., C.-E. Yu, T. D. Bird, and D. W. Tsuang (2010). "Review Article: Genetics of Alzheimer Disease." Journal of Geriatric Psychiatry and Neurology **23**(4): 213-227.
7. Bemporad, F. and F. Chiti (2012). "Protein Misfolded Oligomers: Experimental Approaches, Mechanism of Formation, and Structure-Toxicity Relationships." Chemistry & Biology **19**(3): 315-327.

8. Bitan, G., M. D. Kirkitadze, A. Lomakin, S. S. Vollers, G. B. Benedek and D. B. Teplow (2003). "Amyloid beta;-protein (Abeta) assembly: Abeta 40 and Abeta 42 oligomerize through distinct pathways." Proceedings of the National Academy of Sciences **100**(1): 330-335.
9. Bloom, G. S. (2014). "Amyloid-β and tau: the trigger and bullet in Alzheimer disease pathogenesis." JAMA Neurol **71**(4): 505-508.
10. Bradbury, A. R. M., N. D. Trinklein, H. Thie, I. C. Wilkinson, A. K. Tandon, S. Anderson, C. L. Bladen, B. Jones, S. F. Aldred, M. Bestagno, O. Burrone, J. Maynard, F. Ferrara, J. S. Trimmer, J. Görnemann, J. Glanville, P. Wolf, A. Frenzel, J. Wong, X. Y. Koh, H. Y. Eng, D. Lane, M. P. Lefranc, M. Clark and S. Dübel (2018). "When monoclonal antibodies are not monospecific: Hybridomas frequently express additional functional variable regions." MAbs **10**(4): 539-546.
11. Bressler, S. L., M. D. Gray, B. L. Sopher, Q. Hu, M. G. Hearn, D. G. Pham, M. B. Dinulos, K. Fukuchi, S. S. Sisodia, M. A. Miller, C. M. Disteche and G. M. Martin (1996). "cDNA cloning and chromosome mapping of the human Fe65 gene: interaction of the conserved cytoplasmic domains of the human beta-amyloid precursor protein and its homologues with the mouse Fe65 protein." Hum Mol Genet **5**(10): 1589-1598.
12. Carrillo-Mora, P., R. Luna, and L. Colín-Barenque (2014). "Amyloid beta: multiple mechanisms of toxicity and only some protective effects?" Oxid Med Cell Longev **2014**: 795375.
13. Chalmers, M. J., S. A. Busby, B. D. Pascal, M. R. Southern and P. R. Griffin (2007). "A two-stage differential hydrogen deuterium exchange method for the rapid characterization of protein/ligand interactions." J Biomol Tech **18**(4): 194-204.
14. Chen, G. F., T. H. Xu, Y. Yan, Y. R. Zhou, Y. Jiang, K. Melcher, and H. E. Xu (2017). "Amyloid beta: structure, biology and structure-based therapeutic development." Acta Pharmacol Sin **38**(9): 1205-1235.
15. Coalier, K. A., G. S. Paranjape, S. Karki and M. R. Nichols (2013). "Stability of early-stage amyloid-β (1-42) aggregation species." Biochim Biophys Acta **1834**(1): 65-70.
16. Colvin, B. A., V. A. Rogers, J. A. Kulas, E. A. Ridgway, F. S. Amtashar, C. K. Combs and M. R. Nichols (2017). "The conformational epitope for a new Aβ42 protofibril-selective antibody partially overlaps with the peptide N-terminal region." J Neurochem **143**(6): 736-749.
17. Colvin, M. T., R. Silvers, Q. Z. Ni, T. V. Can, I. Sergeyev, M. Rosay, K. J. Donovan, B. Michael, J. Wall, S. Linse and R. G. Griffin (2016). "Atomic Resolution Structure of Monomorphic Aβ42 Amyloid Fibrils." Journal of the American Chemical Society **138**(30): 9663-9674.
18. Dhami, K. B., S. Karki, A. Parks, C. G. Nichols, and M. R. Nichols (2022). "Development of β-sheet structure in Aβ aggregation intermediates diminishes exposed hydrophobic surface area and enhances proinflammatory activity." Biochimica et Biophysica Acta (BBA) - Proteins and Proteomics **1870**(9): 140817.
19. Englund, H., D. Sehlin, A. S. Johansson, L. N. Nilsson, P. Gellerfors, S. Paulie, L. Lannfelt and F. E. Pettersson (2007). "Sensitive ELISA detection of amyloid-beta protofibrils in biological samples." J Neurochem **103**(1): 334-345.

20. Fernandez, M. A., J. A. Klutkowski, T. Freret and M. S. Wolfe (2014). "Alzheimer presenilin-1 mutations dramatically reduce trimming of long amyloid β-peptides (Aβ) by γ-secretase to increase 42-to-40-residue Aβ." J Biol Chem **289**(45): 31043-31052.
21. Folch, J., M. Ettcheto, D. Petrov, S. Abad, I. Pedrós, M. Marin, J. Olloquequi and A. Camins (2018). "Una revisión de los avances en la terapéutica de la enfermedad de Alzheimer: estrategia frente a la proteína β-amiloide." Neurología **33**(1): 47-58.
22. Golde, T. E. (2022). "Alzheimer's disease – the journey of a healthy brain into organ failure." Molecular Neurodegeneration **17**(1): 18.
23. Gouwens, L. K., M. S. Ismail, V. A. Rogers, N. T. Zeller, E. C. Garrad, F. S. Amtashar, N. J. Makoni, D. C. Osborn and M. R. Nichols (2018). "Aβ42 Protofibrils Interact with and Are Trafficked through Microglial-Derived Microvesicles." ACS Chem Neurosci **9**(6): 1416-1425.
24. Gouwens, L. K., N. J. Makoni, V. A. Rogers and M. R. Nichols (2016). "Amyloid-β42 protofibrils are internalized by microglia more extensively than monomers." Brain Res **1648**(Pt A): 485-495.
25. Gremer, L., D. Schölzel, C. Schenk, E. Reinartz, J. Labahn, R. B. G. Ravelli, M. Tusche, C. Lopez-Iglesias, W. Hoyer, H. Heise, D. Willbold and G. F. Schröder (2017). "Fibril structure of amyloid-β (1-42) by cryo-electron microscopy." Science **358**(6359): 116-119.
26. Gu, L. and Z. Guo (2013). "Alzheimer's Aβ42 and Aβ40 peptides form interlaced amyloid fibrils." Journal of Neurochemistry **126**(3): 305-311.
27. Haass, C. and D. J. Selkoe (2007). "Soluble protein oligomers in neurodegeneration: lessons from the Alzheimer's amyloid β-peptide." Nature Reviews Molecular Cell Biology **8**(2): 101-112.
28. Hampel, H., J. Hardy, K. Blennow, C. Chen, G. Perry, S. H. Kim, V. L. Villemagne, P. Aisen, M. Vendruscolo, T. Iwatsubo, C. L. Masters, M. Cho, L. Lannfelt, J. L. Cummings and A. Vergallo (2021). "The Amyloid-β Pathway in Alzheimer's Disease." Mol Psychiatry **26**(10): 5481-5503.
29. Hardy, J. and D. J. Selkoe (2002). "The amyloid hypothesis of Alzheimer's disease: progress and problems on the road to therapeutics." Science **297**(5580): 353-356.
30. Hardy, J. A. and G. A. Higgins (1992). "Alzheimer's disease: the amyloid cascade hypothesis." Science **256**(5054): 184-185.
31. Harper, J. D., C. M. Lieber and P. T. Lansbury, Jr. (1997). "Atomic force microscopic imaging of seeded fibril formation and fibril branching by the Alzheimer's disease amyloid-beta protein." Chem Biol **4**(12): 951-959.
32. Harper, J. D., S. S. Wong, C. M. Lieber and P. T. Lansbury (1997). "Observation of metastable Abeta amyloid protofibrils by atomic force microscopy." Chem Biol **4**(2): 119-125.
33. Harper, J. D., S. S. Wong, C. M. Lieber and P. T. Lansbury, Jr. (1999). "Assembly of A beta amyloid protofibrils: an in vitro model for a possible early event in Alzheimer's disease." Biochemistry **38**(28): 8972-8980.
34. Hori, Y., T. Hashimoto, H. Nomoto, B. T. Hyman, and T. Iwatsubo (2015). "Role of Apolipoprotein E in β-Amyloidogenesis: ISOFORM-SPECIFIC EFFECTS ON

PROTOFIBRIL TO FIBRIL CONVERSION OF Aβ IN VITRO AND BRAIN Aβ DEPOSITION IN VIVO." J Biol Chem **290**(24): 15163-15174.
35. Huang, Y. R. and R. T. Liu (2020). "The Toxicity and Polymorphism of β-Amyloid Oligomers." Int J Mol Sci **21**(12).
36. Iannuzzi, C., G. Irace and I. Sirangelo (2015). "The effect of glycosaminoglycans (GAGs) on amyloid aggregation and toxicity." Molecules **20**(2): 2510-2528.
37. Ittner, A., S. W. Chua, J. Bertz, A. Volkerling, J. van der Hoven, A. Gladbach, M. Przybyla, M. Bi, A. van Hummel, C. H. Stevens, S. Ippati, L. S. Suh, A. Macmillan, G. Sutherland, J. J. Kril, A. P. Silva, J. P. Mackay, A. Poljak, F. Delerue, Y. D. Ke and L. M. Ittner (2016). "Site-specific phosphorylation of tau inhibits amyloid-β toxicity in Alzheimer's mice." Science **354**(6314): 904-908.
38. Jarrett, J. T. and P. T. Lansbury, Jr. (1993). "Seeding "one-dimensional crystallization" of amyloid: a pathogenic mechanism in Alzheimer's disease and scrapie?" Cell **73**(6): 1055-1058.
39. Jeremic, D., L. Jiménez-Díaz and J. D. Navarro-López (2021). "Past, present and future of therapeutic strategies against amyloid-β peptides in Alzheimer's disease: a systematic review." Ageing Res Rev **72**: 101496.
40. Karran, E. and B. De Strooper (2022). "The amyloid hypothesis in Alzheimer disease: new insights from new therapeutics." Nature Reviews Drug Discovery **21**(4): 306-318.
41. Kayed, R., E. Head, J. L. Thompson, T. M. McIntire, S. C. Milton, C. W. Cotman, and C. G. Glabe (2003). "Common structure of soluble amyloid oligomers implies common mechanism of pathogenesis." Science **300**(5618): 486-489.
42. Kelly, S. C., B. He, S. E. Perez, S. D. Ginsberg, E. J. Mufson and S. E. Counts (2017). "Locus coeruleus cellular and molecular pathology during the progression of Alzheimer's disease." Acta Neuropathol Commun **5**(1): 8.
43. Kinoshita, A., C. M. Whelan, O. Berezovska and B. T. Hyman (2002). "The gamma secretase-generated carboxyl-terminal domain of the amyloid precursor protein induces apoptosis via Tip60 in H4 cells." J Biol Chem **277**(32): 28530-28536.
44. Kirkitadze, M. D., M. M. Condron and D. B. Teplow (2001). "Identification and characterization of key kinetic intermediates in amyloid β-protein fibrillogenesis11Edited by F. Cohen." Journal of Molecular Biology **312**(5): 1103-1119.
45. Klein, W. L. (2002). "Abeta toxicity in Alzheimer's disease: globular oligomers (ADDLs) as new vaccine and drug targets." Neurochem Int **41**(5): 345-352.
46. Kodali, R. and R. Wetzel (2007). "Polymorphism in the intermediates and products of amyloid assembly." Curr Opin Struct Biol **17**(1): 48-57.
47. Kollmer, M., W. Close, L. Funk, J. Rasmussen, A. Bsoul, A. Schierhorn, M. Schmidt, C. J. Sigurdson, M. Jucker and M. Fändrich (2019). "Cryo-EM structure and polymorphism of Aβ amyloid fibrils purified from Alzheimer's brain tissue." Nature Communications **10**(1): 4760.
48. Kwon, S., M. Iba, C. Kim and E. Masliah (2020). "Immunotherapies for Aging-Related Neurodegenerative Diseases-Emerging Perspectives and New Targets." Neurotherapeutics **17**(3): 935-954.

49. Lall, R., R. Mohammed, and U. Ojha (2019). "What are the links between hypoxia and Alzheimer's disease?" Neuropsychiatr Dis Treat **15**: 1343-1354.
50. Lemere, C. A., F. Lopera, K. S. Kosik, C. L. Lendon, J. Ossa, T. C. Saido, H. Yamaguchi, A. Ruiz, A. Martinez, L. Madrigal, L. Hincapie, J. C. Arango, D. C. Anthony, E. H. Koo, A. M. Goate, D. J. Selkoe and J. C. Arango (1996). "The E280A presenilin 1 Alzheimer mutation produces increased A beta 42 deposition and severe cerebellar pathology." Nat Med **2**(10): 1146-1150.
51. Levine III, H. (1993). "Thioflavine T interaction with synthetic Alzheimer's disease β-amyloid peptides: Detection of amyloid aggregation in solution." Protein Science **2**(3): 404-410.
52. Li, S. and D. J. Selkoe (2020). "A mechanistic hypothesis for the impairment of synaptic plasticity by soluble Aβ oligomers from Alzheimer's brain." J Neurochem **154**(6): 583-597.
53. Livingstone, R. W., M. K. Elder, M. C. Barrett, C. M. Westlake, K. Peppercorn, W. P. Tate, W. C. Abraham, and J. M. Williams (2019). "Secreted Amyloid Precursor Protein-Alpha Promotes Arc Protein Synthesis in Hippocampal Neurons." Front Mol Neurosci **12**: 198.
54. Nhan, H. S., K. Chiang, and E. H. Koo (2015). "The multifaceted nature of amyloid precursor protein and its proteolytic fragments: friends and foes." Acta Neuropathol **129**(1): 1-19.
55. Nichols, M. R., B. A. Colvin, E. A. Hood, G. S. Paranjape, D. C. Osborn and S. E. Terrill-Usery (2015). "Biophysical comparison of soluble amyloid-β (1-42) protofibrils, oligomers, and protofilaments." Biochemistry **54**(13): 2193-2204.
56. Nichols, M. R., M. A. Moss, D. K. Reed, W. L. Lin, R. Mukhopadhyay, J. H. Hoh, and T. L. Rosenberry (2002). "Growth of b-amyloid (1-40) protofibrils by monomer elongation and lateral association. Characterization of distinct products by light scattering and atomic force microscopy." Biochemistry **41**: 6115-6127.
57. Nichols, M. R., M. A. Moss, D. K. Reed, W. L. Lin, R. Mukhopadhyay, J. H. Hoh and T. L. Rosenberry (2002). "Growth of beta-amyloid (1-40) protofibrils by monomer elongation and lateral association. Characterization of distinct products by light scattering and atomic force microscopy." Biochemistry **41**(19): 6115-6127.
58. Nilsberth, C., A. Westlind-Danielsson, C. B. Eckman, M. M. Condron, K. Axelman, C. Forsell, C. Stenh, J. Luthman, D. B. Teplow, S. G. Younkin, J. Näslund and L. Lannfelt (2001). "The 'Arctic' APP mutation (E693G) causes Alzheimer's disease by enhanced Abeta protofibril formation." Nat Neurosci **4**(9): 887-893.
59. O'Nuallain, B., D. B. Freir, A. J. Nicoll, E. Risse, N. Ferguson, C. E. Herron, J. Collinge and D. M. Walsh (2010). "Amyloid beta-protein dimers rapidly form stable synaptotoxic protofibrils." J Neurosci **30**(43): 14411-14419.
60. Ono, K., M. M. Condron and D. B. Teplow (2009). "Structure-neurotoxicity relationships of amyloid beta-protein oligomers." Proc Natl Acad Sci U S A **106**(35): 14745-14750.
61. Ono, K., and M. Tsuji (2020). "Protofibrils of Amyloid-β are Important Targets of a Disease-Modifying Approach for Alzheimer's Disease." Int J Mol Sci **21**(3).
62. Palop, J. J., J. Chin, E. D. Roberson, J. Wang, M. T. Thwin, N. Bien-Ly, J. Yoo, K. O. Ho, G. Q. Yu, A. Kreitzer, S. Finkbeiner, J. L. Noebels and L. Mucke (2007).

"Aberrant excitatory neuronal activity and compensatory remodeling of inhibitory hippocampal circuits in mouse models of Alzheimer's disease." Neuron **55**(5): 697-711.
63. Paranjape, G. S., L. K. Gouwens, D. C. Osborn, and M. R. Nichols (2012). "Isolated amyloid-β (1-42) protofibrils, but not isolated fibrils, are robust stimulators of microglia." ACS Chem Neurosci **3**(4): 302-311.
64. Paranjape, G. S., S. E. Terrill, L. K. Gouwens, B. M. Ruck, and M. R. Nichols (2013). "Amyloid-β (1-42) protofibrils formed in modified artificial cerebrospinal fluid bind and activate microglia." J Neuroimmune Pharmacol **8**(1): 312-322.
65. Parhizkar, S. and D. M. Holtzman (2022). "APOE mediated neuroinflammation and neurodegeneration in Alzheimer's disease." Seminars in Immunology: 101594.
66. Perrin, R. J., A. M. Fagan, and D. M. Holtzman (2009). "Multimodal techniques for diagnosis and prognosis of Alzheimer's disease." Nature **461**(7266): 916-922.
67. Ribarič, S. (2018). "Peptides as Potential Therapeutics for Alzheimer's Disease." Molecules **23**(2): 283.
68. Roychaudhuri, R., T.-P. V. Huynh, T. R. Whitaker, E. Hodara, M. M. Condron and D. B. Teplow (2017). "A Critical Role of Ser26 Hydrogen Bonding in Aβ42 Assembly and Toxicity." Biochemistry **56**(48): 6321-6324.
69. Selkoe, D. J. (1991). "The molecular pathology of Alzheimer's disease." Neuron **6**(4): 487-498.
70. Selkoe, D. J. (1998). "The cell biology of beta-amyloid precursor protein and presenilin in Alzheimer's disease." Trends Cell Biol **8**(11): 447-453.
71. Selkoe, D. J. (2004). "Cell biology of protein misfolding: The examples of Alzheimer's and Parkinson's diseases." Nature Cell Biology **6**(11): 1054-1061.
72. Selkoe, D. J. and J. Hardy (2016). "The amyloid hypothesis of Alzheimer's disease at 25 years." EMBO Mol Med **8**(6): 595-608.
73. Sengupta, U., A. N. Nilson and R. Kayed (2016). "The Role of Amyloid-β Oligomers in Toxicity, Propagation, and Immunotherapy." EBioMedicine **6**: 42-49.
74. Serpell, L. C., M. Sunde, M. D. Benson, G. A. Tennent, M. B. Pepys, and P. E. Fraser (2000). "The protofilament substructure of amyloid fibrils11Edited by F. E. Cohen." Journal of Molecular Biology **300**(5): 1033-1039.
75. Seubert, P., C. Vigo-Pelfrey, F. Esch, M. Lee, H. Dovey, D. Davis, S. Sinha, M. Schlossmacher, J. Whaley, C. Swindlehurst et al. (1992). "Isolation and quantification of soluble Alzheimer's beta-peptide from biological fluids." Nature **359**(6393): 325-327.
76. Sevigny, J., P. Chiao, T. Bussière, P. H. Weinreb, L. Williams, M. Maier, R. Dunstan, S. Salloway, T. Chen, Y. Ling, J. O'Gorman, F. Qian, M. Arastu, M. Li, S. Chollate, M. S. Brennan, O. Quintero-Monzon, R. H. Scannevin, H. M. Arnold, T. Engber, K. Rhodes, J. Ferrero, Y. Hang, A. Mikulskis, J. Grimm, C. Hock, R. M. Nitsch and A. Sandrock (2016). "The antibody aducanumab reduces Aβ plaques in Alzheimer's disease." Nature **537**(7618): 50-56.
77. Söllvander, S., E. Nikitidou, L. Gallasch, M. Zyśk, L. Söderberg, D. Sehlin, L. Lannfelt and A. Erlandsson (2018). "The Aβ protofibril selective antibody mAb158 prevents accumulation of Aβ in astrocytes and rescues neurons from Aβ-induced cell death." J Neuroinflammation **15**(1): 98.

78. Southam, K. A., F. Stennard, C. Pavez and D. H. Small (2019). "Knockout of Amyloid β Protein Precursor (APP) Expression Alters Synaptogenesis, Neurite Branching and Axonal Morphology of Hippocampal Neurons." Neurochemical Research **44**(6): 1346-1355.
79. Terrill-Usery, S. E., B. A. Colvin, R. E. Davenport, and M. R. Nichols (2016). "Ab40 has a subtle effect on Ab42 protofibril formation, but to a lesser degree than Ab42 concentration, in Ab42/Ab40 mixtures." Arch Biochem Biophys **597**: 1-11.
80. Terrill-Usery, S. E., M. J. Mohan, and M. R. Nichols (2014). "Amyloid-β(1-42) protofibrils stimulate a quantum of secreted IL-1β despite significant intracellular IL-1β accumulation in microglia." Biochim Biophys Acta **1842**(11): 2276-2285.
81. Touchette, J. C., L. L. Williams, D. Ajit, F. Gallazzi and M. R. Nichols (2010). "Probing the amyloid-beta (1-40) fibril environment with substituted tryptophan residues." Arch Biochem Biophys **494**(2): 192-197.
82. Tycko, R. (2015). "Amyloid Polymorphism: Structural Basis and Neurobiological Relevance." Neuron **86**(3): 632-645.
83. Udan, M. L., D. Ajit, N. R. Crouse, and M. R. Nichols (2008). "Toll-like receptors 2 and 4 mediate Abeta(1-42) activation of the innate immune response in a human monocytic cell line." J Neurochem **104**(2): 524-533.
84. Vandenberghe, R., J. O. Rinne, M. Boada, S. Katayama, P. Scheltens, B. Vellas, M. Tuchman, A. Gass, J. B. Fiebach, D. Hill, K. Lobello, D. Li, T. McRae, P. Lucas, I. Evans, K. Booth, G. Luscan, B. T. Wyman, L. Hua, L. Yang, H. R. Brashear, and R. S. Black (2016). "Bapineuzumab for mild to moderate Alzheimer's disease in two global, randomized, phase 3 trials." Alzheimers Res Ther **8**(1): 18.
85. Walsh, D. M., D. M. Hartley, Y. Kusumoto, Y. Fezoui, M. M. Condron, A. Lomakin, G. B. Benedek, D. J. Selkoe and D. B. Teplow (1999). "Amyloid beta-protein fibrillogenesis. Structure and biological activity of protofibrillar intermediates." J Biol Chem **274**(36): 25945-25952.
86. Walsh, D. M., A. Lomakin, G. B. Benedek, M. M. Condron and D. B. Teplow (1997). "Amyloid beta-protein fibrillogenesis. Detection of a protofibrillar intermediate." J Biol Chem **272**(35): 22364-22372.
87. Wälti, M. A., F. Ravotti, H. Arai, C. G. Glabe, J. S. Wall, A. Böckmann, P. Güntert, B. H. Meier and R. Riek (2016). "Atomic-resolution structure of a disease-relevant Aβ(1-42) amyloid fibril." Proc Natl Acad Sci U S A **113**(34): E4976-4984.
88. Ward, M. W., C. G. Concannon, J. Whyte, C. M. Walsh, B. Corley, and J. H. Prehn (2010). "The amyloid precursor protein intracellular domain (AICD) disrupts actin dynamics and mitochondrial bioenergetics." J Neurochem **113**(1): 275-284.
89. Williams, A. D., E. Portelius, I. Kheterpal, J.-t. Guo, K. D. Cook, Y. Xu, and R. Wetzel (2004). "Mapping Aβ Amyloid Fibril Secondary Structure Using Scanning Proline Mutagenesis." Journal of Molecular Biology **335**(3): 833-842.
90. Wolfe, M. S. (2020). "Substrate recognition and processing by γ-secretase." Biochim Biophys Acta Biomembr **1862**(1): 183016.
91. Wong, C. W., V. Quaranta and G. G. Glenner (1985). "Neuritic plaques and cerebrovascular amyloid in Alzheimer disease are antigenically related." Proc Natl Acad Sci U S A **82**(24): 8729-8732.

92. Xiao, Y., B. Ma, D. McElheny, S. Parthasarathy, F. Long, M. Hoshi, R. Nussinov and Y. Ishii (2015). "Aβ (1–42) fibril structure illuminates self-recognition and replication of amyloid in Alzheimer's disease." Nature Structural & Molecular Biology **22**(6): 499-505.
93. Yang, L., J. Adhikari, M. L. Gross and L. Li (2017). "Kinetic Isotope Effects and Hydrogen/Deuterium Exchange Reveal Large Conformational Changes During the Catalysis of the Clostridium acetobutylicum Spore Photoproduct Lyase." Photochem Photobiol **93**(1): 331-342.
94. Yasumoto, T., Y. Takamura, M. Tsuji, T. Watanabe-Nakayama, K. Imamura, H. Inoue, S. Nakamura, T. Inoue, A. Kimura, S. Yano, H. Nishijo, Y. Kiuchi, D. B. Teplow and K. Ono (2019). "High molecular weight amyloid β (1-42) oligomers induce neurotoxicity via plasma membrane damage." Faseb j **33**(8): 9220-9234.
95. Ye, C. P., D. J. Selkoe and D. M. Hartley (2003). "Protofibrils of amyloid beta-protein inhibit specific K+ currents in neocortical cultures." Neurobiol Dis **13**(3): 177-190.
96. Zhang, Y., O. Guo, Y. Huo, G. Wang and H. Y. Man (2018). "Amyloid-β Induces AMPA Receptor Ubiquitination and Degradation in Primary Neurons and Human Brains of Alzheimer's Disease." J Alzheimers Dis **62**(4): 1789-1801.
97. Zhang, Z. and D. L. Smith (1993). "Determination of amide hydrogen exchange by mass spectrometry: a new tool for protein structure elucidation." Protein Sci **2**(4): 522-531.
98. Yang, Y., D. Arseni, W. Zhang, M. Huang, S. Lövestam, M. Schweighauser, A. Kotecha, A. G. Murzin, S. Y. Peak-Chew, J. Macdonald, I. Lavenir, H. J. Garringer, E. Gelpi, K. L. Newell, G. G. Kovacs, R. Vidal, B. Ghetti, B. Ryskeldi-Falcon, S. H. W. Scheres and M. Goedert (2022). "Cryo-EM structures of amyloid-β 42 filaments from human brains." Science **375**(6577): 167-172.
99. Busciglio, J., A. Lorenzo, and B. A. Yankner (1992). "Methodological variables in the assessment of beta amyloid neurotoxicity." Neurobiol Aging **13**(5): 609-612.
100. Pike, C. J., A. J. Walencewicz, C. G. Glabe and C. W. Cotman (1991). "In vitro aging of beta-amyloid protein causes peptide aggregation and neurotoxicity." Brain Res **563**(1-2): 311-314.
101. Syvänen, S., X. T. Fang, G. Hultqvist, S. R. Meier, L. Lannfelt and D. Sehlin (2017). "A bispecific Tribody PET radioligand for visualization of amyloid-beta protofibrils - a new concept for neuroimaging." Neuroimage **148**: 55-63.
102. Huang, Y. R. and R. T. Liu (2020). "The Toxicity and Polymorphism of β-Amyloid Oligomers." Int J Mol Sci **21**(12).

103. Lannfelt, L., C. Möller, H. Basun, G. Osswald, D. Sehlin, A. Satlin, V. Logovinsky and P. Gellerfors (2014). "Perspectives on future Alzheimer therapies: amyloid-β protofibrils - a new target for immunotherapy with BAN2401 in Alzheimer's disease." Alzheimers Res Ther **6**(2): 16.
104. Logovinsky, V., A. Satlin, R. Lai, C. Swanson, J. Kaplow, G. Osswald, H. Basun and L. Lannfelt (2016). "Safety and tolerability of BAN2401--a clinical study in Alzheimer's disease with a protofibril selective Aβ antibody." Alzheimers Res Ther **8**(1): 14.

105. Dhami, K. B., S. Karki, A. Parks, C. G. Nichols, and M. R. Nichols (2022). "Development of β-sheet structure in Aβ aggregation intermediates diminishes exposed hydrophobic surface area and enhances proinflammatory activity." Biochimica et Biophysica Acta (BBA) - Proteins and Proteomics **1870**(9): 140817.
106. Landles, C. and G. P. Bates (2004). "Huntingtin and the molecular pathogenesis of Huntington's disease. Fourth in molecular medicine review series." EMBO Rep **5**(10): 958-963.
107. Lannfelt, L., C. Möller, H. Basun, G. Osswald, D. Sehlin, A. Satlin, V. Logovinsky and P. Gellerfors (2014). "Perspectives on future Alzheimer therapies: amyloid-β protofibrils - a new target for immunotherapy with BAN2401 in Alzheimer's disease." Alzheimers Res Ther **6**(2): 16.
108. Lee, V. M., M. Goedert and J. Q. Trojanowski (2001). "Neurodegenerative tauopathies." Annu Rev Neurosci **24**: 1121-1159.
109. Nilsberth, C., A. Westlind-Danielsson, C. B. Eckman, M. M. Condron, K. Axelman, C. Forsell, C. Stenh, J. Luthman, D. B. Teplow, S. G. Younkin, J. Näslund and L. Lannfelt (2001). "The 'Arctic' APP mutation (E693G) causes Alzheimer's disease by enhanced Abeta protofibril formation." Nat Neurosci **4**(9): 887-893.
110. Ono, K. and M. Tsuji (2020). "Protofibrils of Amyloid-β are Important Targets of a Disease-Modifying Approach for Alzheimer's Disease." Int J Mol Sci **21**(3).
111. Parkin, E. T., A. Trew, G. Christie, A. Faller, R. Mayer, A. J. Turner and N. M. Hooper (2002). "Structure−Activity Relationship of Hydroxamate-Based Inhibitors on the Secretases that Cleave the Amyloid Precursor Protein, Angiotensin Converting Enzyme, CD23, and Pro-Tumor Necrosis Factor-α." Biochemistry **41**(15): 4972-4981.
112. Selkoe, D. J. (2004). "Cell biology of protein misfolding: The examples of Alzheimer's and Parkinson's diseases." Nature Cell Biology **6**(11): 1054-1061.
113. Walsh, D. M., D. M. Hartley, Y. Kusumoto, Y. Fezoui, M. M. Condron, A. Lomakin, G. B. Benedek, D. J. Selkoe and D. B. Teplow (1999). "Amyloid beta-protein fibrillogenesis. Structure and biological activity of protofibrillar intermediates." J Biol Chem **274**(36): 25945-25952.
114. Yasumoto, T., Y. Takamura, M. Tsuji, T. Watanabe-Nakayama, K. Imamura, H. Inoue, S. Nakamura, T. Inoue, A. Kimura, S. Yano, H. Nishijo, Y. Kiuchi, D. B. Teplow and K. Ono (2019). "High molecular weight amyloid β(1-42) oligomers induce neurotoxicity via plasma membrane damage." Faseb j **33**(8): 9220-9234.

115. Colvin, M. T., R. Silvers, Q. Z. Ni, T. V. Can, I. Sergeyev, M. Rosay, K. J. Donovan, B. Michael, J. Wall, S. Linse and R. G. Griffin (2016). "Atomic Resolution Structure of Monomorphic Aβ42 Amyloid Fibrils." Journal of the American Chemical Society **138**(30): 9663-9674.
116. Li, K. S., D. L. Rempel, and M. L. Gross (2016). "Conformational-Sensitive Fast Photochemical Oxidation of Proteins and Mass Spectrometry Characterize Amyloid Beta 1-42 Aggregation." J Am Chem Soc **138**(37): 12090-12098.
117. Niu, B., B. C. Mackness, D. L. Rempel, H. Zhang, W. Cui, C. R. Matthews, J. A. Zitzewitz and M. L. Gross (2017). "Incorporation of a Reporter Peptide in FPOP Compensates for Adventitious Scavengers and Permits Time-Dependent Measurements." Journal of the American Society for Mass Spectrometry **28**(2): 389-392.
118. Shi, L., T. Liu, M. L. Gross, and Y. Huang (2019). "Recognition of Human IgG1 by Fcγ Receptors: Structural Insights from Hydrogen-Deuterium Exchange and Fast Photochemical Oxidation of Proteins Coupled with Mass Spectrometry." Biochemistry **58**(8): 1074-1080.
119. Yan, Y., G. A. Grant, and M. L. Gross (2015). "Hydrogen-Deuterium Exchange Mass Spectrometry Reveals Unique Conformational and Chemical Transformations Occurring upon [4Fe-4S] Cluster Binding in the Type 2 L-Serine Dehydratase from Legionella pneumophila." Biochemistry **54**(34): 5322-5328.

120. Ajit, D., M. L. Udan, G. Paranjape and M. R. Nichols (2009). "Amyloid-beta (1-42) fibrillar precursors are optimal for inducing tumor necrosis factor-alpha production in the THP-1 human monocytic cell line." Biochemistry **48**(38): 9011-9021.
121. Gouwens, L. K., M. S. Ismail, V. A. Rogers, N. T. Zeller, E. C. Garrad, F. S. Amtashar, N. J. Makoni, D. C. Osborn and M. R. Nichols (2018). "Aβ42 Protofibrils Interact with and Are Trafficked through Microglial-Derived Microvesicles." ACS Chem Neurosci **9**(6): 1416-1425.
122. Gouwens, L. K., N. J. Makoni, V. A. Rogers and M. R. Nichols (2016). "Amyloid-β42 protofibrils are internalized by microglia more extensively than monomers." Brain Res **1648**(Pt A): 485-495.
123. Kodali, R. and R. Wetzel (2007). "Polymorphism in the intermediates and products of amyloid assembly." Curr Opin Struct Biol **17**(1): 48-57.
124. O'Nuallain, B., D. B. Freir, A. J. Nicoll, E. Risse, N. Ferguson, C. E. Herron, J. Collinge and D. M. Walsh (2010). "Amyloid beta-protein dimers rapidly form stable synaptotoxic protofibrils." The Journal of neuroscience: the official journal of the Society for Neuroscience **30**(43): 14411-14419.
125. Paranjape, G. S., L. K. Gouwens, D. C. Osborn, and M. R. Nichols (2012). "Isolated amyloid-β (1-42) protofibrils, but not isolated fibrils, are robust stimulators of microglia." ACS Chem Neurosci **3**(4): 302-311.

126. Paranjape, G. S., S. E. Terrill, L. K. Gouwens, B. M. Ruck, and M. R. Nichols (2013). "Amyloid-β (1-42) protofibrils formed in modified artificial cerebrospinal fluid bind and activate microglia." J Neuroimmune Pharmacol **8**(1): 312-322.
127. Pohanka, M. (2014). "Alzheimer´s disease and oxidative stress: a review." Curr Med Chem **21**(3): 356-364.
128. Terrill-Usery, S. E., M. J. Mohan, and M. R. Nichols (2014). "Amyloid-β (1-42) protofibrils stimulate a quantum of secreted IL-1β despite significant intracellular IL-1β accumulation in microglia." Biochim Biophys Acta **1842**(11): 2276-2285.
129. Udan, M. L., D. Ajit, N. R. Crouse, and M. R. Nichols (2008). "Toll-like receptors 2 and 4 mediate Abeta(1-42) activation of the innate immune response in a human monocytic cell line." J Neurochem **104**(2): 524-533.
130. Walsh, D. M., D. M. Hartley, Y. Kusumoto, Y. Fezoui, M. M. Condron, A. Lomakin, G. B. Benedek, D. J. Selkoe and D. B. Teplow (1999). "Amyloid beta-protein fibrillogenesis. Structure and biological activity of protofibrillar intermediates." J Biol Chem **274**(36): 25945-25952.
131. Walsh, D. M., A. Lomakin, G. B. Benedek, M. M. Condron and D. B. Teplow (1997). "Amyloid beta-protein fibrillogenesis. Detection of a protofibrillar intermediate." J Biol Chem **272**(35): 22364-22372.
132. Ye, C. P., D. J. Selkoe and D. M. Hartley (2003). "Protofibrils of amyloid β-protein inhibit specific K+ currents in neocortical cultures." Neurobiology of Disease **13**(3): 177-190.

133. Bonito-Oliva, A., S. Schedin-Weiss, S. S. Younesi, A. Tiiman, C. Adura, N. Paknejad, M. Brendel, Y. Romin, R. J. Parchem, C. Graff, V. Vukojević, L. O. Tjernberg, L. Terenius, B. Winblad, T. P. Sakmar and W. V. Graham (2019). "Conformation-specific antibodies against multiple amyloid protofibril species from a single amyloid immunogen." J Cell Mol Med **23**(3): 2103-2114.
134. Dragan, A. I., J. R. Casas-Finet, E. S. Bishop, R. J. Strouse, M. A. Schenerman and C. D. Geddes (2010). "Characterization of PicoGreen interaction with dsDNA and the origin of its fluorescence enhancement upon binding." Biophys J **99**(9): 3010-3019.
135. Mora, A. K., P. K. Singh, B. S. Patro, and S. Nath (2016). "PicoGreen: a better amyloid probe than Thioflavin-T." Chemical Communications **52**(82): 12163-12166.

136. Andreasen, N. and K. Blennow (2002). "Beta-amyloid (Abeta) protein in cerebrospinal fluid as a biomarker for Alzheimer's disease." Peptides **23**(7): 1205-1214.
137. Chung, H., M. I. Brazil, T. T. Soe and F. R. Maxfield (1999). "Uptake, degradation, and release of fibrillar and soluble forms of Alzheimer's amyloid beta-peptide by microglial cells." J Biol Chem **274**(45): 32301-32308.

138. Coalier, K. A., G. S. Paranjape, S. Karki and M. R. Nichols (2013). "Stability of early-stage amyloid-β (1-42) aggregation species." Biochim Biophys Acta **1834**(1): 65-70.
139. Daigneault, M., J. A. Preston, H. M. Marriott, M. K. Whyte, and D. H. Dockrell (2010). "The identification of markers of macrophage differentiation in PMA-stimulated THP-1 cells and monocyte-derived macrophages." PLoS One **5**(1): e8668.
140. Hardy, J. (1997). "Amyloid, the presenilins and Alzheimer's disease." Trends Neurosci **20**(4): 154-159.
141. Hardy, J. and D. J. Selkoe (2002). "The amyloid hypothesis of Alzheimer's disease: progress and problems on the road to therapeutics." Science **297**(5580): 353-356.
142. Hashimoto, T., K. Ogino, R. W. Shin, T. Kitamoto, T. Kikuchi and N. Shimizu (2010). "Age-dependent increase in lysosome-associated membrane protein 1 and early-onset behavioral deficits in APPSL transgenic mouse model of Alzheimer's disease." Neurosci Lett **469**(2): 273-277.
143. He, G., W. Luo, P. Li, C. Remmers, W. J. Netzer, J. Hendrick, K. Bettayeb, M. Flajolet, F. Gorelick, L. P. Wennogle and P. Greengard (2010). "Gamma-secretase activating protein is a therapeutic target for Alzheimer's disease." Nature **467**(7311): 95-98.
144. Heneka, M. T., M. J. Carson, J. El Khoury, G. E. Landreth, F. Brosseron, D. L. Feinstein, A. H. Jacobs, T. Wyss-Coray, J. Vitorica, R. M. Ransohoff, K. Herrup, S. A. Frautschy, B. Finsen, G. C. Brown, A. Verkhratsky, K. Yamanaka, J. Koistinaho, E. Latz, A. Halle, G. C. Petzold, T. Town, D. Morgan, M. L. Shinohara, V. H. Perry, C. Holmes, N. G. Bazan, D. J. Brooks, S. Hunot, B. Joseph, N. Deigendesch, O. Garaschuk, E. Boddeke, C. A. Dinarello, J. C. Breitner, G. M. Cole, D. T. Golenbock and M. P. Kummer (2015). "Neuroinflammation in Alzheimer's disease." Lancet Neurol **14**(4): 388-405.
145. Heneka, M. T., D. T. Golenbock and E. Latz (2015). "Innate immunity in Alzheimer's disease." Nat Immunol **16**(3): 229-236.
146. Hölttä, M., O. Hansson, U. Andreasson, J. Hertze, L. Minthon, K. Nägga, N. Andreasen, H. Zetterberg and K. Blennow (2013). "Evaluating amyloid-β oligomers in cerebrospinal fluid as a biomarker for Alzheimer's disease." PLoS One **8**(6): e66381.
147. Iwatsubo, T., A. Odaka, N. Suzuki, H. Mizusawa, N. Nukina and Y. Ihara (1994). "Visualization of Aβ42(43) and Aβ40 in senile plaques with end specific Aβ monoclonals: Evidence that an initially deposited species is Aβ42(43)." Neuron **13**(1): 45-53.
148. Jarrett, J. T., E. P. Berger and P. T. Lansbury, Jr. (1993). "The carboxy terminus of the beta amyloid protein is critical for the seeding of amyloid formation: implications for the pathogenesis of Alzheimer's disease." Biochemistry **32**(18): 4693-4697.
149. Li, J., T. Kanekiyo, M. Shinohara, Y. Zhang, M. J. LaDu, H. Xu and G. Bu (2012). "Differential regulation of amyloid-β endocytic trafficking and lysosomal degradation by apolipoprotein E isoforms." J Biol Chem **287**(53): 44593-44601.

150. Mandrekar, S., Q. Jiang, C. Y. Lee, J. Koenigsknecht-Talboo, D. M. Holtzman and G. E. Landreth (2009). "Microglia mediate the clearance of soluble Abeta through fluid phase macropinocytosis." J Neurosci **29**(13): 4252-4262.
151. Masters, C. L., and D. J. Selkoe (2012). "Biochemistry of amyloid β-protein and amyloid deposits in Alzheimer disease." Cold Spring Harb Perspect Med **2**(6): a006262.
152. McLean, C. A., R. A. Cherny, F. W. Fraser, S. J. Fuller, M. J. Smith, K. Beyreuther, A. I. Bush and C. L. Masters (1999). "Soluble pool of Abeta amyloid as a determinant of severity of neurodegeneration in Alzheimer's disease." Ann Neurol **46**(6): 860-866.
153. Mehta, P. D., T. Pirttilä, S. P. Mehta, E. A. Sersen, P. S. Aisen and H. M. Wisniewski (2000). "Plasma and cerebrospinal fluid levels of amyloid beta proteins 1-40 and 1-42 in Alzheimer disease." Arch Neurol **57**(1): 100-105.
154. Motter, R., C. Vigo-Pelfrey, D. Kholodenko, R. Barbour, K. Johnson-Wood, D. Galasko, L. Chang, B. Miller, C. Clark, R. Green et al. (1995). "Reduction of beta-amyloid peptide42 in the cerebrospinal fluid of patients with Alzheimer's disease." Ann Neurol **38**(4): 643-648.
155. Ono, K., K. Hasegawa, Y. Yoshiike, A. Takashima, M. Yamada, and H. Naiki (2002). "Nordihydroguaiaretic acid potently breaks down pre-formed Alzheimer's beta-amyloid fibrils in vitro." J Neurochem **81**(3): 434-440.
156. Ries, M. and M. Sastre (2016). "Mechanisms of Aβ Clearance and Degradation by Glial Cells." Front Aging Neurosci **8**: 160.
157. Roychaudhuri, R., M. Yang, M. M. Hoshi, and D. B. Teplow (2009). "Amyloid beta-protein assembly and Alzheimer disease." J Biol Chem **284**(8): 4749-4753.
158. Selkoe, D. J. (1998). "The cell biology of beta-amyloid precursor protein and presenilin in Alzheimer's disease." Trends Cell Biol **8**(11): 447-453.
159. Selkoe, D. J. (2011). "Alzheimer's disease." Cold Spring Harb Perspect Biol **3**(7).
160. Walker, D. G. (1998). "Expression and regulation of complement C1q by human THP-1-derived macrophages." Mol Chem Neuropathol **34**(2-3): 197-218.
161. Wälti, M. A., F. Ravotti, H. Arai, C. G. Glabe, J. S. Wall, A. Böckmann, P. Güntert, B. H. Meier and R. Riek (2016). "Atomic-resolution structure of a disease-relevant Aβ(1-42) amyloid fibril." Proc Natl Acad Sci U S A **113**(34): E4976-4984.
162. Youmans, K. L., L. M. Tai, T. Kanekiyo, W. B. Stine Jr, S.-C. Michon, E. Nwabuisi-Heath, A. M. Manelli, Y. Fu, S. Riordan, W. A. Eimer, L. Binder, G. Bu, C. Yu, D. M. Hartley and M. J. LaDu (2012). "Intraneuronal Aβ detection in 5xFAD mice by a new Aβ-specific antibody." Molecular Neurodegeneration **7**(1): 8.
163. Zvěřová, M. (2019). "Clinical aspects of Alzheimer's disease." Clin Biochem **72**: 3-6.

164. Arrighi, H. M., J. Barakos, F. Barkhof, D. Tampieri, C. Jack, D. Melançon, K. Morris, N. Ketter, E. Liu and H. R. Brashear (2016). "Amyloid-related imaging abnormalities-haemosiderin (ARIA-H) in patients with Alzheimer's disease treated with bapineuzumab: a historical, prospective secondary analysis." Journal of Neurology, Neurosurgery & Psychiatry **87**(1): 106-112.

165. Black, R. S., R. A. Sperling, B. Safirstein, R. N. Motter, A. Pallay, A. Nichols, and M. Grundman (2010). "A single ascending dose study of bapineuzumab in patients with Alzheimer disease." Alzheimer disease and associated disorders **24**(2): 198.
166. Blennow, K., H. Zetterberg, J. O. Rinne, S. Salloway, J. Wei, R. Black, M. Grundman, E. Liu, and f. t. AAB-001 201/202 Investigators (2012). "Effect of Immunotherapy with Bapineuzumab on Cerebrospinal Fluid Biomarker Levels in Patients with Mild to Moderate Alzheimer Disease." Archives of Neurology **69**(8): 1002-1010.
167. Brashear, H. R., N. Ketter, J. Bogert, J. Di, S. P. Salloway and R. Sperling (2018). "Clinical evaluation of amyloid-related imaging abnormalities in bapineuzumab phase III studies." Journal of Alzheimer's Disease **66**(4): 1409-1424.
168. Burstein, A. H., Q. Zhao, J. Ross, S. Styren, J. W. Landen, W. W. Ma, F. McCush, C. Alvey, J. W. Kupiec and M. M. Bednar (2013). "Safety and pharmacology of ponezumab (PF-04360365) after a single 10-minute intravenous infusion in subjects with mild to moderate Alzheimer disease." Clin Neuropharmacol **36**(1): 8-13.
169. Cehlar, O., R. Skrabana, V. Revajova and M. Novak (2018). "Structural aspects of Alzheimer's disease immunotherapy targeted against amyloid-beta peptide." Bratislavske lekarske listy **119**(4): 201-204.
170. Doody, R. S., R. G. Thomas, M. Farlow, T. Iwatsubo, B. Vellas, S. Joffe, K. Kieburtz, R. Raman, X. Sun, P. S. Aisen, E. Siemers, H. Liu-Seifert and R. Mohs (2014). "Phase 3 trials of solanezumab for mild-to-moderate Alzheimer's disease." N Engl J Med **370**(4): 311-321.
171. Folch, J., M. Ettcheto, D. Petrov, S. Abad, I. Pedrós, M. Marin, J. Olloquequi and A. Camins (2018). "Review of the advances in treatment for Alzheimer disease: Strategies for combating β-amyloid protein." Neurologia (Engl Ed) **33**(1): 47-58.
172. Goure, W. F., G. A. Krafft, J. Jerecic and F. Hefti (2014). "Targeting the proper amyloid-beta neuronal toxins: a path forward for Alzheimer's disease immunotherapeutics." Alzheimers Res Ther **6**(4): 42.
173. Honig, L. S., B. Vellas, M. Woodward, M. Boada, R. Bullock, M. Borrie, K. Hager, N. Andreasen, E. Scarpini, H. Liu-Seifert, M. Case, R. A. Dean, A. Hake, K. Sundell, V. Poole Hoffmann, C. Carlson, R. Khanna, M. Mintun, R. DeMattos, K. J. Selzler and E. Siemers (2018). "Trial of Solanezumab for Mild Dementia Due to Alzheimer's Disease." N Engl J Med **378**(4): 321-330.
174. Hu, C., O. Adedokun, K. Ito, S. Raje and M. Lu (2015). "Confirmatory population pharmacokinetic analysis for bapineuzumab phase 3 studies in patients with mild to moderate Alzheimer's disease." The Journal of Clinical Pharmacology **55**(2): 221-229.
175. Ivanoiu, A., J. Pariente, K. Booth, K. Lobello, G. Luscan, L. Hua, P. Lucas, S. Styren, L. Yang, D. Li, R. S. Black, H. R. Brashear, and T. McRae (2016). "Long-term safety and tolerability of bapineuzumab in patients with Alzheimer's disease in two phase 3 extension studies." Alzheimer's Research & Therapy **8**(1): 24.
176. Ketter, N., H. R. Brashear, J. Bogert, J. Di, Y. Miaux, A. Gass, D. D. Purcell, F. Barkhof and H. M. Arrighi (2017). "Central review of amyloid-related imaging abnormalities in two phase III clinical trials of bapineuzumab in mild-to-moderate Alzheimer's disease patients." Journal of Alzheimer's Disease **57**(2): 557-573.

177. Klein, G., P. Delmar, N. Voyle, S. Rehal, C. Hofmann, D. Abi-Saab, M. Andjelkovic, S. Ristic, G. Wang, R. Bateman, G. A. Kerchner, M. Baudler, P. Fontoura and R. Doody (2019). "Gantenerumab reduces amyloid-β plaques in patients with prodromal to moderate Alzheimer's disease: a PET substudy interim analysis." Alzheimer's Research & Therapy **11**(1): 101.
178. Kwan, P., H. Konno, K. Y. Chan, and L. Baum (2020). "Rationale for the development of an Alzheimer's disease vaccine." Human Vaccines & Immunotherapeutics **16**(3): 645-653.
179. Lacey, L., J. Bobula, K. Rüdell, J. Alvir and C. Leibman (2015). "Quality of Life and Utility Measurement in a Large Clinical Trial Sample of Patients with Mild to Moderate Alzheimer's Disease: Determinants and Level of Changes Observed." Value in Health **18**(5): 638-645.
180. Landen, J. W., N. Andreasen, C. L. Cronenberger, P. F. Schwartz, A. Börjesson-Hanson, H. Östlund, C. A. Sattler, B. Binneman and M. M. Bednar (2017). "Ponezumab in mild-to-moderate Alzheimer's disease: Randomized phase II PET-PIB study." Alzheimers Dement (N Y) **3**(3): 393-401.
181. Landen, J. W., S. Cohen, C. B. Billing, Jr., C. Cronenberger, S. Styren, A. H. Burstein, C. Sattler, J. H. Lee, C. R. Jack, Jr., K. Kantarci, P. F. Schwartz, W. T. Duggan, Q. Zhao, K. Sprenger, M. M. Bednar and B. Binneman (2017). "Multiple-dose ponezumab for mild-to-moderate Alzheimer's disease: Safety and efficacy." Alzheimers Dement (N Y) **3**(3): 339-347.
182. Landen, J. W., Q. Zhao, S. Cohen, M. Borrie, M. Woodward, C. B. Billing, Jr., K. Bales, C. Alvey, F. McCush, J. Yang, J. W. Kupiec and M. M. Bednar (2013). "Safety and pharmacology of a single intravenous dose of ponezumab in subjects with mild-to-moderate Alzheimer disease: a phase I, randomized, placebo-controlled, double-blind, dose-escalation study." Clin Neuropharmacol **36**(1): 14-23.
183. Liu, E., M. E. Schmidt, R. Margolin, R. Sperling, R. Koeppe, N. S. Mason, W. E. Klunk, C. A. Mathis, S. Salloway, N. C. Fox, D. L. Hill, A. S. Les, P. Collins, K. M. Gregg, J. Di, Y. Lu, I. C. Tudor, B. T. Wyman, K. Booth, S. Broome, E. Yuen, M. Grundman, and H. R. Brashear (2015). "Amyloid-β ¹¹C-PiB-PET imaging results from 2 randomized bapineuzumab phase 3 AD trials." Neurology **85**(8): 692-700.
184. Miyoshi, I., Y. Fujimoto, M. Yamada, S. Abe, Q. Zhao, C. Cronenberger, K. Togo, T. Ishibashi, M. M. Bednar, J. W. Kupiec and B. Binneman (2013). "Safety and pharmacokinetics of PF-04360365 following a single-dose intravenous infusion in Japanese subjects with mild-to-moderate Alzheimer's disease: a multicenter, randomized, double-blind, placebo-controlled, dose-escalation study." Int J Clin Pharmacol Ther **51**(12): 911-923.
185. Ostrowitzki, S., D. Deptula, L. Thurfjell, F. Barkhof, B. Bohrmann, D. J. Brooks, W. E. Klunk, E. Ashford, K. Yoo, Z.-X. Xu, H. Loetscher and L. Santarelli (2012). "Mechanism of Amyloid Removal in Patients with Alzheimer Disease Treated With Gantenerumab." Archives of Neurology **69**(2): 198-207.
186. Ostrowitzki, S., R. A. Lasser, E. Dorflinger, P. Scheltens, F. Barkhof, T. Nikolcheva, E. Ashford, S. Retout, C. Hofmann, P. Delmar, G. Klein, M.

Andjelkovic, B. Dubois, M. Boada, K. Blennow, L. Santarelli, P. Fontoura and S. R. I. for the (2017). "A phase III randomized trial of gantenerumab in prodromal Alzheimer's disease." Alzheimer's Research & Therapy **9**(1): 95.
187. Panza, F., D. Seripa, M. Lozupone, V. Solfrizzi, B. P. Imbimbo, M. R. Barulli, R. Tortelli, R. Capozzo, P. Bisceglia, A. Dimitri, R. Stallone, V. Dibello, N. Quaranta, A. Daniele, A. Bellomo, A. Greco, and G. Logroscino (2018). "The potential of solanezumab and gantenerumab to prevent Alzheimer's disease in people with inherited mutations that cause its early onset." Expert Opin Biol Ther **18**(1): 25-35.
188. Panza, F., V. Solfrizzi, B. P. Imbimbo, M. Giannini, A. Santamato, D. Seripa and G. Logroscino (2014). "Efficacy and safety studies of gantenerumab in patients with Alzheimer's disease." Expert Rev Neurother **14**(9): 973-986.
189. Portron, A., P. Jordan, K. Draper, C. Muenzer, D. Dickerson, T. van Iersel and C. Hofmann (2020). "A Phase I Study to Assess the Effect of Speed of Injection on Pain, Tolerability, and Pharmacokinetics After High-volume Subcutaneous Administration of Gantenerumab in Healthy Volunteers." Clinical Therapeutics **42**(1): 108-120.e101.
190. Ramirez Aguilar, L., J. Acosta-Uribe, M. M. Giraldo, S. Moreno, A. Baena, D. Alzate, R. Cuastumal, D. Aguillón, L. Madrigal, A. Saldarriaga, A. Navarro, G. P. Garcia, D. C. Aguirre-Acevedo, E. G. Geier, J. N. Cochran, Y. T. Quiroz, R. M. Myers, J. S. Yokoyama, K. S. Kosik and F. Lopera (2019). "Genetic origin of a large family with a novel PSEN1 mutation (Ile416Thr)." Alzheimers Dement **15**(5): 709-719.
191. Rinne, J. O., D. J. Brooks, M. N. Rossor, N. C. Fox, R. Bullock, W. E. Klunk, C. A. Mathis, K. Blennow, J. Barakos, A. A. Okello, S. R. M. de Liano, E. Liu, M. Koller, K. M. Gregg, D. Schenk, R. Black, and M. Grundman (2010). "11C-PiB PET assessment of change in fibrillar amyloid-β load in patients with Alzheimer's disease treated with bapineuzumab: a phase 2, double-blind, placebo-controlled, ascending-dose study." The Lancet Neurology **9**(4): 363-372.
192. Salloway, S., R. Sperling, N. C. Fox, K. Blennow, W. Klunk, M. Raskind, M. Sabbagh, L. S. Honig, A. P. P. Porsteinsson and S. Ferris (2014). "Two phase 3 trials of bapineuzumab in mild-to-moderate Alzheimer's disease." New England Journal of Medicine **370**(4): 322-333.
193. Salloway, S., R. Sperling, S. Gilman, N. C. Fox, K. Blennow, M. Raskind, M. Sabbagh, L. S. Honig, R. Doody, C. H. van Dyck, R. Mulnard, J. Barakos, K. M. Gregg, E. Liu, I. Lieberburg, D. Schenk, R. Black, and M. Grundman (2009). "A phase 2 multiple ascending dose trial of bapineuzumab in mild to moderate Alzheimer disease." Neurology **73**(24): 2061-2070.
194. Schwarz, A. J., K. L. Sundell, A. Charil, M. G. Case, R. K. Jaeger, D. Scott, L. Bracoud, J. Oh, J. Suhy, M. J. Pontecorvo, B. C. Dickerson and E. R. Siemers (2019). "Magnetic resonance imaging measures of brain atrophy from the EXPEDITION3 trial in mild Alzheimer's disease." Alzheimer's & Dementia: Translational Research & Clinical Interventions **5**: 328-337.
195. Se Thoe, E., A. Fauzi, Y. Q. Tang, S. Chamyuang and A. Y. Y. Y. Chia (2021). "A review on advances of treatment modalities for Alzheimer's disease." Life Sciences **276**: 119129.

196. Suzuki, K., A. Iwata, and T. Iwatsubo (2017). "The past, present, and future of disease-modifying therapies for Alzheimer's disease." Proceedings of the Japan Academy, Series B **93**(10): 757-771.
197. Vandenberghe, R., J. O. Rinne, M. Boada, S. Katayama, P. Scheltens, B. Vellas, M. Tuchman, A. Gass, J. B. Fiebach, D. Hill, K. Lobello, D. Li, T. McRae, P. Lucas, I. Evans, K. Booth, G. Luscan, B. T. Wyman, L. Hua, L. Yang, H. R. Brashear, and R. S. Black (2016). "Bapineuzumab for mild to moderate Alzheimer's disease in two global, randomized, phase 3 trials." Alzheimers Res Ther **8**(1): 18.
198. Yoshida, K., A. Moein, T. Bittner, S. Ostrowitzki, H. Lin, L. Honigberg, J. Y. Jin and A. Quartino (2020). "Pharmacokinetics and pharmacodynamic effect of crenezumab on plasma and cerebrospinal fluid beta-amyloid in patients with mild-to-moderate Alzheimer's disease." Alzheimer's Research & Therapy **12**(1): 16.

199. Chiao, P., B. J. Bedell, B. Avants, A. P. Zijdenbos, M. Grand'Maison, P. O'Neill, J. O'Gorman, T. Chen, and R. Koeppe (2019). "Impact of Reference and Target Region Selection on Amyloid PET SUV Ratios in the Phase 1b PRIME Study of Aducanumab." Journal of Nuclear Medicine **60**(1): 100-106.
200. Ferrero, J., L. Williams, H. Stella, K. Leitermann, A. Mikulskis, J. O'Gorman, and J. Sevigny (2016). "First-in-human, double-blind, placebo-controlled, single-dose escalation study of aducanumab (BIIB037) in mild-to-moderate Alzheimer's disease." Alzheimers Dement (N Y) **2**(3): 169-176.
201. Logovinsky, V., A. Satlin, R. Lai, C. Swanson, J. Kaplow, G. Osswald, H. Basun and L. Lannfelt (2016). "Safety and tolerability of BAN2401--a clinical study in Alzheimer's disease with a protofibril selective Aβ antibody." Alzheimers Res Ther **8**(1): 14.
202. Panza, F., M. Lozupone, G. Logroscino and B. P. Imbimbo (2019). "A critical appraisal of amyloid-β-targeting therapies for Alzheimer disease." Nature Reviews Neurology **15**(2): 73-88.
203. Satlin, A., J. Wang, V. Logovinsky, S. Berry, C. Swanson, S. Dhadda and D. A. Berry (2016). "Design of a Bayesian adaptive phase 2 proof-of-concept trial for BAN2401, a putative disease-modifying monoclonal antibody for the treatment of Alzheimer's disease." Alzheimers Dement (N Y) **2**(1): 1-12.
204. Sevigny, J., P. Chiao, T. Bussière, P. H. Weinreb, L. Williams, M. Maier, R. Dunstan, S. Salloway, T. Chen, Y. Ling, J. O'Gorman, F. Qian, M. Arastu, M. Li, S. Chollate, M. S. Brennan, O. Quintero-Monzon, R. H. Scannevin, H. M. Arnold, T. Engber, K. Rhodes, J. Ferrero, Y. Hang, A. Mikulskis, J. Grimm, C. Hock, R. M. Nitsch and A. Sandrock (2016). "The antibody aducanumab reduces Aβ plaques in Alzheimer's disease." Nature **537**(7618): 50-56.
205. Swanson, C. J., Y. Zhang, S. Dhadda, J. Wang, J. Kaplow, R. Y. K. Lai, L. Lannfelt, H. Bradley, M. Rabe, A. Koyama, L. Reyderman, D. A. Berry, S. Berry, R. Gordon, L. D. Kramer, and J. L. Cummings (2021). "A randomized, double-blind, phase 2b proof-of-concept clinical trial in early Alzheimer's disease with lecanemab, an anti-Aβ protofibril antibody." Alzheimer's Research & Therapy **13**(1): 80.

206. Attems, J., K. A. Jellinger and F. Lintner (2005). "Alzheimer's disease pathology influences severity and topographical distribution of cerebral amyloid angiopathy." Acta Neuropathol **110**(3): 222-231.
207. Citron, M., C. Vigo-Pelfrey, D. B. Teplow, C. Miller, D. Schenk, J. Johnston, B. Winblad, N. Venizelos, L. Lannfelt and D. J. Selkoe (1994). "Excessive production of amyloid beta-protein by peripheral cells of symptomatic and presymptomatic patients carrying the Swedish familial Alzheimer disease mutation." Proc Natl Acad Sci U S A **91**(25): 11993-11997.
208. Güntert, A., H. Döbeli and B. Bohrmann (2006). "High sensitivity analysis of amyloid-beta peptide composition in amyloid deposits from human and PS2APP mouse brain." Neuroscience **143**(2): 461-475.
209. Haass, C., C. Kaether, G. Thinakaran and S. Sisodia (2012). "Trafficking and proteolytic processing of APP." Cold Spring Harb Perspect Med **2**(5): a006270.
210. Iwatsubo, T., A. Odaka, N. Suzuki, H. Mizusawa, N. Nukina and Y. Ihara (1994). "Visualization of Aβ42(43) and Aβ40 in senile plaques with end specific Aβ monoclonals: Evidence that an initially deposited species is Aβ42(43)." Neuron **13**(1): 45-53.
211. Jarrett, J. T., E. P. Berger and P. T. Lansbury, Jr. (1993). "The carboxy terminus of the beta amyloid protein is critical for the seeding of amyloid formation: implications for the pathogenesis of Alzheimer's disease." Biochemistry **32**(18): 4693-4697.
212. Long, J. M. and D. M. Holtzman (2019). "Alzheimer Disease: An Update on Pathobiology and Treatment Strategies." Cell **179**(2): 312-339.
213. Pagnon de la Vega, M., V. Giedraitis, W. Michno, L. Kilander, G. Güner, M. Zielinski, M. Löwenmark, R. Brundin, T. Danfors, L. Söderberg, I. Alafuzoff, L. N. G. Nilsson, A. Erlandsson, D. Willbold, S. A. Müller, G. F. Schröder, J. Hanrieder, S. F. Lichtenthaler, L. Lannfelt, D. Sehlin and M. Ingelsson (2021). "The Uppsala APP deletion causes early onset autosomal dominant Alzheimer's disease by altering APP processing and increasing amyloid β fibril formation." Sci Transl Med **13**(606).
214. Scheuner, D., C. Eckman, M. Jensen, X. Song, M. Citron, N. Suzuki, T. D. Bird, J. Hardy, M. Hutton, W. Kukull, E. Larson, L. Levy-Lahad, M. Viitanen, E. Peskind, P. Poorkaj, G. Schellenberg, R. Tanzi, W. Wasco, L. Lannfelt, D. Selkoe and S. Younkin (1996). "Secreted amyloid β–protein similar to that in the senile plaques of Alzheimer's disease is increased in vivo by the presenilin 1 and 2 and APP mutations linked to familial Alzheimer's disease." Nature Medicine **2**(8): 864-870.
215. Suzuki, N., T. T. Cheung, X. D. Cai, A. Odaka, L. Otvos, Jr., C. Eckman, T. E. Golde and S. G. Younkin (1994). "An increased percentage of long amyloid beta protein secreted by familial amyloid beta protein precursor (beta APP717) mutants." Science **264**(5163): 1336-1340.
216. Thal, D. R., J. Walter, T. C. Saido and M. Fändrich (2015). "Neuropathology and biochemistry of Aβ and its aggregates in Alzheimer's disease." Acta Neuropathol **129**(2): 167-182.
217. Yang, Y., D. Arseni, W. Zhang, M. Huang, S. Lövestam, M. Schweighauser, A. Kotecha, A. G. Murzin, S. Y. Peak-Chew, J. Macdonald, I. Lavenir, H. J. Garringer,

E. Gelpi, K. L. Newell, G. G. Kovacs, R. Vidal, B. Ghetti, B. Ryskeldi-Falcon, S. H. W. Scheres and M. Goedert (2022). "Cryo-EM structures of amyloid-β 42 filaments from human brains." Science **375**(6577): 167-172.

218. Syvänen, S., X. T. Fang, G. Hultqvist, S. R. Meier, L. Lannfelt and D. Sehlin (2017). "A bispecific Tribody PET radioligand for visualization of amyloid-beta protofibrils - a new concept for neuroimaging." Neuroimage **148**: 55-63.
219. Tomic, J. L., A. Pensalfini, E. Head and C. G. Glabe (2009). "Soluble fibrillar oligomer levels are elevated in Alzheimer's disease brain and correlate with cognitive dysfunction." Neurobiol Dis **35**(3): 352-358.

220. van Dyck, C. H., C. J. Swanson, P. Aisen, R. J. Bateman, C. Chen, M. Gee, M. Kanekiyo, D. Li, L. Reyderman, S. Cohen, L. Froelich, S. Katayama, M. Sabbagh, B. Vellas, D. Watson, S. Dhadda, M. Irizarry, L. D. Kramer, and T. Iwatsubo (2022). "Lecanemab in Early Alzheimer's Disease." New England Journal of Medicine.

221. van Dyck, C. H., C. J. Swanson, P. Aisen, R. J. Bateman, C. Chen, M. Gee, M. Kanekiyo, D. Li, L. Reyderman, S. Cohen, L. Froelich, S. Katayama, M. Sabbagh, B. Vellas, D. Watson, S. Dhadda, M. Irizarry, L. D. Kramer, and T. Iwatsubo (2022). "Lecanemab in Early Alzheimer's Disease." New England Journal of Medicine.

222. Benilova, I., E. Karran and B. De Strooper (2012). "The toxic Aβ oligomer and Alzheimer's disease: an emperor in need of clothes." Nature Neuroscience **15**(3): 349-357.
223. Bitan, G., M. D. Kirkitadze, A. Lomakin, S. S. Vollers, G. B. Benedek and D. B. Teplow (2003). "Amyloid b-protein (Ab) assembly: Ab40 and Ab42 oligomerize through distinct pathways." Proc. Natl. Acad. Sci. USA **100**(1): 330-335.
224. Bohrmann, B., K. Baumann, J. Benz, F. Gerber, W. Huber, F. Knoflach, J. Messer, K. Oroszlan, R. Rauchenberger, W. F. Richter, C. Rothe, M. Urban, M. Bardroff, M. Winter, C. Nordstedt and H. Loetscher (2012). "Gantenerumab: a novel human anti-Aβ antibody demonstrates sustained cerebral amyloid-β binding and elicits cell-mediated removal of human amyloid-β." J Alzheimers Dis **28**(1): 49-69.
225. Colvin, M. T., R. Silvers, Q. Z. Ni, T. V. Can, I. Sergeyev, M. Rosay, K. J. Donovan, B. Michael, J. Wall, S. Linse and R. G. Griffin (2016). "Atomic resolution structure of monomorphic Ab_{42} amyloid fibrils." J Am Chem Soc **138**(30): 9663-9674.
226. Deshpande, A., H. Kawai, R. Metherate, C. G. Glabe and J. Busciglio (2009). "A role for synaptic zinc in activity-dependent Ab oligomer formation and accumulation at excitatory synapses." J Neurosci **29**(13): 4004-4015.
227. Dhami, K. B., S. Karki, A. Parks, C. G. Nichols and M. R. Nichols (2022). "Development of β-sheet structure in Aβ aggregation intermediates diminishes

exposed hydrophobic surface area and enhances proinflammatory activity." Biochim Biophys Acta Proteins Proteom **1870**(9): 140817.
228. Englund, H., D. Sehlin, A. S. Johansson, L. N. Nilsson, P. Gellerfors, S. Paulie, L. Lannfelt and F. E. Pettersson (2007). "Sensitive ELISA detection of amyloid-beta protofibrils in biological samples." J Neurochem **103**(1): 334-345.
229. Evangelisti, E., R. Cascella, M. Becatti, G. Marrazza, C. M. Dobson, F. Chiti, M. Stefani, and C. Cecchi (2016). "Binding affinity of amyloid oligomers to cellular membranes is a generic indicator of cellular dysfunction in protein misfolding diseases." Scientific Reports **6**(1): 32721.
230. Georganopoulou, D. G., L. Chang, J. M. Nam, C. S. Thaxton, E. J. Mufson, W. L. Klein and C. A. Mirkin (2005). "Nanoparticle-based detection in cerebral spinal fluid of a soluble pathogenic biomarker for Alzheimer's disease." Proc. Natl. Acad. Sci. USA **102**(7): 2273-2276.
231. Golde, T. E. (2022). "Alzheimer's disease – the journey of a healthy brain into organ failure." Molecular Neurodegeneration **17**(1): 18.
232. Goure, W. F., G. A. Krafft, J. Jerecic and F. Hefti (2014). "Targeting the proper amyloid-beta neuronal toxins: a path forward for Alzheimer's disease immunotherapeutics." Alzheimers Res Ther **6**(4): 42.
233. Gravina, S. A., L. Ho, C. B. Eckman, K. E. Long, L. Otvos, Jr., L. H. Younkin, N. Suzuki and S. G. Younkin (1995). "Amyloid b protein (Ab) in Alzheimer's disease brain. Biochemical and immunocytochemical analysis with antibodies specific for forms ending at Ab40 or Ab42(43)." J. Biol. Chem. **270**(13): 7013-7016.
234. Gremer, L., D. Scholzel, C. Schenk, E. Reinartz, J. Labahn, R. B. G. Ravelli, M. Tusche, C. Lopez-Iglesias, W. Hoyer, H. Heise, D. Willbold and G. F. Schroder (2017). "Fibril structure of amyloid-β (1-42) by cryo-electron microscopy." Science **358**(6359): 116-119.
235. Gu, L. and Z. Guo (2013). "Alzheimer's Aβ42 and Aβ40 peptides form interlaced amyloid fibrils." Journal of Neurochemistry **126**(3): 305-311.
236. Haass, C. and D. J. Selkoe (2007). "Soluble protein oligomers in neurodegeneration: lessons from the Alzheimer's amyloid b-peptide." Nat Rev Mol Cell Biol **8**(2): 101-112.
237. Harper, J. D., C. M. Lieber and P. T. Lansbury, Jr. (1997). "Atomic force microscopic imaging of seeded fibril formation and fibril branching by the Alzheimer's disease amyloid-b protein." Chem. Biol. **4**: 951-959.
238. Harper, J. D., S. S. Wong, C. M. Lieber and P. T. Lansbury, Jr. (1997). "Observation of metastable Ab amyloid protofibrils by atomic force microscopy." Chem. Biol. **4**(2): 119-125.
239. Harper, J. D., S. S. Wong, C. M. Lieber and P. T. Lansbury, Jr. (1999). "Assembly of Ab amyloid peptides: an *in vitro* model for a possible early event in Alzheimer's disease." Biochemistry **38**: 8972-8980.
240. Janelidze, S., S. Palmqvist, A. Leuzy, E. Stomrud, I. M. W. Verberk, H. Zetterberg, N. J. Ashton, P. Pesini, L. Sarasa, J. A. Allué, C. E. Teunissen, J. L. Dage, K. Blennow, N. Mattsson-Carlgren and O. Hansson (2022). "Detecting amyloid positivity in early Alzheimer's disease using combinations of plasma Aβ42/Aβ40 and p-tau." Alzheimers Dement **18**(2): 283-293.

241. Jarrett, J. T., E. P. Berger and P. T. Lansbury, Jr. (1993). "The carboxy terminus of the b amyloid protein is critical for the seeding of amyloid formation: Implications for the pathogenesis of Alzheimer's disease." Biochemistry **32**(18): 4693-4697.
242. Katzmarski, N., S. Ziegler-Waldkirch, N. Scheffler, C. Witt, C. Abou-Ajram, B. Nuscher, M. Prinz, C. Haass and M. Meyer-Luehmann (2020). "Aβ oligomers trigger and accelerate Aβ seeding." Brain Pathol **30**(1): 36-45.
243. Kayed, R., E. Head, F. Sarsoza, T. Saing, C. W. Cotman, M. Necula, L. Margol, J. Wu, L. Breydo, J. L. Thompson, S. Rasool, T. Gurlo, P. Butler and C. G. Glabe (2007). "Fibril specific, conformation dependent antibodies recognize a generic epitope common to amyloid fibrils and fibrillar oligomers that is absent in prefibrillar oligomers." Mol Neurodegener **2**(1): 18.
244. Kayed, R., E. Head, J. L. Thompson, T. M. McIntire, S. C. Milton, C. W. Cotman, and C. G. Glabe (2003). "Common structure of soluble amyloid oligomers implies common mechanism of pathogenesis." Science **300**: 486-489.
245. Kodali, R. and R. Wetzel (2007). "Polymorphism in the intermediates and products of amyloid assembly." Curr Opin Struct Biol.
246. Koffie, R. M., M. Meyer-Luehmann, T. Hashimoto, K. W. Adams, M. L. Mielke, M. Garcia-Alloza, K. D. Micheva, S. J. Smith, M. L. Kim, V. M. Lee, B. T. Hyman, and T. L. Spires-Jones (2009). "Oligomeric amyloid b associates with postsynaptic densities and correlates with excitatory synapse loss near senile plaques." Proc Natl Acad Sci USA **106**(10): 4012-4017.
247. Koike, H., Y. Iguchi, K. Sahashi and M. Katsuno (2021). "Significance of Oligomeric and Fibrillar Species in Amyloidosis: Insights into Pathophysiology and Treatment." Molecules **26**(16).
248. Kwon, S., M. Iba, C. Kim and E. Masliah (2020). "Immunotherapies for aging-related neurodegenerative diseases-emerging perspectives and new targets." Neurotherapeutics.
249. Lambert, M. P., K. L. Viola, B. A. Chromy, L. Chang, T. E. Morgan, J. Yu, D. L. Venton, G. A. Krafft, C. E. Finch and W. L. Klein (2001). "Vaccination with soluble Ab oligomers generates toxicity-neutralizing antibodies." J Neurochem **79**(3): 595-605.
250. Langer, F., Y. S. Eisele, S. K. Fritschi, M. Staufenbiel, L. C. Walker and M. Jucker (2011). "Soluble Aβ Seeds Are Potent Inducers of Cerebral β-Amyloid Deposition." The Journal of Neuroscience **31**(41): 14488-14495.
251. Lannfelt, L., C. Moller, H. Basun, G. Osswald, D. Sehlin, A. Satlin, V. Logovinsky and P. Gellerfors (2014). "Perspectives on future Alzheimer therapies: Amyloid-b protofibrils - a new target for immunotherapy with BAN2401 in Alzheimer's disease." Alzheimers Res Ther **6**(2): 16.
252. Lee, E. B., L. Z. Leng, B. Zhang, L. Kwong, J. Q. Trojanowski, T. Abel and V. M. Lee (2006). "Targeting amyloid-b peptide (Ab) oligomers by passive immunization with a conformation-selective monoclonal antibody improves learning and memory in Ab precursor protein (APP) transgenic mice." J Biol Chem **281**(7): 4292-4299.
253. Lesne, S., M. T. Koh, L. Kotilinek, R. Kayed, C. G. Glabe, A. Yang, M. Gallagher, and K. H. Ashe (2006). "A specific amyloid-b protein assembly in the brain impairs memory." Nature **440**(7082): 352-357.

254. Masters, C. L., R. Bateman, K. Blennow, C. C. Rowe, R. A. Sperling, and J. L. Cummings (2016). "Alzheimer's disease." Nat Rev Dis Primers **1**: 15056.
255. McDade, E., J. L. Cummings, S. Dhadda, C. J. Swanson, L. Reyderman, M. Kanekiyo, A. Koyama, M. Irizarry, L. D. Kramer, and R. J. Bateman (2022). "Lecanemab in patients with early Alzheimer's disease: detailed results on biomarker, cognitive, and clinical effects from the randomized and open-label extension of the phase 2 proof-of-concept study." Alzheimers Res Ther **14**(1): 191.
256. Mittag, J. J., S. Milani, D. M. Walsh, J. O. Radler and J. J. McManus (2014). "Simultaneous measurement of a range of particle sizes during Ab_{1-42} fibrillogenesis quantified using fluorescence correlation spectroscopy." Biochem Biophys Res Commun **448**(2): 195-199.
257. Nichols, M. R., B. A. Colvin, E. A. Hood, G. S. Paranjape, D. C. Osborn and S. E. Terrill-Usery (2015). "Biophysical comparison of soluble amyloid-β (1-42) protofibrils, oligomers, and protofilaments." Biochemistry **54**: 2193-2204.
258. Ono, K., and M. Tsuji (2020). "Protofibrils of amyloid-b are important targets of a disease-modifying approach for Alzheimer's disease." Int J Mol Sci **21**(3): 952.
259. Paranjape, G. S., L. K. Gouwens, D. C. Osborn, and M. R. Nichols (2012). "Isolated amyloid-β (1-42) protofibrils, but not isolated fibrils, are robust stimulators of microglia." ACS Chem Neurosci **3**: 302-311.
260. Schilling, S., J. U. Rahfeld, I. Lues and C. A. Lemere (2018). "Passive Ab immunotherapy: current achievements and future perspectives." Molecules **23**(5).
261. Seubert, P., C. Vigo-Pelfrey, F. Esch, M. Lee, H. Dovey, D. Davis, S. Sinha, M. Schlossmacher, J. Whaley, C. Swindlehurst, R. McCormack, R. Wolfert, D. J. Selkoe, I. Lieberberg and D. Schenk (1992). "Isolation and quantification of soluble Alzheimer's b-peptide from biological fluids." Nature **359**(6393): 325-327.
262. Sevigny, J., P. Chiao, T. Bussiere, P. H. Weinreb, L. Williams, M. Maier, R. Dunstan, S. Salloway, T. Chen, Y. Ling, J. O'Gorman, F. Qian, M. Arastu, M. Li, S. Chollate, M. S. Brennan, O. Quintero-Monzon, R. H. Scannevin, H. M. Arnold, T. Engber, K. Rhodes, J. Ferrero, Y. Hang, A. Mikulskis, J. Grimm, C. Hock, R. M. Nitsch and A. Sandrock (2016). "The antibody aducanumab reduces Ab plaques in Alzheimer's disease." Nature **537**(7618): 50-56.
263. Söllvander, S., E. Nikitidou, L. Gallasch, M. Zyśk, L. Söderberg, D. Sehlin, L. Lannfelt and A. Erlandsson (2018). "The Aβ protofibril selective antibody mAb158 prevents accumulation of Aβ in astrocytes and rescues neurons from Aβ-induced cell death." J Neuroinflammation **15**(1): 98.
264. Terry, R. D., N. K. Gonatas, and M. Weiss (1964). "Ultrastructural studies in Alzheimer's presenile dementia." A. J. Pathol. **44**: 269-297.
265. Tucker, S., C. Möller, K. Tegerstedt, A. Lord, H. Laudon, J. Sjödahl, L. Söderberg, E. Spens, C. Sahlin, E. R. Waara, A. Satlin, P. Gellerfors, G. Osswald and L. Lannfelt (2015). "The murine version of BAN2401 (mAb158) selectively reduces amyloid-β protofibrils in brain and cerebrospinal fluid of tg-ArcSwe mice." J Alzheimers Dis **43**(2): 575-588.
266. van Dyck, C. H., C. J. Swanson, P. Aisen, R. J. Bateman, C. Chen, M. Gee, M. Kanekiyo, D. Li, L. Reyderman, S. Cohen, L. Froelich, S. Katayama, M. Sabbagh,

B. Vellas, D. Watson, S. Dhadda, M. Irizarry, L. D. Kramer, and T. Iwatsubo (2022). "Lecanemab in Early Alzheimer's Disease." N Engl J Med.

267. Walsh, D. M., D. M. Hartley, Y. Kusumoto, Y. Fezoui, M. M. Condron, A. Lomakin, G. B. Benedek, D. J. Selkoe and D. B. Teplow (1999). "Amyloid b-protein fibrillogenesis: Structure and biological activity of protofibrillar intermediates." J. Biol. Chem. **274**: 25945-25952.
268. Walsh, D. M., A. Lomakin, G. B. Benedek, M. M. Condron and D. B. Teplow (1997). "Amyloid b-protein fibrillogenesis: Detection of a protofibrillar intermediate." J. Biol. Chem. **272**(35): 22364-22372.
269. Walsh, S., R. Merrick, E. Richard, S. Nurock and C. Brayne (2022). "Lecanemab for Alzheimer's disease." Bmj **379**: o3010.
270. Wong, C. W., V. Quaranta and G. G. Glenner (1985). "Neuritic plaques and cerebrovascular amyloid in Alzheimer disease are antigenically related." Proc Natl Acad Sci USA **82**(24): 8729-8732.
271. Xu, C., L. Zhao, and C. Dong (2022). "A Review of Application of Aβ 42/40 Ratio in Diagnosis and Prognosis of Alzheimer's Disease." Journal of Alzheimer's Disease **90**: 495-512.
272. Yang, Y., D. Arseni, W. Zhang, M. Huang, S. Lövestam, M. Schweighauser, A. Kotecha, A. G. Murzin, S. Y. Peak-Chew, J. Macdonald, I. Lavenir, H. J. Garringer, E. Gelpi, K. L. Newell, G. G. Kovacs, R. Vidal, B. Ghetti, B. Ryskeldi-Falcon, S. H. W. Scheres and M. Goedert (2022). "Cryo-EM structures of amyloid-β 42 filaments from human brains." Science **375**(6577): 167-172.
273. Yasumoto, T., Y. Takamura, M. Tsuji, T. Watanabe-Nakayama, K. Imamura, H. Inoue, S. Nakamura, T. Inoue, A. Kimura, S. Yano, H. Nishijo, Y. Kiuchi, D. B. Teplow and K. Ono (2019). "High molecular weight amyloid β (1-42) oligomers induce neurotoxicity via plasma membrane damage." Faseb j **33**(8): 9220-9234.

274. Adolfsson, O., M. Pihlgren, N. Toni, Y. Varisco, A. L. Buccarello, K. Antoniello, S. Lohmann, K. Piorkowska, V. Gafner, J. K. Atwal, J. Maloney, M. Chen, A. Gogineni, R. M. Weimer, D. L. Mortensen, M. Friesenhahn, C. Ho, R. Paul, A. Pfeifer, A. Muhs and R. J. Watts (2012). "An effector-reduced anti-b-amyloid (Ab) antibody with unique Ab binding properties promotes neuroprotection and glial engulfment of Ab." J Neurosci **32**(28): 9677-9689.
275. Bonito-Oliva, A., S. Schedin-Weiss, S. S. Younesi, A. Tiiman, C. Adura, N. Paknejad, M. Brendel, Y. Romin, R. J. Parchem, C. Graff, V. Vukojević, L. O. Tjernberg, L. Terenius, B. Winblad, T. P. Sakmar and W. V. Graham (2019). "Conformation-specific antibodies against multiple amyloid protofibril species from a single amyloid immunogen." J Cell Mol Med **23**(3): 2103-2114.
276. Coalier, K. A., G. S. Paranjape, S. Karki and M. R. Nichols (2013). "Stability of early-stage amyloid-β (1-42) aggregation species." Biochim Biophys Acta **1834**(1): 65-70.
277. Dhami, K. B., S. Karki, A. Parks, C. G. Nichols, and M. R. Nichols (2022). "Development of β-sheet structure in Aβ aggregation intermediates diminishes

exposed hydrophobic surface area and enhances proinflammatory activity." Biochim Biophys Acta Proteins Proteom **1870**(9): 140817.
278. Goure, W. F., G. A. Krafft, J. Jerecic and F. Hefti (2014). "Targeting the proper amyloid-beta neuronal toxins: a path forward for Alzheimer's disease immunotherapeutics." Alzheimers Res Ther **6**(4): 42.
279. Gouwens, L. K., M. S. Ismail, V. A. Rogers, N. T. Zeller, E. C. Garrad, F. S. Amtashar, N. J. Makoni, D. C. Osborn and M. R. Nichols (2018). "Ab42 protofibrils interact with and are trafficked through microglial-derived microvesicles." ACS Chem Neurosci **9**(6): 1416-1425.
280. Gouwens, L. K., N. J. Makoni, V. A. Rogers and M. R. Nichols (2016). "Amyloid-b42 protofibrils are internalized by microglia more extensively than monomers." Brain Res **1648**(Pt A): 485-495.
281. Hellstrand, E., B. Boland, D. M. Walsh, and S. Linse (2009). "Amyloid b-protein aggregation produces highly reproducible kinetic data and occurs by a two-phase process." ACS Chem Neurosci **1**(1): 13-18.
282. Huang, Y. R., and R. T. Liu (2020). "The Toxicity and Polymorphism of β-Amyloid Oligomers." Int J Mol Sci **21**(12).
283. Karran, E. and B. De Strooper (2022). "The amyloid hypothesis in Alzheimer disease: new insights from new therapeutics." Nat Rev Drug Discov **21**(4): 306-318.
284. Nichols, M. R., M. A. Moss, D. K. Reed, W. L. Lin, R. Mukhopadhyay, J. H. Hoh, and T. L. Rosenberry (2002). "Growth of bβ-amyloid (1-40) protofibrils by monomer elongation and lateral association. Characterization of distinct products by light scattering and atomic force microscopy." Biochemistry **41**: 6115-6127.
285. Ono, K. and M. Tsuji (2020). "Protofibrils of amyloid-b are important targets of a disease-modifying approach for Alzheimer's disease." Int J Mol Sci **21**(3): 952.
286. Paranjape, G. S., L. K. Gouwens, D. C. Osborn, and M. R. Nichols (2012). "Isolated amyloid-β (1-42) protofibrils, but not isolated fibrils, are robust stimulators of microglia." ACS Chem Neurosci **3**(4): 302-311.
287. Paranjape, G. S., S. E. Terrill, L. K. Gouwens, B. M. Ruck, and M. R. Nichols (2013). "Amyloid-β (1-42) protofibrils formed in modified artificial cerebrospinal fluid bind and activate microglia." J Neuroimmune Pharmacol **8**(1): 312-322.
288. Paranjape, G. S., S. E. Terrill, L. K. Gouwens, B. M. Ruck, and M. R. Nichols (2013). "Amyloid-β (1-42) protofibrils formed in modified artificial cerebrospinal fluid bind and activate microglia." J Neuroimmune Pharmacol **8**(1): 312-322.
289. Udan, M. L., D. Ajit, N. R. Crouse, and M. R. Nichols (2008). "Toll-like receptors 2 and 4 mediate Aβ (1-42) activation of the innate immune response in a human monocytic cell line." J Neurochem **104**: 524-533.
290. Walsh, D. M., D. M. Hartley, Y. Kusumoto, Y. Fezoui, M. M. Condron, A. Lomakin, G. B. Benedek, D. J. Selkoe and D. B. Teplow (1999). "Amyloid b-protein fibrillogenesis: Structure and biological activity of protofibrillar intermediates." J. Biol. Chem. **274**: 25945-25952.
291. Long, J. M. and D. M. Holtzman (2019). "Alzheimer Disease: An Update on Pathobiology and Treatment Strategies." Cell **179**(2): 312-339.

292. Masters, C. L., and D. J. Selkoe (2012). "Biochemistry of amyloid β-protein and amyloid deposits in Alzheimer disease." Cold Spring Harb Perspect Med **2**(6): a006262.
293. Perrin, R. J., A. M. Fagan, and D. M. Holtzman (2009). "Multimodal techniques for diagnosis and prognosis of Alzheimer's disease." Nature **461**(7266): 916-922.
294. Selkoe, D. J. (1998). "The cell biology of beta-amyloid precursor protein and presenilin in Alzheimer's disease." Trends Cell Biol **8**(11): 447-453.
295. Selkoe, D. J. and J. Hardy (2016). "The amyloid hypothesis of Alzheimer's disease at 25 years." EMBO Mol Med **8**(6): 595-608.

296. Haass, C., C. Kaether, G. Thinakaran and S. Sisodia (2012). "Trafficking and proteolytic processing of APP." Cold Spring Harb Perspect Med **2**(5): a006270.
297. Selkoe, D. J. (2004). "Cell biology of protein misfolding: The examples of Alzheimer's and Parkinson's diseases." Nature Cell Biology **6**(11): 1054-1061.

298. Attems, J., K. A. Jellinger and F. Lintner (2005). "Alzheimer's disease pathology influences severity and topographical distribution of cerebral amyloid angiopathy." Acta Neuropathol **110**(3): 222-231.
299. Chen, G. F., T. H. Xu, Y. Yan, Y. R. Zhou, Y. Jiang, K. Melcher, and H. E. Xu (2017). "Amyloid beta: structure, biology and structure-based therapeutic development." Acta Pharmacol Sin **38**(9): 1205-1235.
300. Citron, M., C. Vigo-Pelfrey, D. B. Teplow, C. Miller, D. Schenk, J. Johnston, B. Winblad, N. Venizelos, L. Lannfelt and D. J. Selkoe (1994). "Excessive production of amyloid beta-protein by peripheral cells of symptomatic and presymptomatic patients carrying the Swedish familial Alzheimer disease mutation." Proc Natl Acad Sci U S A **91**(25): 11993-11997.
301. Coalier, K. A., G. S. Paranjape, S. Karki and M. R. Nichols (2013). "Stability of early-stage amyloid-β (1-42) aggregation species." Biochim Biophys Acta **1834**(1): 65-70.
302. Gu, L., and Z. Guo (2013). "Alzheimer's Aβ42 and Aβ40 peptides form interlaced amyloid fibrils." Journal of Neurochemistry **126**(3): 305-311.
303. Harper, J. D., C. M. Lieber and P. T. Lansbury, Jr. (1997). "Atomic force microscopic imaging of seeded fibril formation and fibril branching by the Alzheimer's disease amyloid-beta protein." Chem Biol **4**(12): 951-959.
304. Harper, J. D., S. S. Wong, C. M. Lieber and P. T. Lansbury, Jr. (1999). "Assembly of A beta amyloid protofibrils: an in vitro model for a possible early event in Alzheimer's disease." Biochemistry **38**(28): 8972-8980.
305. McLean, C. A., R. A. Cherny, F. W. Fraser, S. J. Fuller, M. J. Smith, K. Beyreuther, A. I. Bush and C. L. Masters (1999). "Soluble pool of Abeta amyloid as a determinant of severity of neurodegeneration in Alzheimer's disease." Ann Neurol **46**(6): 860-866.
306. Pagnon de la Vega, M., V. Giedraitis, W. Michno, L. Kilander, G. Güner, M. Zielinski, M. Löwenmark, R. Brundin, T. Danfors, L. Söderberg, I. Alafuzoff, L. N.

G. Nilsson, A. Erlandsson, D. Willbold, S. A. Müller, G. F. Schröder, J. Hanrieder, S. F. Lichtenthaler, L. Lannfelt, D. Sehlin and M. Ingelsson (2021). "The Uppsala APP deletion causes early onset autosomal dominant Alzheimer's disease by altering APP processing and increasing amyloid β fibril formation." Sci Transl Med **13**(606).
307. Roychaudhuri, R., T.-P. V. Huynh, T. R. Whitaker, E. Hodara, M. M. Condron and D. B. Teplow (2017). "A Critical Role of Ser26 Hydrogen Bonding in Aβ42 Assembly and Toxicity." Biochemistry **56**(48): 6321-6324.
308. Scheuner, D., C. Eckman, M. Jensen, X. Song, M. Citron, N. Suzuki, T. D. Bird, J. Hardy, M. Hutton, W. Kukull, E. Larson, L. Levy-Lahad, M. Viitanen, E. Peskind, P. Poorkaj, G. Schellenberg, R. Tanzi, W. Wasco, L. Lannfelt, D. Selkoe and S. Younkin (1996). "Secreted amyloid β–protein similar to that in the senile plaques of Alzheimer's disease is increased in vivo by the presenilin 1 and 2 and APP mutations linked to familial Alzheimer's disease." Nature Medicine **2**(8): 864-870.
309. Selkoe, D. J. (2004). "Cell biology of protein misfolding: The examples of Alzheimer's and Parkinson's diseases." Nature Cell Biology **6**(11): 1054-1061.
310. Selkoe, D. J. and J. Hardy (2016). "The amyloid hypothesis of Alzheimer's disease at 25 years." EMBO Mol Med **8**(6): 595-608.
311. Suzuki, N., T. T. Cheung, X. D. Cai, A. Odaka, L. Otvos, Jr., C. Eckman, T. E. Golde and S. G. Younkin (1994). "An increased percentage of long amyloid beta protein secreted by familial amyloid beta protein precursor (beta APP717) mutants." Science **264**(5163): 1336-1340.
312. van Dyck, C. H., C. J. Swanson, P. Aisen, R. J. Bateman, C. Chen, M. Gee, M. Kanekiyo, D. Li, L. Reyderman, S. Cohen, L. Froelich, S. Katayama, M. Sabbagh, B. Vellas, D. Watson, S. Dhadda, M. Irizarry, L. D. Kramer, and T. Iwatsubo (2022). "Lecanemab in Early Alzheimer's Disease." New England Journal of Medicine.

VITA

Shikha Grover was born and raised in Delhi, the capital city of India. She received her high school education from a catholic school Rosary Sr. Sec School. She earned her bachelor's degree in chemistry from Hansraj College, Delhi University, and her Master of Science degree in Organic Chemistry from the department of Chemistry, Delhi University. She worked in India for 1.5 years in India before she got accepted in PhD Chemistry (Biochemistry) program at University of Missouri-St. Louis in Spring 2018 and began her journey for the very first time away from family. Little did she know that

she would come across many people from various cultures who would become her family. She obtained her master's in science degree in Chemistry from UMSL in Spring 2020. She has a great family she lives with and is gearing up for upcoming adventures in the circle of life.